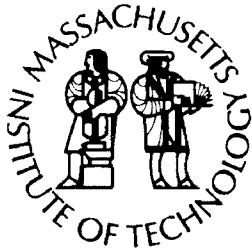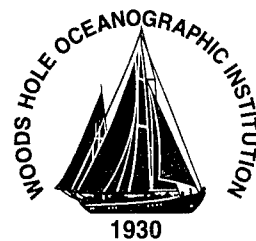# Massachusetts Institute of Technology

Woods Hole Oceanographic Institution

Joint Program in Oceanography/ Applied Ocean Science and Engineering

1930

DOCTORAL DISSERTATION

Scale Closure in Upper Ocean Optical Properties:
From Single Particles to Ocean Color

by

Rebecca E. Green

June 2002

20021231 099

MIT/WHOI

2002-10

Scale Closure in Upper Ocean Optical Properties:
From Single Particles to Ocean Color

by

Rebecca E. Green

Massachusetts Institute of Technology
Cambridge, Massachusetts 02139

and

Woods Hole Oceanographic Institution
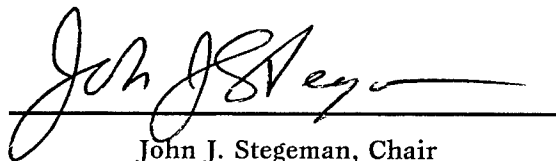Woods Hole, Massachusetts 02543

June 2002

DOCTORAL DISSERTATION

Approved for Distribution:

John J. Stegeman, Chair
Department of Biology

Paola Malanotte-Rizzoli
MIT Director of Joint Program

John W. Farrington
WHOI Dean of Graduate
Studies

SCALE CLOSURE IN UPPER OCEAN OPTICAL PROPERTIES:
FROM SINGLE PARTICLES TO OCEAN COLOR

By

Rebecca E. Green

B.S., California Institute of Technology, 1994

Submitted in partial fulfillment for the requirements for the degree of

Doctor of Philosophy

at the

MASSACHUSETTS INSTITUTE OF TECHNOLOGY

and the

WOODS HOLE OCEANOGRAPHIC INSTITUTION

June 2002

© 2002 Rebecca E. Green
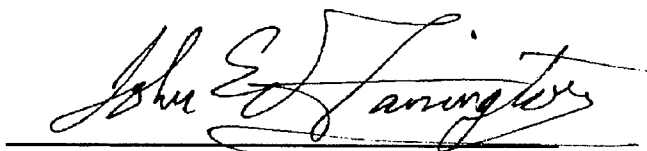All rights reserved

The author hereby grants to MIT and WHOI permission to reproduce paper and
electronic copies of this in whole or in part, and to distribute them publicly.

Signature of author_____

Joint Program in Biological Oceanography
Massachusetts Institute of Technology /
Woods Hole Oceanographic Institution
May 2002

Certified by_____

Heidi M. Sosik
Thesis Supervisor

Accepted by_____

Mark E. Hahn
Chairman, Joint Committee for Biological Oceanography
Massachusetts Institute of Technology
Woods Hole Oceanographic Institution

SCALE CLOSURE IN UPPER OCEAN OPTICAL PROPERTIES: FROM SINGLE PARTICLES TO OCEAN COLOR

by

Rebecca E. Green

Submitted to the MIT/WHOI Joint Program in Biological Oceanography in partial fulfillment of the requirements for the degree of Doctor in Philosophy

ABSTRACT

Predictions of chlorophyll concentration from satellite ocean color are an indicator of phytoplankton primary productivity, with implications for foodweb structure, fisheries, and the global carbon cycle. Current models describing the relationship between optical properties and chlorophyll do not account for much of the optical variability observed in natural waters, because of the presence of seawater constituents that do not covary with phytoplankton pigment concentration. In an attempt to better understand variability in these models, the contributions of seawater constituents to ocean optical properties were investigated. A combination of Mie theory and flow cytometry was used to determine the diameter, complex refractive index (n+n'i), and optical cross-sections of individual particles, based on a method developed in the laboratory using phytoplankton cultures.

Individual particle measurements were used to interpret variability in concurrently measured bulk optical properties in New England continental shelf waters in two seasons. The summed contribution to scattering of individual particles in the size range of 0.1-50 μm accounted for approximately the entire scattering coefficient measured independently using bulk methods. In surface waters in both seasons, the large diameters and n' of eukaryotic phytoplankton caused them to be the main particle contributors to both absorption and scattering. Minerals were the main contributor to backscattering, b_b, in the spring, whereas in the summer both minerals and detritus contributed to b_b. *Synechococcus* and heterotrophic bacteria were less important optically, contributing ≤11% each to attenuation in either season.

The role of seawater constituents in determining remote sensing reflectance, R_{rs}, was determined using radiative transfer theory. Seasonal differences in the spectral shape of R_{rs} were contributed to approximately equally by eukaryotic phytoplankton absorption, dissolved absorption, and non-phytoplankton b_b. A higher inverse wavelength dependence of non-phytoplankton b_b in the summer was caused by the contribution of small detritus, in contrast to larger minerals in the spring. Measurements of b_b and R_{rs} were compared to values from bio-optical models based on chlorophyll concentration. Differences in measured and modeled b_b and R_{rs} were

caused by higher dissolved absorption and higher backscattering efficiencies and scattering by non-phytoplankton than were assumed by the model.

Thesis Supervisor: Heidi M. Sosik, Associate Scientist
                    Woods Hole Oceanographic Institution

ACKNOWLEDGEMENTS

friend and partner, Raz Popescu. He has given me extensive help in the proofreading and formatting of my thesis, and has lovingly supported me during the last several months of thesis writing.

TABLE OF CONTENTS

CHAPTER 1:

INTRODUCTION

A primary motivation of this dissertation was to interpret, in a detailed manner, bulk optical properties in the ocean with the objective of improving model predictions of chlorophyll concentration from satellite ocean color. This motivation is in keeping with a longstanding goal in ocean optics of deriving ecologically important quantities, including chlorophyll concentration, phytoplankton absorption, and particulate carbon concentration, from measurements of bulk optical properties. Predictions of chlorophyll concentration from satellite ocean color are an indicator of phytoplankton primary productivity, with implications for foodweb structure, fisheries, and the global carbon cycle. Research began over 25 years ago on the development of bio-optical algorithms for the determination of chlorophyll concentration in the ocean from remotely sensed reflectance data (e.g. Clarke et al. 1970; Gordon et al. 1980), and this topic continues to be a major focus of current research (e.g. Morel and Maritorena 2001; Sathyendranath et al. 2001).

Bio-optical algorithms rely on the relationship between pigment concentration in the water and the bulk optical properties of the water. Bulk optical properties include both IOPs, which depend solely on the constituents of seawater (e.g. absorption, scattering, and backscattering), and AOPs which depend both on the constituents of seawater and the ambient light field (e.g. diffuse attenuation and reflectance). Unexplained variability exists in bio-optical algorithms in open ocean

waters, and even more so in coastal waters, due to a lack of knowledge of seawater

constituents besides phytoplankton. Recently, models have been developed for the

inversion of reflectance spectra to determine IOPs, including absorption by

phytoplankton, absorption by dissolved and detrital materials, and backscattering by

particulates (Roesler and Perry 1995; Garver and Siegel 1997; Carder et al. 1999).

Such models suggest that future research should focus on better understanding the

ratio between absorption by phytoplankton and absorption by dissolved and detrital

materials and on the types and optical properties of particles which contribute to

backscattering. On the basis of recent measurements, it may also be possible to use

satellite reflectance data in the estimation of particulate organic carbon in the ocean.

Stramski et al. (1999) reported a relationship between measurements of particulate

organic carbon and particulate backscattering in the Southern Ocean, suggesting that a

similar relationship may exist for remote sensing reflectance.

The quantification of relationships between bulk optical properties and

ecologically important quantities, such as chlorophyll and particulate organic carbon,

depends on the ability to account for the seawater constituents that contribute to bulk

optical properties. This dependence is an issue of "scale closure", defined as the use

of measurements of single particles to account for changes in bulk properties (Mobley

1994). Model simulations have been performed to determine expected mean particle

contributions to inherent optical properties in open ocean waters (Stramski and Kiefer

1991; Stramski and Mobley 1997; Stramski et al. 2001) and to apparent optical

properties in both open ocean and coastal waters with two types of phytoplankton

blooms (Mobley and Stramski 1997). These simulations show the power of summing over individual seawater consituents to explain modeled variability in optical properties and suggest that similar studies could describe important variability when applied to natural samples. Three studies have aimed at understanding scale closure in natural samples, all in Case 1 waters (DuRand and Olson 1996; Chung et al. 1998; Claustre et al. 1999). Variability in beam attenuation due to particles (c_p) at 660 nm was partially explained by accounting for changes in microbial particle types measured using flow cytometry. Based on these studies, eukaryotic phytoplankton of 0.2-20 µm in size accounted for 30-45% of total beam c_p, *Prochlorococcus* and heterotrophic bacteria accounted for ~10% each, *Synechococcus* contributed a negligible amount (≤5%), and non-plankton (not measured) were inferred to account for 40-50% of c_p. The results of Chung et al. (1998) for phytoplankton groups were not considered here because of seemingly erroneous findings (Binder and DuRand, 2002).

The application of flow cytometry in oceanography has allowed for the rapid determination of individual particle properties in mixed marine particle assemblages (Olson et al. 1993). The basis of modern flow cytometry, the sheath-flow principle, was first developed as a medical tool for the optical counting of red blood cells (Crosland-Taylor 1953). In the late 1970's and early 1980's, flow cytometry was applied to laboratory studies of phytoplankton in culture (Paau et al. 1978; Paau et al. 1979; Trask et al. 1982; Olson et al. 1983; Yentsch et al. 1983), and in 1985, flow cytometry was first used at sea for the study of marine phytoplankton distributions in

natural samples (Olson et al. 1985). Since its initial application to the marine environment, methods have been developed for the identification of numerous particle types using flow cytometric forward and side angle scattering, fluorescence and labeling techniques. A comparison of forward scattering, red fluorescence, and/or orange fluorescence allows populations of *Prochlorococcus*, eukaryotic picophytoplankton, coccolithophorids, pennate diatoms, cryptophytes, *Synechococcus*, and non-phytoplankton particles to be enumerated and sized (Olson et al. 1993). Additionally, fluorescent staining techniques have allowed for the flow cytometric identification of heterotrophic bacteria (Marie et al. 1997), possibly viruses (Marie et al. 1999), and organic and inorganic particles (Moreira-Turcq and Martin 1998).

Mie theory provides the theoretical link between flow cytometric measurement of individual particles and the determination of their inherent optical properties. The absorption and scattering of light by a homogenous sphere, including the angular distribution of the scattered intensity, is solved using Mie theory (Mie 1908; Bohren and Hoffman 1983). The application of Mie theory to flow cytometry requires an understanding of how the optical properties of natural particles are related to those of homogenous spheres, as assumed by the theory. Measurements of angular scattering for phytoplankton cultures have shown deviations from angular scattering predicted by Mie theory (Quinby-Hunt et al. 1989; Volten et al. 1998), and modeling work has focused on better understanding the effects of non-sphericity and inhomogeneities on theoretical determinations of angular scattering (e.g. Quinby-Hunt et al. 1989; Kitchen and Zaneveld 1992; Herring and Boss 2000). With its assumptions in mind, Mie

theory can provide a framework for calculating scattering at all angles from the forward and side angle scattering measurements of flow cytometry. Mie theory (or an approximation there of) has been applied to flow cytometric measurements of particles to determine particle diameter and real refractive index (n) (Ackleson and Spinrad 1988; Ackleson and Robins 1990) and the contribution of different phytoplankton species to beam attenuation (DuRand and Olson 1996; Claustre et al. 1999).

In addition to single particle measurements, the study of scale closure relies on the measurement of bulk optical properties. Remote sensing measurements of reflectance (ocean color) from space began with the launch of the Coastal Zone Color Scanner (CZCS) by NASA (National Aeronautics and Space Administration) in 1978 and have undoubtedly generated the widest interest in optical properties in the history of optical oceanography. As well, in situ methods exist for measuring AOPs using profiling radiometers, and measurement is generally made at wavelengths corresponding to those of current ocean color satellite sensors, such as the Sea Viewing Wide Field-of-View Sensor (SeaWiFS) (e.g. Morrow et al. 1994). In comparison to AOPs which depend on the ambient light field, instrumentation for measuring bulk IOPs is based on shining a characterized light source, such as a light emitting diode (LED), into or through a volume of water. Commercial, in situ instrumentation exists for measuring absorption, attenuation, backscattering, and the volume scattering function at selected angles (Zaneveld et al. 1990; Maffione and Dana 1997; Dana and Maffione 2000; Moore et al. 2001). In situ absorption is routinely measured on both filtered and unfiltered seawater to discriminate between

particulate and dissolved absorption. Ideally, single particle and bulk optical measurements would be made simultaneously, however, in practice bulk optical measurements are made in situ or from space and flow cytometry is performed on discrete water samples in the laboratory.

My thesis is organized into five chapters with the three data chapters covering a range of measurements from single particle optical properties to comparison with bulk inherent and apparent optical properties. In Chapter 2, I present results for the application of Mie theory to flow cytometry to determine particle diameter, real refractive index (n), and imaginary refractive index (n') (referred to as the "FCM-Mie method"). For phytoplankton cultures measured in the laboratory, estimates of cell properties from flow cytometry are compared to estimates of cell properties from bulk optical measurements. In Chapter 3, I apply Mie theory and flow cytometry, using methods developed in Chapter 2, to determine the contributions of particle groups to bulk inherent optical properties for natural samples collected in New England continental shelf waters. The contributions of seven seawater constituents are considered including seawater itself, dissolved materials, and five particle groups: eukaryotic pico/nanophytoplankton, *Synechococcus*, heterotrophic bacteria, detritus, and minerals. Variability in the IOPs of these constituents and in concentration, diameter, n, and n' for the particle groups is used to explain variability in bulk IOPs. Chapter 4 is a continuation of the use of seawater constituents to account for optical variability. In this chapter I use the contributions of constituents to account for variability in the apparent optical properties of diffuse attenuation (K_d) and remote

sensing reflectance (R_{rs}). Contributions of constituents to AOPs are modeled using the Hydrolight radiative transfer program and spectral IOPs, which are based on the use of Mie theory and flow cytometric measurements at 488 nm. General conclusions of the thesis are presented in Chapter 5. In Appendix A, I discuss the optimization between Mie theory and flow cytometric measurements used for heterotrophic bacteria. Appendix B contains a summary of the various flow cytometry experiments used to evaluate the FCM-Mie method.

REFERENCES

Ackleson, S.G., and D.B. Robins. 1990. Flow cytometric determinations of North Sea phytoplankton optical properties. Netherlands J. Sea Res. **25**: 11-18.

Ackleson, S.G., and R.W. Spinrad. 1988. Size and refractive index of individual marine particulates: a flow cytometric approach. Appl. Opt. **27**: 1270-1277.

Bohren, C.F., and D.R. Hoffman. 1983. Absorption and scattering of light by small particles. J. Wiley.

Carder, K.L., F.R. Chen, Z.P. Lee, and S.K. Hawes. 1999. Semianalytic Moderate-Resolution Imaging Spectrometer algorithms for chlorophyll a and absorption with bio-optical domains based on nitrate-depletion temperatures. J. Geophys. Res. **104**: 5403-5421.

Chung, S.P., W.D. Gardner, M.R. Landry, M.J. Richardson, and I.D. Walsh. 1998. Beam attenuation by microorganisms and detrital particles in the equatorial Pacific. J. Geophys. Res. **103**: 12669-12681.

Clarke, G.L., G.C. Ewing, and C.J. Lorenzen. 1970. Spectra of backscattered light from the sea obtained from aircraft as a measure of chlorophyll concentration. Science **167**: 1119-1121.

Claustre, H., A. Morel, M. Babin, C. Cailliau, D. Marie, J.C. Marty, D. Tailliez, and D. Vaulot. 1999. Variability in particle attenuation and chlorophyll fluorescence in the tropical Pacific: Scales, patterns, and biogeochemical implications. J. Geophys. Res. **104**: 3401-3422.

Crosland-Taylor, P.J. 1953. A device for counting small particles suspended in a fluid through a tube. Nature **171**: 37-38.

Dana, D.R., and R.A. Maffione. 2000. HydroBeta: A new instrument for measuring the volume scattering function from 10 to 170 degrees in situ. In *Ocean Optics XV*.

DuRand, M.D., and R.J. Olson. 1996. Contributions of phytoplankton light scattering and cell concentration changes to diel variations in beam attenuation in the

equatorial Pacific from flow cytometric measurements of pico-, ultra- and nanoplankton. Deep-Sea Res. II **43**: 891-906.

Garver, S., and D. Siegel. 1997. Inherent optical property inversion of ocean color spectra and its biogeochemical interpretation 1. Time Series from the Sargasso Sea. J. Geophys. Res. **102**: 18607-18625.

Gordon, H.R., D.K. Clark, J.L. Mueller, and W.A. Hovis. 1980. Phytoplankton pigments from the Nimbus-7 Coastal Zone Color Scanner: Comparisons with surface measurements. Science **210**: 63-66.

Herring, S., and E. Boss. 2000. Optical properties of spheroidal marine particles. Paper read at Ocean Optics XV.

Kitchen, J.C., and J.R.V. Zaneveld. 1992. A three-layered sphere model of the optical properties of phytoplankton. Limnol. Oceanogr. **37**: 1680-1690.

Maffione, R.A., and D.R. Dana. 1997. Instruments and methods for measuring the backward-scattering coefficient of ocean waters. Appl. Opt. **36**: 6057-6067.

Marie, D., C.P.D. Brussaard, R. Thyrhaug, G. Bratbak, and D. Vaulot. 1999. Enumeration of marine viruses in culture and natural samples by flow cytometry. Appl. Environ. Microbiol. **65**: 45-52.

Marie, D., F. Partensky, S. Jacquet, and D. Vaulot. 1997. Enumeration and cell cycle analysis of natural populations of marine picoplankton by flow cytometry using the nucleic acid stain SYBR Green I. Appl. Environ. Microbiol. **63**: 186-193.

Mie, G. 1908. Beiträge zur optik trüber median, speziell kolloidaler metallösungen. Annals of Physics **25**: 377-442.

Mobley, C.D. 1994. Light and water; radiative transfer in natural waters. Academic Press, Inc.

Mobley, C.D., and D. Stramski. 1997. Effects of microbial particle on oceanic optics: Methodology for radiative transfer modeling and example simulations. Limnol. Oceanogr. **42**: 550-560.

Moore, C.C., M.S. Twardowski, and J.R. Zaneveld. 2001. The ECO VSF - A sensor for determination of the volume scattering function in the backward direction. In *Proc. of Ocean Optics XV*.

Moreira-Turcq, P.F., and J.M. Martin. 1998. Characterisation of fine particles by flow cytometry in estuarine and coastal Arctic waters. J. Sea Res. **39**: 217-226.

Morel, A., and S. Maritorena. 2001. Bio-optical properties of oceanic waters: A reappraisal. J. Geophys. Res. **106**: 7163-7180.

Morrow, J.H., M.S. Duhig, and C.R. Booth. 1994. Design and evaluation of a cosine collector for a SeaWiFS-compatible marine reflectance radiometer. Paper read at SPIE Ocean Optics XII.

Olson, R.J., S.L. Frankel, S.W. Chisholm, and H.M. Shapiro. 1983. An inexpensive flow cytometer for analysis of fluorescence signlad in phytoplankton: Chlorophyll and DNA distributions. J. Exp. Mar. Biol. Ecol. **68**: 129-144.

Olson, R.J., D. Vaulot, and S.W. Chisholm. 1985. Marine phytoplankton distributions measured using shipboard flow cytometry. Deep-Sea Res. **32**: 1273-1280.

Olson, R.J., E.R. Zettler, and M.D DuRand. 1993. Phytoplankton Analysis Using Flow Cytometry, p. 175-186. *In* P. F. Kemp, B. F. Sherr, E. B. Sherr and J. J. Cole, [eds.]. Aquatic Microbial Ecology. Lewis Publishers.

Paau, A.S., J.R. Cowles, J. Oro, A. Bartel, and E. Hungerford. 1979. Separation of algal mixtures and bacterial mixtures with flow- microfluorometer using chlorophyll and ethidium bromide fluorescence. Archives of Microbiology **120**: 271-273.

Paau, A.S., J. Oro, and J.R. Cowles. 1978. Application of flow cytometry to the study of algal cells and isolated chloroplasts. J. Exp. Bot. **29**: 1011-1020.

Quinby-Hunt, M.S., A.J. Hunt, L. Lofftus, and D. Shapiro. 1989. Polarized-light scattering studies of marine *Chlorella*. Limnol. Oceanogr. **34**: 1587-1600.

Roesler, C.S., and M.J. Perry. 1995. In situ phytoplankton absorption, fluorescence emission, and particulate backscattering spectra determined from reflectance. J. Geophys. Res. **100**: 13279-13294.

Sathyendranath, S., G. Cota, V. Stuart, H. Maass, and T. Platt. 2001. Remote sensing of phytoplankton pigments: a comparison of empirical and theoretical approaches. International J. Remote Sensing **22**: 249-273.

Stramski, D., A. Bricaud, and A. Morel. 2001. Modeling the inherent optical properties of the ocean based on the detailed composition of the planktonic community. Appl. Opt. **40**: 2929-2945.

Stramski, D., and D.A. Kiefer. 1991. Light scattering by microorganisms in the open ocean. Prog. Oceanogr. **28**: 343-383.

Stramski, D., and C.D. Mobley. 1997. Effects of microbial particles on oceanic optics: A database of single-particle optical properties. Limnol. Oceanogr. **42**: 538-549.

Stramski, D., R.A. Reynolds, M. Kahru, and B.G. Mitchell. 1999. Estimation of particulate organic carbon in the ocean from satellite remote sensing. Science **285**: 239-242.

Trask, B.J., G.J. Van den Engh, and J.H.B.W. Elgershuizen. 1982. Analysis of phytoplankton by flow cytometry. Cytometry **2**: 258-267.

Volten, H., J.F. de Haan, J.W. Hovenier, R. Schreurs, W. Vassen, A.G. Dekker, H.J. Hoogenboom, F. Charlton, and R. Wouts. 1998. Laboratory measurements of angular distributions of light scattered by phytoplankton and silt. Limnol. Oceanogr. **43**: 1180-1197.

Yentsch, C.M., P.K. Horan, K. Muirhead, Q. Dortch, E.M. Haugen, L. Legendre, L.S. Murphy, M.J. Perry, D. Phinney, S.A. Pomponi, R.W. Spinrad, and A.M. Wood. 1983. Flow cytometry and sorting: A powerful technique with potential applications in aquatic sciences. Limnol. Oceanogr. **28**: 1275-1280.

Zaneveld, J.R.V., R. Bartz, and J.C. Kitchen. 1990. A reflective-tube absorption meter. Paper read at SPIE Ocean Optics X.

CHAPTER 2:

FLOW CYTOMETRIC DETERMINATION OF SIZE AND COMPLEX

REFRACTIVE INDEX FOR MARINE PARTICLES: COMPARISON WITH BULK

MEASUREMENTS

ABSTRACT

Flow cytometry is the only method currently available for measuring the distributions of size and complex refractive index of suspended particulate matter, quantities which are significant determinants of the optical properties of the ocean. I have advanced a method to determine diameter (D) and complex refractive index (n+n'i) of marine particles from flow cytometric (FCM) measurements of forward scattering, side scattering and chlorophyll fluorescence combined with Mie theory. I have evaluated my "FCM-Mie" method by comparing its results for phytoplankton cultures with independent estimates of cell D, n, and n' from electronic particle counter and bulk optical measurements. For a variety of phytoplankton species, cell D initially estimated from the FCM-Mie method was lower than independent estimates, and n and n' were generally higher than independent estimates. These differences reflected lower forward scattering and higher side scattering for single cell measurements than predicted by Mie theory, most likely due to deviation of cells from the assumption of homogenous spheres. To address this problem, I derived empirical scattering corrections based on measurements of nine species of phytoplankton. With these corrections, FCM-Mie estimates of size, n, and n' were improved for cells in the laboratory and were determined to within 13%, 28%, and 36% of measured values; notably, size was determined accurately for cells grown under both high- and low-light conditions. The values of n' determined from the FCM-Mie method were significantly correlated with intracellular chlorophyll concentration (p = 0.002), while values of n were not significantly correlated with intracellular carbon concentration. I applied the method to natural mixtures of particles including phytoplankton and non-phytoplankton from New England continental shelf waters. For a springtime depth profile, eukaryotic pico/nanophytoplankton and cells of the genus *Synechococcus* had minimum mean values of n' in surface waters, and non-phytoplankton particles had higher values of n than phytoplankton at all depths.

INTRODUCTION

The properties of the suspended particulate matter in the upper ocean are an important determinant of optical variability (Morel and Prieur 1977; Kirk 1983; Lewis and Cullen 1991), affecting how sunlight is attenuated with depth in the ocean and how it is reflected from surface waters, two important factors in ocean color algorithms. The primary factors that determine how a particle suspension interacts with the ambient light field, include particle concentration and the distributions of size and complex refractive index (n+n'i). The complex refractive index is composed of a real part (n) which describes scattering at interfaces and an imaginary part (n') which is indicative of the particle's light absorption properties. Changes in particle properties affect the particle's inherent optical properties of absorption, scattering, and backscattering. For example, smaller particles and particles with higher values of n tend to have higher ratios of backscattering to scattering. In simulations of the optical properties of oligotrophic waters, Stramski et al. (2001) found that phytoplankton dominated absorption at most wavelengths mainly because of their high values of n', while inorganic particles were the most important contributors to both scattering and backscattering mainly because of their high values of n. Based on the applicability of their simulations, these authors concluded that an increased effort is needed to characterize the types and concentrations of particles suspended in seawater, both in situ and in the laboratory.

Flow cytometry is one of the few tools available for analyzing the optical properties of large numbers of individual particles. Flow cytometric (FCM) forward and side angle scattering, fluorescence and labeling techniques can be used to enumerate, classify, and size various phytoplankton and non-phytoplankton particles (Olson et al. 1993). Using flow cytometry, it is possible to enumerate and distinguish specific groups of particles in the ocean, including *Prochlorococcus, Synechococcus,* eukaryotic pico- and nanophytoplankton, coccolithophorids, pennate diatoms, cryptophytes, and heterotrophic bacteria (Olson et al. 1989; Olson et al. 1993; Marie et al. 1997). Cell size has been estimated based on empirical relationships between FCM forward scattering and cell volume developed using laboratory cultures (Olson et al. 1989; DuRand 1995; Gin et al. 1999) and field populations of phytoplankton (Cavender-Bares 1999). As well, cell size has been determined from FCM scattering based on a time-of-transit measurement through the illuminating beam, an approach which avoids the effects of cell refractive index on scattering versus volume relationships (Chan and Un 2001).

In this paper I develop a method for determining the size, real refractive index, n, and imaginary refractive index, n', of individual particles using flow cytometry and Mie theory. I have advanced an approach first developed by Ackleson and Spinrad (1988) who applied Mie theory to angular scattering measurements from flow cytometry to determine size and n for phytoplankton cells of less than 10 μm in diameter. Given the size, n, and n' of a homogenous spherical particle, Mie theory

describes how incident light is absorbed and scattered, including the angular distribution and polarization of the scattered light (Mobley 1994). The method for applying Mie theory to flow cytometry involves comparison of theoretical and measured angular scattering for particles of known size and/or n and n', including polystyrene beads and oil suspensions; I have added silica beads, because they are within the range of n expected for phytoplankton cells. In addition to size and n, I have incorporated the determination of n' for phytoplankton cells, using an empirical relationship between FCM chlorophyll red fluorescence and absorption cross-section (Perry and Porter 1989).

Mie theory is the theoretical basis in my approach for determining size and complex refractive index from flow cytometric angular scattering and fluorescence measurements. Inherent in the theory is the assumption that particles are spherical and homogenous, an assumption from which natural particles, such as phytoplankton cells, are known to deviate. Mie theory (or approximations of the theory) have previously been applied to bulk optical measurements to infer n and n' of phytoplankton cultures, and these values of n and n' have been within the ranges expected for phytoplankton and were correlated with intracellular carbon and chlorophyll concentrations (Bricaud et al. 1988; DuRand and Olson 1998; Stramski et al. 2001). Recently, Volten et al. (1998) compared angular distributions of light scattered by phytoplankton suspensions measured in the laboratory to Mie theory estimates of angular scattering based on bulk optical determinations of n and n', and they found significant differences between

measured and theoretical angular scattering. They suggested that these deviations were due to the fact that phytoplankton are not homogenous spheres, as assumed for Mie calculations. Perhaps for this reason, Ackleson et al. (1988) observed that their estimates of n from single-cell optical measurements tended to be higher than previously published estimates of phytoplankton n using bulk optical properties. Given these discrepancies, I have further investigated the accuracy of FCM determinations of size, n, and n' using Mie theory by comparing them to independent estimates of these values.

The purpose of my research is to improve upon the application of Mie theory to flow cytometric measurements in order to determine the properties of phytoplankton and non-phytoplankton particles in natural samples. The accurate determination of individual particle properties is necessary for interpreting variability in bulk optical properties. I have developed a method for determining cell diameter, n, and n' from single-particle measurements based on validation with bulk estimates of these values for cultures of phytoplankton. I have found that the successful application of Mie theory to phytoplankton depends on characterization of how their forward and side scattering compares to that of spherical, homogenous particles, an assumption inherent in the theory. My new approach for the analysis of individual particle measurements accurately determines cell properties for different species of phytoplankton and under different growth conditions. For non-phytoplankton particles, I have used my method to determine diameter and n, however assumptions

need to be made for n' and how the scattering of these particles relates to that of homogenous spheres. I have applied my method to natural mixtures of particles containing phytoplankton and non-phytoplankton from New England continental shelf waters to exemplify how particle properties vary in natural samples.

METHODS FOR PARTICLE MEASUREMENTS

Flow Cytometry

A modified Epics V flow cytometer (FCM; Coulter Electronics Corp.) interfaced with a Cicero acquisition system (Cytomation, Inc.) was used to measure forward light scattering (FLS, ~3-19° at 488 nm), side angle light scattering (SSC, ~54-126° at 488 nm), chlorophyll fluorescence (CHL, 660-700 nm), and the concentration of particles. The dynamic range of FLS, SSC, and CHL measurements was increased by splitting the optical signals and independently detecting and amplifying them with separate photomultipliers and 3-decade log amplifiers. For each property, the relative sensitivities of the two measurements were adjusted to have one decade overlap, and thus the potential measurement range was expanded to five orders of magnitude. Particles were injected into a saline sheath flow and illuminated by light from an argon ion laser beam polarized parallel to the fluid stream. The samples were delivered with a peristaltic pump (Harvard Apparatus), and cell concentration was determined from pump flow rate and sample analysis time. Polystyrene microspheres of various sizes (from 0.57 μm to 6.2 μm YG beads from Polysciences, Inc.) were measured as reference particles. Data were saved as listmodes and

23

analyzed using a version of "CYTOWIN" software (originally written by D. Vaulot; http://www.sb-roscoff.fr/Phyto/cyto.html) modified to merge data from two logarithmic amplifiers. For populations of beads and cultured cells, arithmetic means of FLS, SSC, and CHL were computed following transformation of distributions to linear values.

Absorption and Attenuation

Spectral absorption coefficients (a) of phytoplankton suspensions were measured on a Perkin-Elmer Lambda 18 UV/VIS spectrophotometer equipped with a 60-mm integrating sphere. Samples were placed in a 1-cm quartz cuvette at the entrance to the integrating sphere, and measurements were made over the spectral range of 300 to 900 nm with a speed of 240 nm s^{-1}, a slit width of 4 nm, and a scan interval of 1 nm. Optical density of cultures was measured relative to syringe-filtered (0.22 μm) culture or fresh media (depending on the experiment) in the reference cuvette. A dilution series was measured at the start of each experiment to ensure that, in subsequent measurements, multiple scattering effects were negligible. All spectra were offset to zero optical density at 750 nm.

A flow through absorption and attenuation meter with a 25-cm pathlength (ac-9, WETLabs) was used to measure the spectral beam attenuation coefficient (c) at nine wavelengths (412, 440, 488, 510, 532, 555, 650, 676, and 715 nm). Two reservoirs were attached with tubing to the inlet and outlet of the ac-9, samples were gravity fed through the instrument, and data collection was monitored to ensure the absence of air

bubbles. Filtered seawater was used to dilute phytoplankton cultures before measurement and was analyzed between samples and subtracted as a blank. A dilution series was measured at the start of the experiment to ensure that there were no concentration dependent effects on the measurements. During data processing, temperature correction was applied based on the difference between water temperature at the time of sampling and during instrument calibration (Pegau et al. 1997). Values of a measured with the spectrophotometer and ac-9 were similar, and I chose to use the spectrophotometric values since they are less susceptible to noise and other sampling errors.

Ancillary Measurements

Cell size distributions were determined with a Coulter Multisizer (Coulter Corp.) equipped with either a 30-μm, 50-μm, or 100-μm aperture, depending on the size of the cells. The instrument was calibrated using 5.11, 9.32, and 19.61 μm microspheres for the 30-μm, 50-μm, and 100-μm apertures, respectively. Cultures were diluted with filtered seawater in order to obtain coincidence rates of 6% or less. The size distributions of replicate samples were averaged and normalized to the cell concentration from flow cytometric analysis. Size distributions of the smaller cells were fit with a Gaussian curve in order to extrapolate distributions where signal-to-noise was low. The 256-channel data of cell diameter distributions were used to calculate the diameter of the mean cell (D) and the geometric projected area of the

mean cell to include the effects of polydispersion in my calculations (Stramski and Reynolds 1993; Reynolds et al. 1997).

Duplicate samples of 1- to 2-ml of culture were filtered onto GF/F filters and frozen in liquid nitrogen for later fluorometric chlorophyll *a* analysis. The fluorometer (Turner 10-AU with optical filter kit 10-040R) was calibrated with a dilution series of pure chlorophyll *a* (Sigma Chemical Co.) in 90% acetone. Filtered samples were removed from liquid nitrogen, extracted overnight in cold 90% acetone, agitated, and the supernatant was removed after 5 min in a clinical centrifuge (~4000 x g). Fluorometer readings were made before and after acidification to account for the effects of phaeophytin in the calculation of chlorophyll *a* concentration (Jeffrey and Welschmeyer 1997). Consistent with previous work (Wright et al. 1997), I found that the extraction approach was ineffective for *Nannochloris* sp. and two unidentified eukaryotes ("t6" and "isb"), all of which are small (< 3 μm) cells containing chlorophyll *b*. These species were excluded from data analysis involving chlorophyll relationships.

Duplicate 25-ml samples of each culture were also filtered onto pre-combusted GF/F filters, frozen, and later dried overnight at 60°C before analysis on a Perkin-Elmer 2400 CHN analyzer with acetanilide as the standard. Carbon values of wet and dry filter blanks were a few percent of sample carbon signals and were subtracted from sample values. Intracellular carbon concentration ($kg\ m^{-3}$) was calculated by averaging replicate samples and dividing raw carbon values by volume filtered, cell concentration, and mean cell volume.

Particle Types

A dataset of physical and optical measurements was compiled for numerous types of phytoplankton ranging in size from 1 to 10 μm, polystyrene and silica microspheres (beads), and suspensions of oil droplets. Phytoplankton data were derived from a combination of several laboratory experiments, as well as from analysis of natural seawater samples, and a variety of measurements were made on them as described below. For the beads and oil droplets, only flow cytometry measurements were made.

I divided the phytoplankton laboratory experiments into "calibration" and "evaluation" datasets for which measurements were made independently (Table 1). The methodology for applying Mie theory to FCM measurements was developed using the calibration dataset, and then evaluated by applying it to the evaluation dataset. The calibration dataset included ten species of phytoplankton. The evaluation dataset contained 21 cultures, with thirteen species each of phytoplankton grown at low-light levels and high-light levels (for experimental details for a subset of these cultures, see Shalapyonok et al. (2001)). The evaluation dataset also included two diel studies, of *Micromonas pusilla* (DuRand et al. 2002) and *Nannochloris* sp. (DuRand and Olson 1998), for which measurements were made every two hours over a 24-hour period. I did not include in my measurements phytoplankton cells which were far from spherical (e.g. pennate diatoms or chains of cells) or contained gas vacuoles.

For the laboratory experiments, monospecific but non-axenic cultures were grown in f/2 medium (Guillard 1975) under defined conditions of light intensity and

temperature, and various measurements were made. All cultures were grown under either natural light conditions ("high light", summertime in Woods Hole, MA) or Cool-White fluorescent lights ("low light", 50-120 μmol photons $m^{-2}s^{-1}$); all light levels were constant, except in the case of the natural light studies and the diel studies of *Micromonas* and *Nannochloris* for which cultures were grown under a 12:12 light:dark cycle. In each case, temperature was held constant at a value between 20 and 24°C. A variety of measurements were made on cultures in either the exponential or stationary phase of growth. For all cultures in the calibration dataset and for the two diel experiments in the evaluation dataset, a full suite of measurements was made, including FCM FLS, SSC, and CHL, spectral *a* and *c*, Coulter Counter size distributions, and carbon concentrations; chlorophyll concentrations were measured only for cultures in the calibration dataset and the *Micromonas* diel experiment. Spectral c was measured using an ac-9 (as previously described), except in the case of the *Nannochloris* diel experiment for which c was measured at 665 nm on a SeaTech transmissometer (25-cm pathlength) and converted to 488 nm by applying an average ratio observed between n at 665 nm and n at 488 nm for *Nannochloris* in the calibration dataset. For all other cultures in the evaluation dataset, a more limited set of measurements was made which included FCM FLS, SSC, and CHL, Coulter Counter size distributions, and in some cases spectrophotometric measurements.

Oil suspensions were measured on the FCM and used as calibration particles with known refractive index. Suspensions of heptane, nonane, or dodecane (Sigma Chemical, Co.) were made by adding a small amount of oil to a syringe of filtered

seawater and shaking vigorously to form a polydispersion of droplet sizes (Ackleson and Spinrad 1988). Refractive indices of the oils were measured on a refractometer (Fisher Scientific) in the laboratory as 1.0325, 1.0467, and 1.0590 (relative to water), respectively, for heptane, nonane, and dodecane. These values differ slightly from those in the CRC Handbook of Chemistry and Physics (1998-1999), which were published as 1.0364, 1.0496, and 1.0617, respectively. Values measured on the laboratory refractometer gave accurate readings for a set of standards and were used in my analyses. The oils were assumed to be non-absorbing.

Beads of known size and refractive index were measured on the FCM and used as calibration particles. Polystyrene beads of several sizes (0.57, 2.14, 2.9, 3.79, 5.2, and 6.2 μm) and n of 1.19 were analyzed in conjunction with each laboratory and field experiment. A silica bead of 1.58 μm (Duke Scientific, Inc.) was also included in the calibration and *Micromonas* diel experiments, and is of particular interest because its refractive index of 1.09 is closer than that of polystyrene beads to values within the plausible range for phytoplankton cells, generally from 1.01 to 1.10. Polystyrene bead absorption was measured spectrophotometrically for the 2.14 μm bead and was calculated for the other sizes of polystyrene beads by multiplying the ratio of each bead's mean FCM CHL to that of the 2.14 μm bead. The silica beads were assumed to be non-absorbing.

Selected field samples analyzed during the Coastal Mixing and Optics (CMO) Experiment (Dickey and Williams 2001) were chosen to exemplify the application of

my analyses to field data. The sampling site was located on the New England Shelf in 70 meters of water at a single location (70° 30′ N, 40° 30′ W). I have analyzed FCM samples collected during a noon depth profile on May 6th of a spring, 1997 CMO cruise (Sosik et al. 2001). Flow cytometric measurements were made on water samples collected with Niskin bottles on a rosette equipped with CTD. Eukaryotic pico/nanophytoplankton populations were discriminated from non-phytoplankton particles based on their FCM CHL signal, and *Synechococcus* cells were discriminated based on their orange fluorescence. Using my methodology for applying Mie theory to FCM measurements, I analyzed each particle in a sample and created size and refractive index distributions for eukaryotic phytoplankton, *Synechococcus*, and non-phytoplankton.

THEORETICAL DEVELOPMENT

Mie Theory and Estimation of Bulk n and n′

Bulk estimates of n and n′ at 488 nm were derived through an inverse method, using Mie scattering theory. Assumptions of the theory include that particles are spherical and homogenous. Refractive indices were derived through an iterative procedure using optimization routines provided with the MATLAB software package (Mathworks, Inc.), in which the differences between Mie-modeled and measured values of the efficiency factors for absorption and attenuation were minimized. Initial values of n and n′ for the Mie modeling approach were computed using the anomalous diffraction approximation (Van de Hulst 1957) through iteration (following the

30

approach described by Bricaud and Morel (1986). Additional Mie inputs included D and the efficiency factors for absorption and attenuation which were determined from a and c, respectively, D, and cell concentration.

Mie Theory and Flow Cytometry

My objective was to use Mie theory to infer particle D, n, and n' from FCM measurements of FLS, SSC, and CHL. For this, we need to know the particle's absorption cross-section (σ_a), the magnitudes of FLS and SSC, and the scattering angles associated with each of these. For phytoplankton, σ_a can be estimated from an empirical relationship with FCM CHL (see Results). I measure the magnitudes of FLS and SSC, but I do not know the optical geometry of FCM scattering precisely enough for the application of Mie theory. In order to infer the angles of FLS and SSC, I developed an optimization approach using FCM measurements of calibration particles and Mie theory calculations of scattering for these particles. The optimization allows for variation both in the range of angles contributing to FLS and SSC and in the weighting of contributions from different angles.

I performed an unconstrained, nonlinear minimization for calibration particles of known refractive index and /or size using optimization routines provided with the MATLAB software package. Embedded in my optimization is the program for Mie scattering which was provided by E. Boss based on Fortran code of Bohren and Hoffman (1983), and my application of Mie scattering to flow cytometry is a modification of code originally written in Fortran by Ackleson and Spinrad (1988).

Particles used in my optimization included polydisperse oil suspensions of heptane, nonane, and dodecane, polystyrene beads, and a silica bead. There were four variables in the optimization, two that were used to weight contributions to forward scattering (fls1 and f1) and two that were used to weight contributions to side scattering (ssc1 and f2). For my FCM configuration, horizontal beam obscuration bars block the collection lens for both the forward and side scattering detectors and, additionally, the entire lower half of the lenses for the forward detector is obscured. The geometry of FLS scattering is sufficiently constrained to determine an empirical function, leading to a weighting function for the forward detector of:

$$w_{fls}(\theta) = f1*(1-fls1*2/(\pi*d_1*\tan(\theta*2*\pi/360))) \tag{1}$$

where $3° \leq \theta \leq 19°$, d_1 = distance from particle to collection lens (= 24.9 mm), fls1 = 1/2 width of the obscuration bar, and f1 is a scalar multiplier. In contrast to FLS, the collection of light scattered to side angles is too complex to define empirically for the FCM configuration, and a sine function was chosen to represent the weighting for SSC because it gives a good fit between FCM measurements and Mie theory. The weighting for the side detector is described by the following equation:

$$w_{ssc}(\theta) = f2*\sin(\pi*(w_a*\theta+w_b)/180) \tag{2}$$

where $ssc1 < \leq \theta \leq (180-ssc1)$, $w_a = 180/(180-2*ssc1)$, $w_b = -w_a*ssc1$, and f2 is a scalar multiplier. As in Ackleson and Spinrad (1988), differential scattering cross-sections in

the FLS and SSC directions were calculated by multiplying the FLS and SSC

weightings, $w_{fls}(\theta)$ and $w_{ssc}(\theta)$, by the first two elements of the scattering matrix to

account for polarization (S11 and S12 in the notation of Bohren and Hoffman (1983)),

and summing over all angles contributing to detected scattering signals.

FCM-Mie Method Development and Testing

Using this optimization, a 3-dimensional lookup table of Mie theory-based

solutions for particle FLS, SSC, and σ_a was created over the expected ranges of

particle D (0-10 μm at 0.1 μm resolution), n (1-1.10 at 0.002 resolution; 1.10-1.15 at

0.005 resolution), and n′ (0-0.010 at 5×10^{-4} resolution; 0.010-0.030 at 1×10^{-3}

resolution) for the marine particles of interest. For any particle of interest, measured

values of particle FLS, SSC, and σ_a can be compared to values in the lookup table, and

a solution (i.e. associated with values of D, n, and n′) chosen based on minimum

distance, where

distance=

$$(\log_{10}(\sigma'_{b,t}(\theta_{fls})) - \log_{10}(\sigma'_{b,o}(\theta_{fls})))^2 + (\log_{10}(\sigma'_{b,t}(\theta_{ssc})) - \log_{10}(\sigma_{b,o}(\theta_{ssc})))^2 + (\log_{10}(\sigma_{a,t}) - \log_{10}(\sigma_{a,o}))^2$$

(3);

here the subscripts o and t refer to observed and theoretical values (i.e., from the

lookup table), respectively. Forward and side scattering cross-sections (normalized to

that of a reference bead) are represented by $\sigma'_{b,o}$ and $\sigma'_{b,t}$ for angles in the FLS (θ_{fls})

and SSC (θ_{ssc}) directions. Absorption cross-section is represented by $\sigma_{a,o}$ and $\sigma_{a,t}$. At

the position of minimum distance between observed and theoretical values, D, n, and n' are chosen from the lookup table as the particle's estimated properties. I refer to this approach for applying Mie theory to FCM measurements as the "FCM-Mie method".

RESULTS AND DISCUSSION

Single Particle Absorption

Phytoplankton absorption for laboratory and natural samples was calculated based on FCM CHL. A regression was determined between spectrophotometrically derived σ_a (m^2 $cell^{-1}$) at 488 nm and FCM CHL at 680 nm; this regression was based on results for fourteen phytoplankton species measured in the laboratory taken from both the calibration and evaluation datasets. Spectrophotometric σ_a was calculated by normalizing spectrophotometric a to cell concentration. The cultures used are representative of major taxonomic groups and range in size from 1 to 10 μm. A high correlation was observed between σ_a and FCM CHL ($r^2 = 0.96$ with a power fit; Fig. 1). When the regression was applied to FCM CHL values for the cultures, a mean error of 30% was observed between modeled and measured σ_a. Previously, a relationship between FCM CHL and σ_a was described by Perry and Porter (1989) who reported a strong correlation between FCM CHL and σ_a for sixteen phytoplankton cultures using a linear fit ($r^2 = 0.93$).

FCM and Mie Theory Optimization

I applied my optimization routine for matching FCM scattering measurements of oils and beads to Mie theory. Little difference was seen between oils and beads measured for the different experiments even though there were often months to years between measurements. Thus, one optimization was performed on an averaged dataset of oil and bead measurements. A close fit was observed between theoretical and measured FLS and SSC, especially in the size range of phytoplankton cells of interest, between 1 and 10 μm (Fig. 2). Significant deviation of the oil measurements from theory does not occur until below approximately 1 μm and above 15 μm. For the silica and polystyrene beads, the mean deviation between theory and measurements was 7% for logarithmic values of FLS and 5% for logarithmic values of SSC.

Using this optimization and the resulting Mie-based lookup table, estimates of bead D, n, and n' from the FCM-Mie method were compared to known values. (Analysis of the polystyrene beads required addition of calculations to the lookup table for particles in the range for n of 1.15-1.30, 0.005 resolution.) Comparison between FCM-Mie estimates of D, n, and n' and measured values for all polystryrene beads analyzed, resulted in the FCM-Mie method underestimating D by an average of 6%, overestimating n by 29%, and overestimating n' by 48%. For the silica bead, the FCM-Mie method overestimated D by 14%, underestimated n by 20%, and accurately determined n'. Because n for silica is within the range of phytoplankton cells, the

error values for the silica bead are most representative of those which can be expected with application of my FCM-Mie method to phytoplankton.

Evaluation of Method (for Phytoplankton)

To evaluate the validity of the FCM-Mie solutions, I compared estimates of D, n, and n' to independent estimates of these values from measurements of phytoplankton cultures in the laboratory. Only cells less than 10 μm in size were used due to limitations of my FCM approach using Mie theory, and because it is difficult to determine independent values of n from bulk optical measurements for larger cells, because unique solutions can not be found.

Initially, values of D, n, and n' estimated from the FCM-Mie method were compared to the independent determinations of these quantities for the calibration dataset (Table 1). The culture of *Emiliania huxleyi* was excluded from analysis, because no independent solution was found for n or n'. For the ten species of phytoplankton studied, cell D were underestimated (slope = 0.9 forced through zero; Fig. 3(a)), and n and n' were generally overestimated (slope = 1.5 and 1.7, forced through one and zero, respectively; Fig. 3(b) and 3(c)). The unidentified culture denoted "isb" was not included in the statistics for n and n', because its independent estimate of n of 1.12 is considered to be outside of the range plausible for phytoplankton cells. One explanation for the high value of n for this culture could be the presence in the sample of non-phytoplankton particles, such as bacteria or cell debris.

I have confidence in my independent values of n and n′, because bulk estimates of n at 488 nm were well correlated with intracellular carbon concentration ($r^2 = 0.61$, data not shown), and bulk estimates of n′ at 675 nm were correlated with intracellular chlorophyll concentration ($r^2 = 0.47$). These findings agree with previous work by Stramski (1999) who has reported intracellular carbon concentration to be correlated with n at 660 nm and intracellular chlorophyll concentration to be correlated with n′ at 675 nm for *Thalassiosira pseudonana* and *Synechococcus*. One explanation for the differences I observe between FCM-Mie and independent determinations of *D*, n, and n′ is that many phytoplankton cells deviate from sphericity and homogeneity, both of which are assumptions of Mie theory.

In an effort to characterize and correct for the deviations between FCM-Mie and independent estimates of cell properties, I investigated the relationship between modeled- and FCM-measured FLS and SSC. Modeled values of FLS and SSC were calculated using Mie theory with measurements of *D* and bulk estimates of n and n′. Flow cytometric measurements of FLS were generally lower than modeled FLS by an average of 39%. The opposite trend existed for SSC with measurements generally higher than modeled values by an average of 19%. A second order polynomial fit between logarithmic values of modeled and measured FLS gave a high correlation coefficient ($r^2 = 0.97$; Fig. 4). For SSC, there was not a simple relationship between measured and modeled values, so I used a linear fit (forced through the position of *Synechococcus*) to describe the general bias; this fit explained 50% of the total

variance. My general findings for SSC agree with those of Volten et al. (1998) who found that, for 13 of the 15 phytoplankton cultures they analyzed, measured polarized scattering at side angles was significantly higher than that estimated from Mie theory. Notably, and contrary to the general trend I observed in SSC, the smallest cell I measured, *Synechococcus*, had similar or higher modeled than measured SSC values. Volten et al. (1998) also found this trend for the two smallest cells they measured, *Prochlorothrix hallandica* and *Selenastrum capricornutum*. Thus, there is either some size dependence in the fit between modeled and measured volume scattering functions, or else smaller cells are more like homogenous spheres.

I used the regression results between modeled and measured FLS and SSC to adjust FCM FLS and SSC before particle measurements were compared to values in the Mie-based lookup table. This represents a crude approach to account for general effects of shape and structure in phytoplankton. It can not be expected to provide highly accurate results for every phytoplankton cell type, but should provide improved estimates of D, n, and n′ for many types. As expected, when applied to the calibration dataset, the results showed better agreement for all three parameters, D, n, and n′ (Fig. 5). Cell D was the most accurately predicted of the three properties (slope = 1.0, r^2 = 0.96). The correlations between FCM-Mie and independent estimates of n and n′ were still not significant, but the bias in the data was reduced (slope = 0.9 and 0.8 for n and n′, respectively) and mean values were more accurately predicted. Most likely, my fit for SSC between modeled and measured values has higher variance than the FLS fit,

because FLS is highly dependent on diameter, whereas SSC is a more complex function of diameter, refractive index reflecting cell structure, and cell shape. This is supported by the fact that D is accurately predicted from FCM measurements for the calibration dataset with only an FLS correction, but that, in order to determine n and n', an SSC correction is also needed. Since the correction approach was developed with the calibration dataset, these results do not represent independent verification that the approach is reasonable; for this I used results from other experiments.

Laboratory Application

I evaluated my modified FCM-Mie approach (i.e. with FLS and SSC correction) by applying it to independent data from the *Micromonas* and *Nannochloris* diel experiments (DuRand and Olson 1998; DuRand et al. 2002). For both species, cell D, n, and n' were better resolved by my FCM-Mie method with FLS and SSC corrections (Figs. 6 and 7). The mean error in estimates of D were 4% and 6% for the *Micromonas* and *Nannochloris* diel experiments, respectively. Significant diel changes in D for both experiments were resolved by the FCM-Mie method ($r^2 = 0.90$ and 0.81, respectively, for linear fits). As expected, diel changes were not observed in FCM-Mie n and n'; no significant diel patterns were observed in independent determinations of n and n' (DuRand and Olson 1998; DuRand et al. 2002). Mean errors in FCM-Mie n for the *Micromonas* and *Nannochloris* diel experiments were 35 and 8%, respectively, and mean errors for n' were 67% and 22%, respectively. FCM-Mie n and n' were more accurately determined for *Nannochloris* than for *Micromonas*,

because *Micromonas* is further from the regression line determined for the SSC correction.

Previously, the majority of FCM studies (with the exception of Ackleson et al. (1988), Ackleson and Spinrad (1988), and Ackleson and Robins (1990)) have used FCM FLS to determine cell D from an empirical fit with cell volume measured with an electronic particle counter using phytoplankton (Olson et al. 1989; DuRand 1995; Gin et al. 1999; DuRand et al. 2001; Shalapyonok et al. 2001). Using this approach, different empirical relationships are necessary to determine D for cells grown at low and high light levels (Fig. 8) (Shalapyonok et al. 2001). The high-light empirical fit presented here was based on cells grown in high light from the evaluation dataset, and the low-light empirical fit was based on cells grown in low light from the evaluation dataset. The high- and low-light empirical fits are significantly different in their estimate of cell D from FCM FLS and increasingly so as cell D increases. For example, for cells at the upper end of the diameter range of interest, an FCM FLS of 15 gives a predicted cell D of 9.9 µm from the low-light empirical fit and 7.4 µm from the high-light empirical fit. At the smaller end of the diameter range of interest, an FCM FLS of 1 corresponds to cell D of 2.1 µm from the low-light empirical fit and 1.9 µm from the high-light empirical fit.

I applied my FCM-Mie approach to data from the evaluation dataset to evaluate its performance with cultures grown under different light intensities and thus with different optical properties. Applying the FCM-Mie approach, I found that the

resulting values of D were well correlated with measured values for cells grown under both high- and low-light intensities (Fig. 9; slope = 0.97, r^2 = 0.86 and 0.98, respectively). In contrast, the low-light empirical fit (as discussed in the previous paragraph) overestimates D for cultures grown in high light (Fig. 9a; slope = 1.16), and a high-light empirical fit underestimates D for cultures grown in low light (Fig. 9b; slope = 0.73). This result shows that the modified FCM-Mie method accounts for absorption and scattering such that I am able to accurately predict changes in cell size under different light regimes. The application of the FCM-Mie approach to the determination of D for cells grown at different light levels becomes increasingly important as cell size increases, as can be seen by the increasing deviation between the low- and high-light empirical fits with increasing cell D (Figs. 8 and 9).

I determined the level of accuracy that can be expected for D, n, and n' from the FCM-Mie method. All statistics utilizing the *Micromonas* and *Nannochloris* diel experiments include two points from each experiment at the values of the smallest and largest D. Based on the evaluation dataset (44 measurements of cultures grown at both low and high light levels) there was a mean error of 13% for D. Bulk values of n and n' were available only for the calibration dataset and the two diel studies in the evaluation dataset, so although not ideal (i.e. not entirely based on independent data), a level of accuracy for n and n' was determined from these studies. Based on these experiments, mean errors of 28% and 36% were observed for n and n', respectively. The values of n' determined from the FCM-Mie method are significantly correlated

with intracellular chlorophyll concentration (p = 0.002) with a linear model explaining

60% of the variability, while values of n are not significantly correlated with

intracellular carbon concentration.

Field Application

I applied my methodology to natural samples collected on May 6th, 1997 in

New England continental shelf waters. Distributions of D, n, and n′ were computed

for *Synechococcus* and eukaryotic pico/nanophytoplankton from measurements of

FCM FLS, SSC, and CHL using the modified FCM-Mie method. For non-

phytoplankton particles, absorption was assumed to be zero, and distributions of D and

n were computed from FCM FLS and SSC using the FCM-Mie method without the

FLS and SSC corrections determined for phytoplankton. Analysis was limited to

particles of less than approximately 10 μm in size for both phytoplankton and non-

phytoplankton. In size distributions for the surface sample, populations of

Synechococcus and eukaryotes had peaked distributions with mean D of 1.36 μm and

3.02 μm, respectively. Non-phytoplankton increased in concentration with decreasing

size with a Junge slope of 4.1, within the range of values (2-5, with 3-4 typical)

previously reported for marine particle size distributions (Fig. 10; refs. in Mobley

(1994)). Real refractive index distributions for *Synechococcus* and eukaryotes were in

the range expected for phytoplankton (1.01-1.10), and the means (1.061 and 1.062,

respectively) were approximately the same for the two populations. Non-

phytoplankton had a mean n of 1.104, which was higher than the mean n for the

phytoplankton. Imaginary refractive index distributions for *Synechococcus* and eukaryotes were in the range expected for phytoplankton (generally from 0-0.02; Stramski et al. (2001)); the mean value for *Synechococcus* of 0.0022 was lower than that for eukaryotes of 0.0058, presumably because *Synechococcus* contain phycoerythrin, a pigment which does not absorb as well as the accessory pigments of eukaryotes at 488 nm (Olson et al. 1990). Distributions of D, n, and n′ had a broader range for eukaryotes than for *Synechococcus*, as expected, because the eukaryotes contain a broad range of species.

I also examined the depth dependence of particle properties in relation to the physical structure of the water column. Properties were estimated for each individual particle in a water sample, and then mean values were determined for each group of similar particles (i.e. *Synechococcus*, eukaryotes, and non-phytoplankton). The water column was thermally stratified with a surface mixed layer of about 16 meters in which bulk chlorophyll fluorescence was elevated. For particle properties that exhibited variation with depth, mean D was higher within the mixed layer than below, and mean n and n′ were lower (Fig. 11). Depth distributions of D and n were more variable for eukaryotes than for *Synechococcus*, while n′ changed approximately 2-fold with depth for each population. Based on mean property values within versus below the mixed layer, eukaryotes were 29% larger in surface waters (a difference of 0.87 μm), n was 14% lower (a difference of 0.01), and n′ was 49% lower (a difference of 0.0052). *Synechococcus* were 5% larger in surface waters (a difference of 0.066

43

μm), and n' was 51% lower (a difference of 0.002); n did not change significantly with depth. Mean D, n, and n' were higher for eukaryotes than for *Synechococcus* at all depths, except for n within the mixed layer, which was not significantly different between the two populations. The mean non-phytoplankton particle was smaller and more refractive than the mean phytoplankton cell at all depths. Non-phytoplankton mean D was 3% larger (a difference of 0.024 μm) within the mixed layer, and mean n was 13% lower (a difference of 0.016).

Values of real refractive index for non-phytoplankton should be indicative of the relative contributions of organic and inorganic particles. Mean n for non-phytoplankton (1.104-1.128) were higher than n for phytoplankton (1.0609-1.0751) at all depths. In comparison to phytoplankton, these results imply that non-phytoplankton had higher mineral content or, in the case of organic particles, lower water content. My findings are consistent with a recent study by Twardowski et al. (2001) who employed an inverse method to derive average real refractive index for natural particle assemblages from optical measurements and size distributions. In their study, values of n were generally lower in areas of high phytoplankton concentrations and higher in areas of high detrital content. In my example, values of n for non-phytoplankton were lower in the mixed layer than below, which is consistent with biological processes (e.g., cell death, production of fecal material) as a source of organic particles within the mixed layer and resuspension of bottom sediments as a source of inorganic particles below the mixed layer. There are two caveats in the

interpretation of non-phytoplankton n determined from the FCM-Mie method. First, I assumed these particles were non-absorbing; this is consistent with low values of n' previously reported, on the order of 3×10^{-5} at 488 nm (Stramski et al. 2001). Second, and more importantly, I did not account for the effects of non-sphericity and inhomogeneities. The deviation of non-phytoplankton from homogenous spheres is a topic for further study and will be complicated, because non-phytoplankton contain a broad range of different types of particles, including mineral particles, heterotrophic organisms, cell debris, and fecal matter.

Changes in average phytoplankton properties can be caused by changes at the cellular level and/or in the species composition of the population. The depth profile shown here is associated with a stratified water column with reduced nutrient levels in the surface mixed layer and the end of a phytoplankton bloom in surface waters (Sosik et al. 2001). Differences seen in eukaryotic cell D, with the largest cells in surface waters, are most likely caused by differences in species composition associated with the bloom within versus below the mixed layer. In contrast, variability in n' is more likely caused by changes at the cellular level which probably happen to all species due to the effects of a stratified water column with high light levels and low nutrients in surface waters compared to below the mixed layer. Values of n' for both eukaryotic phytoplankton and *Synechococcus* are lower in surface waters, which is consistent with previous findings that cells have less pigment per cell under conditions of high light and low nutrients (e.g. Mitchell and Kiefer (1988), Sosik et al. (1989), and Sosik

and Mitchell (1991)). The increase in n for eukaryotes with depth suggests that cells have higher intracellular carbon content below the mixed layer, which may be caused by changes in species composition and/or rearrangements in internal structures. In previous studies, the modification of internal cell structures caused changes in angular scattering, especially at side angles (Witkowski et al. 1994; Witkowski et al. 1998); these changes in scattering would presumably affect estimates of n and may be responsible for differences in eukaryotic n above and below the mixed layer.

SUMMARY

I developed a method to determine the D, n, and n′ of marine particles from FCM measurements of FLS, SSC, and CHL combined with Mie theory. Particles of known D, n, and n′ were measured in order to characterize FCM parameters before they were used in Mie calculations. An empirical laboratory calibration was needed for a variety of phytoplankton species to convert from FCM CHL to σ_a at 488 nm. For each particle, FCM measurements of FLS, SSC, and σ_a was compared to values in a Mie-based lookup table from which values of D, n, and n′ was determined. Based on the initial comparison of these values to independent values from electronic particle counter and bulk optical measurements, I found that cell D was underestimated and n and n′ were overestimated by the FCM-Mie method. For phytoplankton cells, an FLS and SSC correction was determined from comparison of FCM measurements and modeled values and was necessary in order to accurately determine cell properties from the FCM-Mie method. The FLS and SSC corrections were needed most likely

because cells deviate from the Mie theory assumptions of particle sphericity and homogeneity.

My modified FCM-Mie method (i.e. with FLS and SSC corrections) was able to determine phytoplankton cell properties for a variety of cultures. The FCM-Mie method provided estimates of cell D to within 13% of directly measured values, and the estimates were better than those obtained from empirical correlation of FLS with cell D. A significant improvement is that cells grown under different light intensities, whose FLS:D relationships differ, could be accurately analyzed with the FCM-Mie approach. FCM-Mie estimates of n and n' were obtained to within a mean of 28% and 36%, respectively, of independently determined values from bulk measurements. The higher degree of error in n and n' in comparison to D is probably caused by higher unexplained variance in the SSC correction than in the FLS correction. Values of FCM-Mie n' were significantly correlated with intracellular chlorophyll concentration, while FCM-Mie n were positively but not significantly correlated with intracellular carbon concentration. In order to improve the determination of refractive index from single particle measurements, further work is needed in the development of modeling angular scattering from phytoplankton cells of diverse types.

In future work, I will apply the FCM-Mie methodology to determining spatial and temporal changes in D, n, and n' for phytoplankton and non-algal particles, including bacteria, organic detritus, and inorganic detritus, measured during both the summer, 1996 and spring, 1997 CMO cruises. Estimates of individual particle

properties will be used to interpret variability in bulk inherent and apparent optical properties, which were measured concurrently with single particle properties. These studies will allow us to compare how intra-particle variability (changes in D, n, and n′) versus inter-particle variability (changes in the relative concentrations of particle types) accounts for variability in bulk optical properties. I expect that the application of the FCM-Mie method to natural assemblages will significantly improve our understanding of how changes in cell properties, such as D, n, and n′, cause variability in bulk optical properties in the ocean.

Table 1. Specifications for Cultures in the Calibration and Evaluation Datasets

Dataset	Phytoplankton Species	Light Level (μmol photons m^{-2} s^{-1})	Average D (μm)
Calibration	Synechococcus sp. (7D95m)	90	1.21
	unidentified eukaryote (isb)		1.27
	unidentified eukaryote (t6)		2.19
	Nannochloris sp.		2.59
	unidentified eukaryote (islow1)		2.61
	Isochrysis galbana		4.42
	Emiliania huxleyi (no coccoliths; Clone BT6)[1]		4.57
	Thalassiosira pseudonana		4.81
	Monochrysis lutheri		5.26
	Dunaliella tertiolecta		7.93
Evaluation	Synechococcus sp. (WH8109)	50-100	0.93
	Synechococcus sp. (WH7803)	50-100	1.01
	Synechococcus sp. (WH8012)	50-100	1.10
	Synechococcus sp. (WH8103)	50-100	1.13
	Synechococcus sp. (7d95m)	Natural[3], 70 [3]	1.16
	Micromonas pusilla	120 [2]	1.63
	unidentified eukaryote (t6)	Natural, 70 [3]	2.41
	Pycnococcus provasolii	50-100	2.63
	Nannochloris sp.	Natural[3], 70 [3], Natural[2], 50-100	2.68
	unidentified eukaryote (islow1)	Natural[3]	2.76
	Minutocellus polymorphous (13DT11)	Natural[3]	3.72
	Emiliania huxleyi (with coccoliths; Clone 12-1)	Natural[3], 50-100	3.98
	unidentified eukaryote (t11)	Natural[3]	4.10
	Isochrysis galbana	50-100	4.72
	Monochrysis lutheri	Natural[3], 50-100	5.10
	Isochrysis sp.	Natural[3], 70 [3]	5.13
	Emiliania huxleyi	Natural[3]	5.58
	Dunaliella tertiolecta	Natural[3], 70 [3], 50-100	7.81
	Amphidinium carteri	50-100	9.25
	Hymenomonas carterae	50-100	9.29
	Platymonas sp.	Natural[3]	9.66
	Olisthodiscus sp.	Natural[3]	9.82

The growth irradiance "natural" denotes cultures acclimated for growth in natural light during the summertime (June-August) in Woods Hole, Massachusetts.

When multiple irradiances are specified they refer to separate experiments.

[1]Culture excluded from analysis, because no independent solution was found for n or n'.

[2]Cultures for which diel measurements were made(DuRand and Olson 1998; DuRand et al. 2002).

[3]Data from Shalapyonok et al.(Shalapyonok et al. 2001).
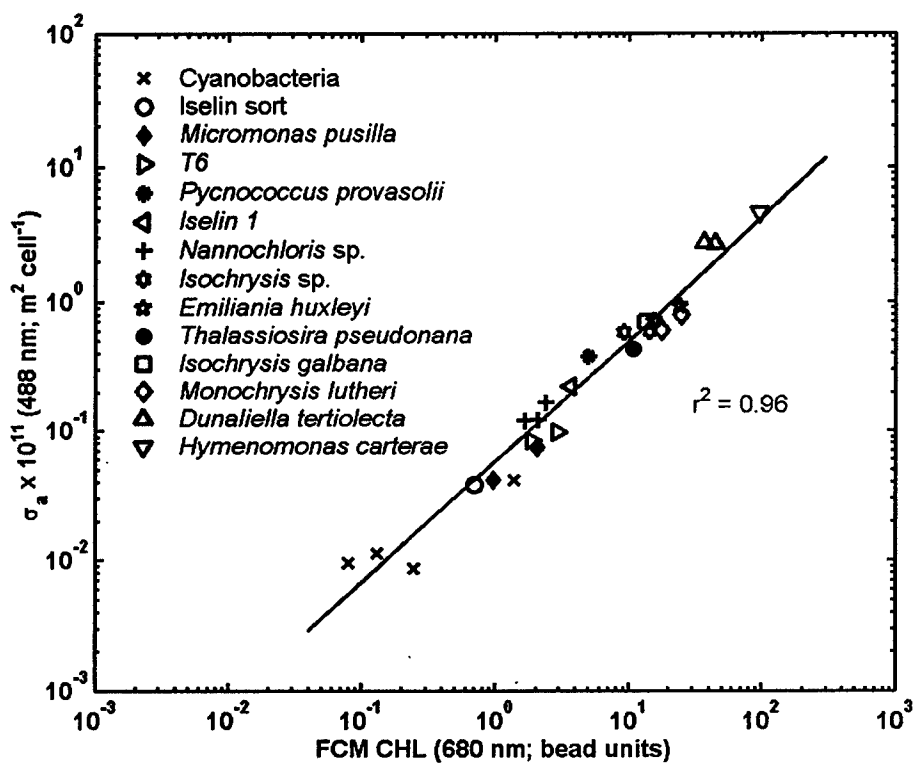
Fig. 1. Relationship between spectrophotometrically determined absorption cross-section, σ_a (488 nm), and flow cytometrically determined chlorophyll fluorescence, FCM CHL (680 nm), for a variety of phytoplankton cultures.
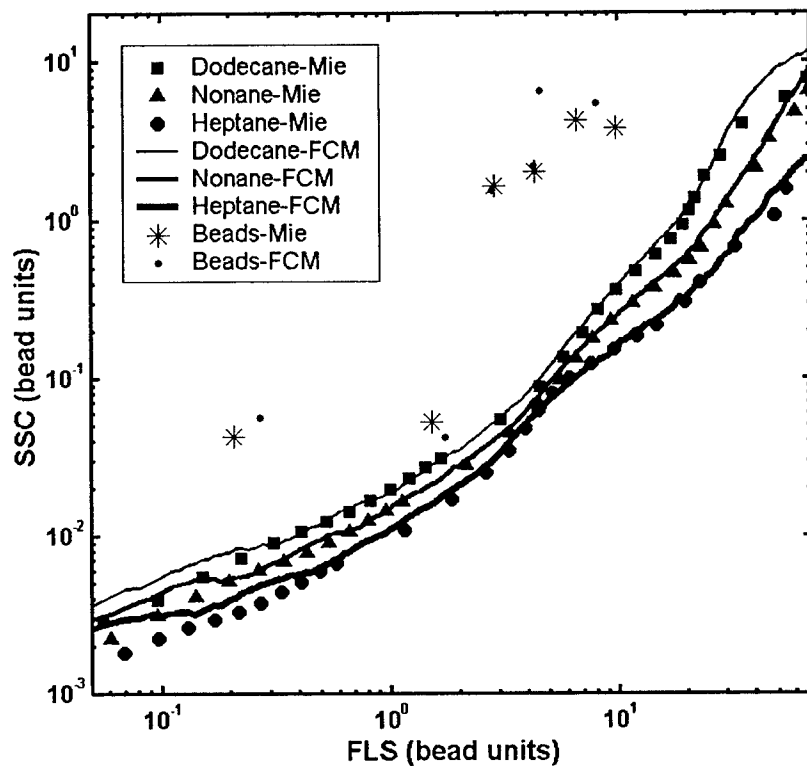
Fig. 2. Comparison of theory-based estimates (asterisks) and FCM measurements (lines and dots) of forward angle light scattering, FLS, and side angle light scattering, SSC, for beads and oil dispersions. The bead and oil measurements are an averaged dataset over all experiments. Several bead types were used in this comparison, including 0.66, 2.9, 3.79, 5.2, and 6.2 μm polystyrene beads and 1.58 μm silica beads. Oil dispersions of heptane, nonane, and dodecane are shown.
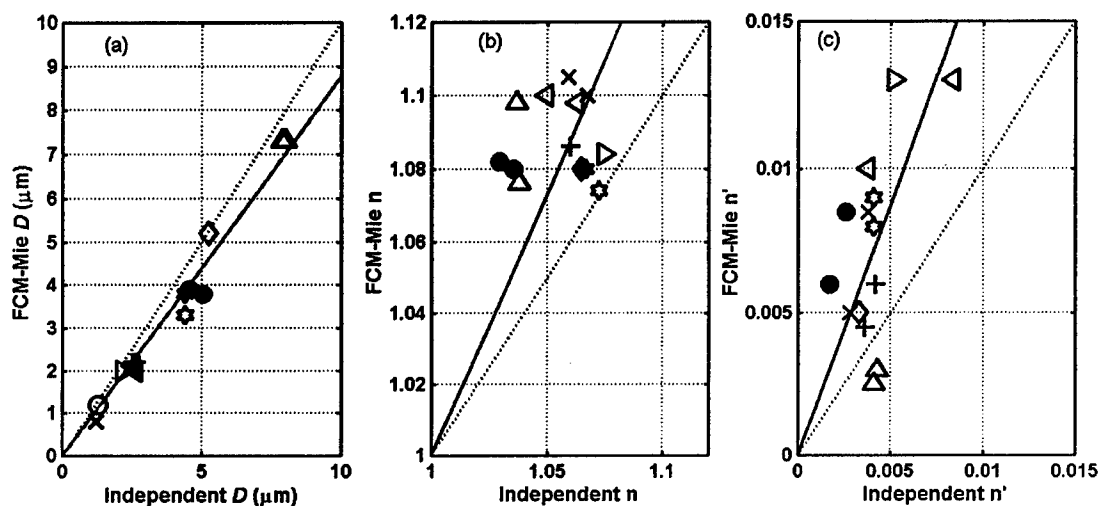
Fig. 3. Comparison of cell properties, (a) mean diameter, D, (b) real refractive index, n, and (c) imaginary refractive index, n′, estimated using the FCM-Mie approach with independent estimates based on direct measurements of cultures in the calibration dataset. See legend in Fig. 1. Independent D is from electronic particle counter measurements, and independent n and n′ are determined from bulk optical measurements. The dotted line on each plot is the 1:1 line and the solid line is a linear regression of the data forced through zero in the case of D and n′ and through one in the case of n.
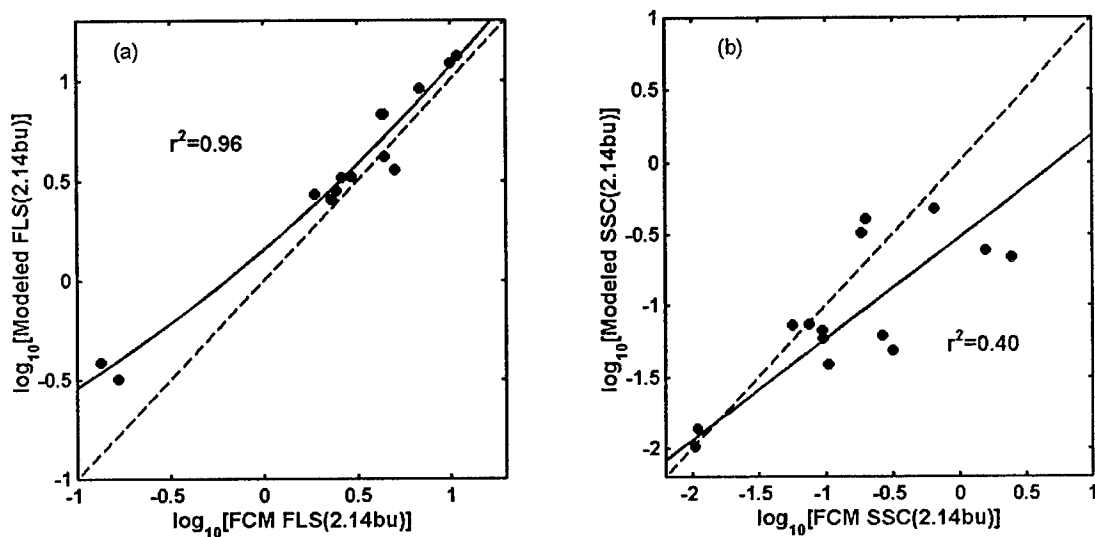
Fig. 4. Relationships between FCM-measured and Mie-modeled values of (a) forward angle light scattering, FLS, and (b) side angle light scattering, SSC, for the calibration dataset. Mie-modeled FLS and SSC values were determined from independent estimates of D, n, and n'. 1:1 lines are indicated by dashed lines and least squares regression results between logarithmic measured and modeled values are shown as solid lines.
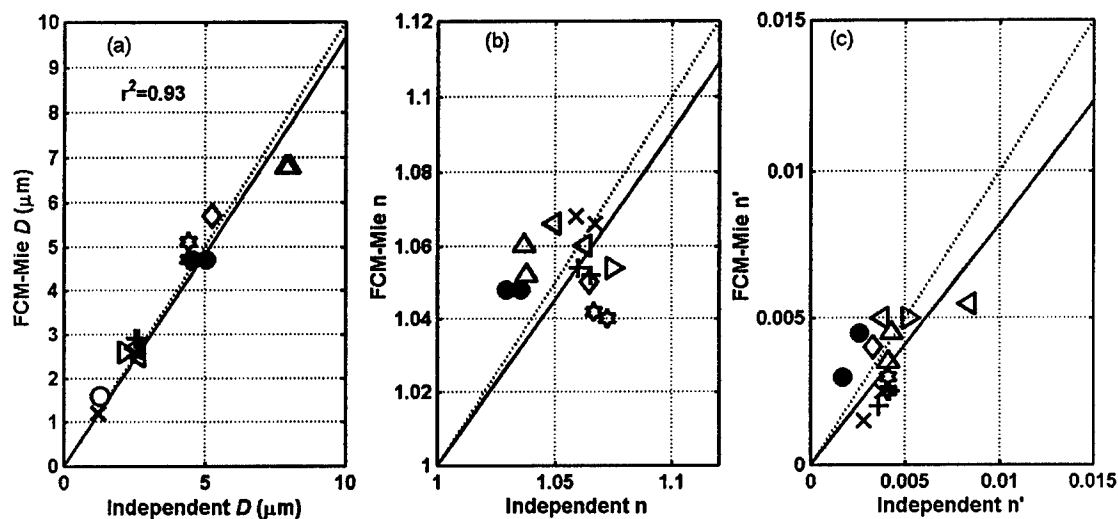
Fig. 5. Comparison of cell properties, (a) diameter, D, (b) real refractive index, n, and
(c) imaginary refractive index, n', calculated from the modified FCM-Mie method (i.e.
with FLS and SSC corrections) with cell properties measured independently for the
calibration dataset. See legend in Fig. 1. The correlation coefficients for the n and n'
relationships are not significant. The 1:1 line (dotted line) and least squares regression
results between independent and FCM-Mie values (solid line) are shown on each plot.
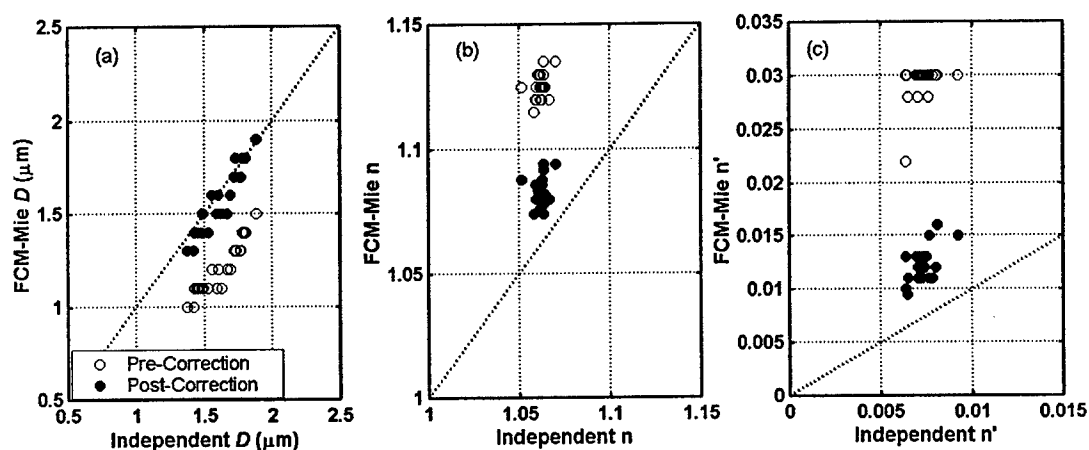
Fig. 6. Comparison of cell properties, (a) diameter, D, (b) real refractive index, n, and (c) imaginary refractive index, n′, estimated using the modified FCM-Mie method with independent estimates based on direct measurements of *Micromonas* sampled every two hours over a 24-hour period. FCM-Mie estimates of D, n, and n′ are shown before (open circles) and after (closed circles) FLS and SSC corrections are applied. The 1:1 line is shown on each plot (dotted line).
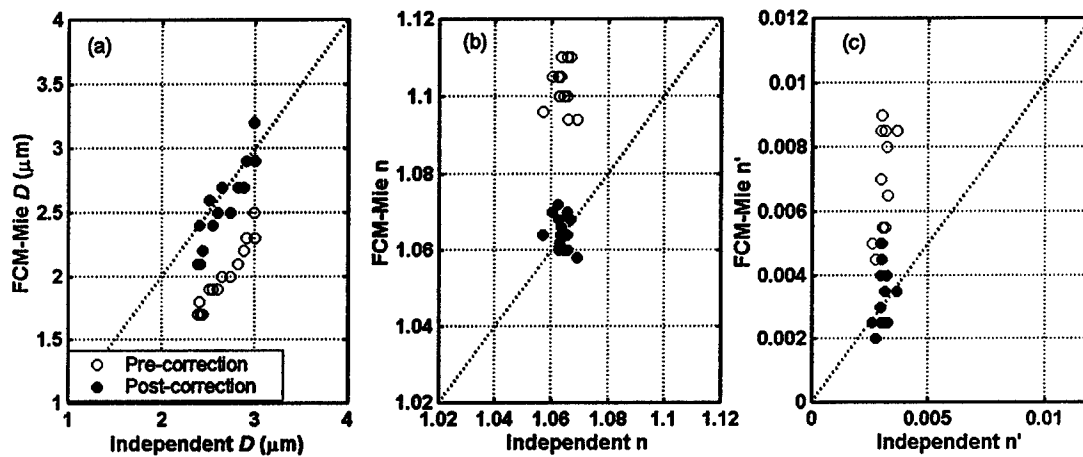
Fig. 7. Comparison of cell properties, (a) diameter, D, (b) real refractive index, n, and (c) imaginary refractive index, n', estimated using the modified FCM-Mie approach with independent estimates based on direct measurements of *Nannochloris* sampled every two hours over a 24-hour period. FCM-Mie estimates of D, n, and n' are shown before (open circles) and after (closed circles) FLS and SSC corrections are applied. The 1:1 line is shown on each plot (dotted line).
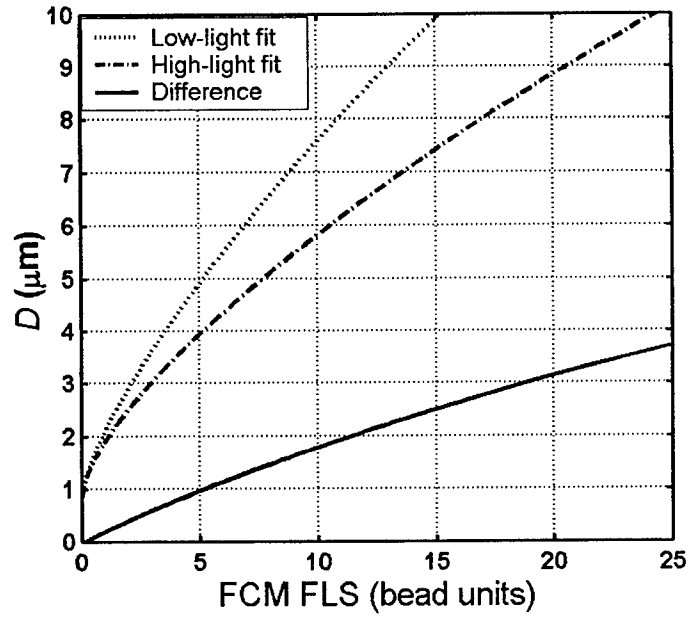
Fig. 8. Empirical relationships between FCM forward angle light scattering, FLS, and measured cell diameter, D, for cells grown under conditions of low and high light levels. A third line shows the difference in D between the two fits as a function of FCM FLS. Similar empirical relationships have been previously used for the determination of cell D from measurements of FCM FLS.
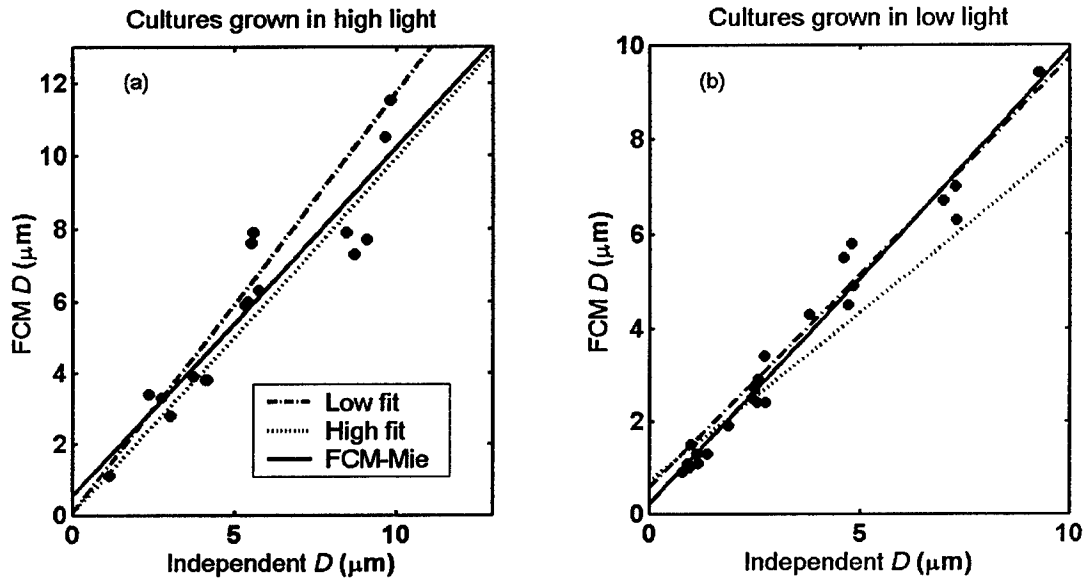
Fig. 9. Comparison of cell diameter (D) estimates from the modified FCM-Mie method and from empirical calibrations of FLS versus measured cell D for cultures grown at (a) high and (b) low light in the evaluation dataset. In each plot, lines for the "High-Light Calibration", "Low-Light Calibration", and "FCM-Mie" are linear regression results for cultures grown at high- and low-light levels, respectively; for clarity only the data points associated with the FCM-Mie approach are shown. Values of FCM-Mie D show a good correlation with independent D under both high and low-light levels, whereas the high and low-light calibrations work well only for the intensities at which they were determined.
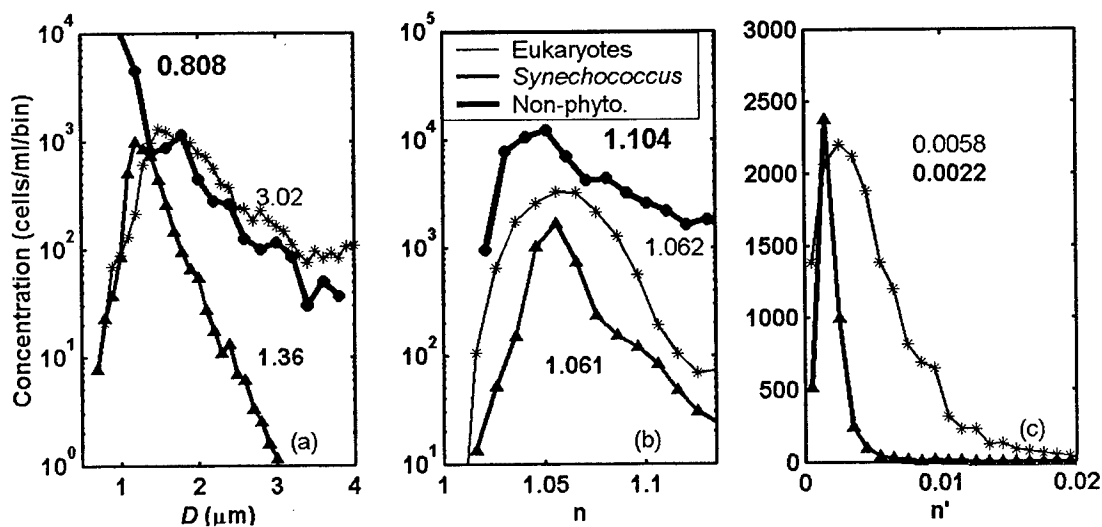
Fig. 10. Distributions of (a) diameter, D, (b) real refractive index, n, and (c) imaginary refractive index, n', for *Synechococcus*, eukaryotic phytoplankton, and non-phytoplankton estimated with the modified FCM-Mie method for a sample from 1 m depth collected on May 6, 1997 from New England shelf waters. Mean values are indicated next to each distribution. The n' distribution for non-phytoplankton is not plotted, because these particles have been assumed to be non-absorbing.
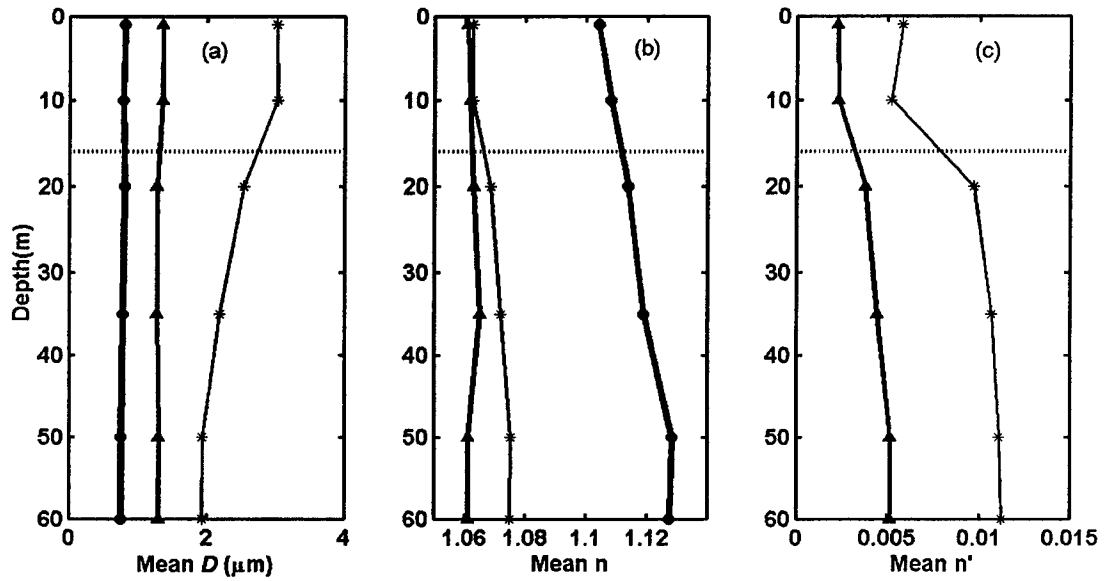
Fig. 11. A depth profile of mean (a) diameter, D, (b) real refractive index, n, and (c) imaginary refractive index, n', for *Synechococcus*, eukaryotic phytoplankton, and non-phytoplankton estimated with the modified FCM-Mie method for water samples collected on May 6, 1997. Mean values are calculated from property distributions based on analysis of each particle in a sample. The bottom of the mixed layer is represented by the dashed line at 16 meters depth on each plot.

REFERENCES

Ackelson, S.G., and R.W. Spinrad. 1988. Size and refractive index of individual marine particulates: a flow cytometric approach. Appl.Optics **27**: 1270-1277.

Ackleson, S.G., and D.B. Robins. 1990. Flow cytometric determinations of North Sea phytoplankton optical properties. Netherlands J. Sea Res. **25**: 11-18.

Ackleson, S.G., D.B. Robins, and J.A. Stephens. 1988. Distributions in phytoplankton refractive index and size within the North Sea. Paper read at Ocean Optics IX.

Bohren, C.F., and D.R. Hoffman. 1983. Absorption and scattering of light by small particles. J. Wiley.

Bricaud, A., A.L. Bedhomme, and A. Morel. 1988. Optical properties of diverse phytoplanktonic species: experimental results and theoretical interpretation. J.Plankton Res. **10**: 851-873.

Bricaud, A., and A. Morel. 1986. Light attenuation and scattering by phytoplankton cells: a theoretical modeling. Appl. Opt. **25**: 571-580.

Cavender-Bares, K.K. 1999. Size distributions, population dynamics, and single-cell properties of marine plankton in diverse nutrient environments. Ph.D. thesis, Massachusetts Institute of Technology.

Chan, R.K.Y., and K.M. Un. 2001. Real-time size distribution, concentration, and biomass measurement of marine phytoplankton with a novel dual-beam laser fluorescence Doppler cytometer. Appl. Opt. **40**: 2956-2965.

Dickey, T.D., and A.J. Williams III. 2001. Interdisciplinary ocean process studies on the New England shelf. J. Geophys. Res. **106**: 9427-9434.

DuRand, M.D. 1995. Phytoplankton growth and diel variations in beam attenuation through individual cell analysis. Ph.D. thesis, Massachusetts Institute of Technology, Woods Hole Oceanographic Institution.

DuRand, M.D., R.E. Green, H.M. Sosik, and R.J. Olson. 2002. Diel variations in optical properties of Micromonas pusilla (Prasinophyceae). J.Phycol. **submitted**.

DuRand, M.D., and R.J. Olson. 1998. Diel patterns in optical properties of the chlorophyte Nannochloris sp.: relating individual-cell to bulk measurements. Limnol. Oceanogr. **43**: 1107-1118.

DuRand, M.D., R.J. Olson, and S.W. Chisholm. 2001. Phytoplankton population dynamics at the Bermuda Atlantic time-series station in the Sargasso Sea. Deep-Sea Res. II **48**: 1983-2003.

Gin, K.Y.H., S.W. Chisholm, and R.J. Olson. 1999. Seasonal and depth variation in microbial size spectra at the Bermuda Atlantic time series station. Deep-Sea Res. I **46**: 1221-1245.

Guillard, R.R.L. 1975. Culture of phytoplankton for feeding marine invertebrates, p. 29-60. *In* W. L. Smith and M. H. Chanely, [eds.]. Culture of marine invertebrate animals. Plenum Press.

Jeffrey, S. W., and N. A. Welschmeyer. 1997. Spectrophotometric and fluorometric equations in common use in oceanography, p. 597-615. *In* S. W. Jeffrey, R. F.

C. Mantoura and S. W. Wright, [eds.]. Phytoplankton Pigments in Oceanography: Guidelines to Modern Methods. UNESCO Publishing.

Kirk, J.T.O. 1983. Light and photosynthesis in aquatic ecosystems. Cambridge University Press.

Lewis, M.R., and J.J. Cullen. 1991. From cells to the ocean: Satellite ocean color, p. 325-337. *In* S. Demers, [eds.]. Particle Analysis in Oceanography. Springer-Verlag.

Marie, D., F. Partensky, S. Jacquet, and D. Vaulot. 1997. Enumeration and cell cycle analysis of natural populations of marine picoplankton by flow cytometry using the nucleic acid stain SYBR Green I. Appl.Environ.Microbiol. **63**: 186-193.

Mitchell, B.G., and D.A. Kiefer. 1988. Chlorophyll *a* specific absorption and fluorescence excitation spectra for light-limited phytoplankton. Deep-Sea Res. **35**: 639-663.

Mobley, C.D. 1994. Light and water; radiative transfer in natural waters. Academic Press, Inc.

Morel, A., and L. Prieur. 1977. Analysis of variations in ocean color. Limnol. Oceanogr. **22**: 709-722.

Olson, R.J., S.W. Chisholm, E.R. Zettler, M.A. Altabet, and J.A. Dusenberry. 1990. Spatial and temporal distributions of prochlorophyte picoplankton in the North Atlantic Ocean. Deep-Sea Res. **37**: 1033-1051.

Olson, R.J., E.R. Zettler, and o.k. Anderson. 1989. Discrimination of eukaryotic phytoplankton cell types from light scatter and autofluorescence properties measured by flow cytometry. Cytometry **10**: 636-643.

Olson, R.J., E.R. Zettler, and M.D DuRand. 1993. Phytoplankton Analysis Using Flow Cytometry, p. 175-186. *In* P. F. Kemp, B. F. Sherr, E. B. Sherr and J. J. Cole, [eds.]. Aquatic Microbial Ecology. Lewis Publishers.

Pegau, W.S., G. Deric, and J.R.V. Zaneveld. 1997. Absorption and attenuation of visible and near-infrared light in water: dependence on temperature and salinity. Appl.Optics **36**.

Perry, M.J., and S.M. Porter. 1989. Determination of the cross-section absorption coefficient of individual phytoplankton cells by analytical flow cytometry. Limnol.Oceanogr. **34**: 1727-1738.

Reynolds, R.A., D. Stramski, and D.A. Kiefer. 1997. The effect of nitrogen limitation on the absorption and scattering properties of the marine diatom Thalassiosira pseudonana. Limnol.Oceanogr. **42**: 881-892.

Shalapyonok, A., R. J. Olson, and L. S. Shalapyonok. 2001. Arabian Sea phytoplankton during Southwest and Northeast Monsoons 1995: composition, size structure and biomass from individual cell properties measured by flow cytometry. Deep-Sea Res. II **48**: 1231-1262.

Sosik, H.M., S.W. Chisholm, and R.J. Olson. 1989. Chlorophyll fluorescence from single cells: Interpretation of flow cytometric signals. Limnol. Oceanogr. **34**: 1749-1761.

Sosik, H.M., R.E. Green, W.S. Pegau, and C.S. Roesler. 2001. Temporal and vertical variability in optical properties of New England shelf waters during late summer and spring. J. Geophys. Res. **106**: 9455-9472.

Sosik, H.M., and B.G. Mitchell. 1991. Absorption, fluorescence and quantum yield for growth in nitrogen limited *Dunaliella tertiolecta*. Limnol. Oceanogr. **36(5)**: 910-921.

Stramski, D. 1999. Refractive index of planktonic cells as a measure of cellular carbon and chlorophyll a content. Deep-Sea Research I **46**: 335-351.

Stramski, D., A. Bricaud, and A. Morel. 2001. Modeling the inherent optical properties of the ocean based on the detailed composition of the planktonic community. Appl. Opt. **40**: 2929-2945.

Stramski, D., and R.A. Reynolds. 1993. Diel variations in the optical properties of a marine diatom. Limnol.Oceanogr. **38**: 1347-1364.

Twardowski, M.S., E. Boss, J.B. Macdonald, W.S. Pegau, A.H. Barnard, and J.R.V. Zaneveld. 2001. A model for estimating bulk refractive index from the optical backscattering ratio and the implications for understanding particle composition in case I and case II waters. J. Geophys. Res. **106**: 14129-14142.

Van de Hulst, H.C. 1957. Light scattering by small particles. John Wiley and Sons.

Volten, H., J.F. de Haan, J.W. Hovenier, R. Schreurs, W. Vassen, A.G. Dekker, H.J. Hoogenboom, F. Charlton, and R. Wouts. 1998. Laboratory measurements of angular distributions of light scattered by phytoplankton and silt. Limnol. Oceanogr. **43**: 1180-1197.

Witkowski, K., T. Krol, and M. Lotocka. 1994. The light scattering matrix of Chlorella vulgaris cells and its variability due to cell modification. Oceanologia **36**: 19-31.

Witkowski, K., T. Krol, A. Zielinski, and E. Kuten. 1998. A light-scattering matrix for unicellular marine phytoplankton. Limnol. Oceanogr. **43**: 859-869.

Wright, S.W., S.W. Jeffrey, and R.F.C. Mantoura. 1997. Evaluation of methods and solvents for pigment extraction, p. 661. *In* S. W. Jeffrey, R. F. C. Mantoura and S. W. Wright, [eds.]. Phytoplankton pigments in oceanography. UNESCO Publishing.

CHAPTER 3:

THE CONTRIBUTION OF PHYTOPLANKTON AND NON-PHYTOPLANKTON

PARTICLES TO VARIABILITY IN INHERENT OPTICAL PROPERTIES

ABSTRACT

The contributions of particle groups to inherent optical properties (IOPs) in New England continental shelf waters was determined in order to better understand unexplained variability in bio-optical algorithms based on chlorophyll concentration. Bio-optical algorithms rely on the relationship between pigment concentration in the water and the inherent optical properties (IOPs) of scattering and absorption by phytoplankton. Unexplained variability exists in bio-optical algorithms in open ocean waters, and even more so in coastal waters, due to a lack of knowledge of seawater constituents besides phytoplankton. Contributions to inherent optical properties (IOPs) were computed for optically important particle groups, including eukaryotic pico/nanophytoplankton, *Synechococcus*, heterotrophic bacteria, detritus, and minerals. Determinations of particle sum absorption (a_p) and scattering (b_p) were validated with independent bulk optical measurements of a_p and b_p during summer and spring sampling on the New England continental shelf. In both the summer and spring, the major contributors to IOPs in surface waters were eukaryotic phytoplankton for a_p and b_p and detritus and minerals for particulate backscattering (b_{bp}). For each particle group, concentration, size distribution, n, and n' were determined and were used to explain differences observed in the contributions to IOPs. Eukaryotic phytoplankton were the most important contributors to a_p and b_p, even though they were the least abundant particles, because of their large diameters and high values of n' compared to other particles. Detritus and minerals were the most important determinants of b_{bp} because of their high abundance in the range of small (submicron) particles, which are highly efficient backscatterers, and, in the case of minerals, because of high values of n. Detritus was more important to b_{bp} in the summer and minerals were more important in the spring, because detritus was more abundant, especially in the submicron size range, in the summer compared to spring. Heterotrophic bacteria were the second most important contributor to b_{bp} in the spring after minerals, and *Synechococcus* were the second most important contributors to subsurface maxima in a_p and b_p in the summer after eukaryotic phytoplankton.

INTRODUCTION

Knowledge of particle properties is important for the interpretation of variability in the inherent optical properties (IOPs) of the upper ocean, but most particle properties are difficult to measure. The accurate parameterization of inherent optical properties in terms of particle composition is the basis of bio-optical algorithms for deriving chlorophyll concentration from satellite ocean color. Results of model simulations have shown how changes in particle composition can give significantly different IOPs, even at the same chlorophyll concentration (Mobley and Stramski 1997; Stramski et al. 2001). These simulations are based on assumptions of the types of particle groups present and the distributions of size and complex refractive index for each particle group modeled. Certain of these particle properties are difficult to measure, especially distributions of the complex refractive index. Inferences of bulk refractive indices have been made by a variety of optical methods, in conjunction with Mie theory (e.g. Zaneveld et al. 1974; Morel and Bricaud 1986; Stramski and Morel 1990; Twardowski et al. 2001), but detailed distributions of particle properties can not be determined from bulk optical approaches. One approach to determining distributions of particle properties for natural populations is through the rapid measurement of individual particles using flow cytometry. Flow cytometry has been used to enumerate and distinguish specific groups of particles, and advances have been made towards determining distributions of particle size and complex refractive index with application to determining particle contributions to IOPs (Ackelson and Spinrad

1988; Olson et al. 1989; Perry and Porter 1989; Olson et al. 1993; Marie et al. 1997; DuRand and Olson 1998).

Total inherent optical properties are determined by the additive contributions of the individual components which absorb and scatter light within a water body. Typically, bulk IOPs have been modeled considering the contributions of a small number of components, including dissolved organic matter, phytoplankton, organic detritus, and water (Mobley 1994). Recently, Stramski et al. (2001) extended this modeling by performing simulations of IOPs which included 18 planktonic components (from viruses to microplanktonic species 30 μm in diameter), organic detritus, mineral particles, and air bubbles. Their simulations were based on assumed sizes, complex refractive indices, and concentrations of the different particle types. In order to extend this type of analysis to natural assemblages, the authors' concluded that there needed to be an increased effort to characterize the types and concentrations of particles suspended in seawater, using advanced techniques, such as flow cytometry. My goal in this work was to apply flow cytometry to the modeling of IOPs by measuring and describing populations of natural particles which are optically important.

As individual particle studies can not practically consider *all* particle types, Mobley and Stramski (1997) have outlined two criteria which should be considered in defining functional particle categories. First, the studied particulate components should account for the total bulk optical properties in a water body as accurately as possible. Second, each of the particle categories should play a specific, well-defined

role in the marine ecosystem. In the open ocean, the dominant paradigm is that phytoplankton and their detrital products are important in determining absorption, bacteria are the main contributors to scattering, and particles less than 1 μm in size, most likely submicron detrital particles of unknown origin, determine backscattering (Kirk 1983; Lewis and Cullen 1991; Morel and Ahn 1991; Stramski and Kiefer 1991). In contrast, Stramski et al.'s (2001) modeling work showed that minerals and detritus were the most important contributors to scattering, and that minerals were by far the most important contributors to backscattering. The contribution of viruses to absorption, scattering, and backscattering was determined to be negligible. I have included all of the optically important particles in my IOP budgets, including phytoplankton, heterotrophic bacteria, detritus, and minerals.

The Coastal Mixing and Optics experiment (CMO) presented the opportunity for the determination of particle contributions to IOPs for natural assemblages. During this experiment, there was intensive sampling of optical and physical properties at a site on the New England shelf during late summer 1996 and spring 1997. Measurements were made of bulk IOPs and individual particle properties. During both seasons, particles were found to be the primary source of temporal and vertical variability in optical properties since light absorption by dissolved material, though significant in magnitude, was relatively constant (Sosik et al. 2001). Phytoplankton was determined to be responsible for much of the observed variability in particle absorption, a_p, on the basis of spectrophotometric measurements of phytoplankton absorption. As well, it was inferred that phytoplankton and covarying

particles were responsible for variability in particle scattering, b_p, given similar trends in a_p and b_p.

The objective of this work was to achieve scale closure between particle sum and measured bulk inherent optical properties, and to use particle properties to describe variability in IOPs. I used Mie theory to analyze flow cytometric (FCM) measurements of optically important particle types, including eukaryotic pico/nanophytoplankton, *Synechococcus*, heterotrophic bacteria, detritus, and minerals. Each particle group was enumerated and property distributions were determined for size, complex refractive index, and cross-sections for absorption, scattering, and backscattering. Particle sum IOPs were calculated as a sum over the optical cross-sections of all particles in a given volume and compared well with measured IOPs on both the summer and spring CMO cruises. Variability in IOPs was then described using changes in the particle properties of the different particle groups. In surface waters, the main contributors to particle absorption (a_p) and scattering (b_p) were eukaryotic phytoplankton, and to particle backscattering (b_{bp}) were minerals, detritus, and heterotrophic bacteria.

METHODS

Bulk Optical Properties

Vertical profiles for water sampling and measurements of optical properties were made as part of the CMO Experiment (Sosik et al. 2001). The CMO site is located on the southern New England shelf, south of Martha's Vineyard (40° 30′ N,

70° 30′ W), in a region known as the "Mud Patch" and has a water depth of ~70 m. Data were collected during two 3 week cruises in the late summer of 1996 aboard the R/V *Seward Johnson* (cruise SJ9610, 17 August - 7 September) and spring of 1997 aboard the R/V *Knorr* (cruise KN150, 24 April - 13 May). Profiles were carried out approximately three times per day during daylight hours at the main CMO site. Inherent optical properties were measured in situ with dual path absorption and attenuation meters (ac-9, WetLabs, Inc.), designed to measure absorption (a) and beam attenuation (c) coefficients in 9 spectral bands (412, 440, 488, 510, 532, 555, 650, 676, and 715 nm). During both CMO cruises, ac-9 meters were mounted on a profiling package, and unfiltered and filtered (<0.2 μm) seawater was pumped through two separate meters to measure particulate absorption (a_p), dissolved absorption (a_g), and particulate scattering ($b_p=c-a$). Additionally, optical measurements (e.g. spectrophotometry and flow cytometry) were made shipboard on water samples collected from six depths throughout the water column using a conductivity-temperature-depth profiler/rosette system equipped with sampling bottles. Absorption coefficients for particulate material collected on GF/F filters (pore size of 0.7 μm) were determined spectrophotometrically (using a Cary 3E dual beam UV/visible spectrophotometer). Subsequent to the initial optical density measurements, filters were extracted in methanol and reanalyzed to determine the residual particulate absorption (a_{dm}; detritus + minerals) (Kishino et al., 1985); the absorption coefficient

due to methanol-extractable phytoplankton pigments (a_{ph}) was estimated by difference between the initial and post-extraction measurements.

Flow Cytometry

An Epics V flow cytometer (FCM; Coulter Electronics Corp.) modified for high sensitivity and interfaced with a Cicero acquisition system (Cytomation, Inc.) was used to measure forward angle light scattering (FLS, ~3-19° at 488 nm), side angle light scattering (SSC, ~54-126° at 488 nm), chlorophyll fluorescence (CHL, 660-700 nm), and the concentration of particles. The dynamic range of FLS, SSC, and CHL measurements was increased by splitting the optical signals and independently detecting and amplifying them with separate photomultipliers and 3-decade log amplifiers. For each property, the relative sensitivities of the two measurements were adjusted to have one decade overlap, and thus the potential measurement range was expanded to five orders of magnitude. Particles were injected into a saline sheath flow and illuminated by light from an argon ion laser beam polarized parallel to the fluid stream. The samples were delivered with a peristaltic pump (Harvard Apparatus), and cell concentration was determined from pump flow rate and sample analysis time. Three types of reference particles were measured, including polystyrene microspheres of various sizes (from 0.57 μm to 6.2 μm YG beads from Polysciences, Inc.), a silica bead of 1.58 μm (Duke Scientific, Inc.), and oil suspensions (heptane, nonane, and dodecane; Sigma Chemical, Co.). For populations of beads, arithmetic means of FLS, SSC, and CHL were computed following transformation of distributions to linear

values. All FCM measurements were referenced to the 2.14 μm bead and here are reported in these bead units.

Flow cytometric measurements were made of four particle groups, including eukaryotic pico/nanophytoplankton ("eukaryotic phytoplankton"), *Synechococcus*, heterotrophic bacteria, and non-phytoplankton. Phytoplankton and non-phytoplankton of ~0.75 μm to 50 μm in diameter were analyzed in 569 and 515 samples in summer and spring, respectively, on a shipboard flow cytometer. Non-phytoplankton are here defined as particles measured on the flow cytometer which include detritus, minerals, and microheterotrophs such as ciliates and flagellates. Eukaryotic phytoplankton populations were discriminated from non-phytoplankton particles based on their FCM CHL signal, and *Synechococcus* cells were discriminated based on their orange fluorescence. Samples were generally run on the flow cytometer until 230,000 events were collected, on average for 6.5 minutes at 0.5 ml/min on the summer cruise and for 11.5 minutes at 0.5ml/min on the spring cruise. Selected 1-ml samples (from noon hydrocasts) were preserved in glutaraldehyde and frozen in liquid nitrogen; following the cruises, these samples were analyzed for heterotrophic bacteria on a flow cytometer in the laboratory (~146 samples in summer and 185 in spring). Heterotrophic bacteria were enumerated by staining samples with a nucleic acid stain (SYBR Green I, Molecular Probes, Inc.), following the protocol of Marie et al. (1997). The samples were incubated for 15 minutes in the dark, the discriminator was set on green fluorescence, and the samples were analyzed on average for 3.3 minutes at a rate of 0.01 ml min^{-1}. All FCM data was saved as 2-D histograms and listmodes which

were analyzed using a version of "CYTOWIN" software (originally written by D. Vaulot; http://www.sb-roscoff.fr/Phyto/cyto.html) modified to create files containing FLS, SSC, and CHL for each particle.

Flow cytometric counts for each particle group in a sample were large (on the order of 10^4-10^5), and FCM measurements were binned to minimize computation time. Following the creation of files with CYTOWIN, all data analysis was performed using the MATLAB software package (Mathworks, Inc.). Initially, FCM measurements were linearized and merged from the two logarithmic amplifiers for each of FLS, SSC, and CHL. For each particle group, a grid was created of logarithmically spaced increments of FLS, SSC, and CHL based on the minimum and maximum values observed across all samples for a cruise, and the number of particles in each bin was calculated. For eukaryotic phytoplankton and *Synechococcus*, measurements of FCM FLS, SSC, and CHL were binned, and for non-phytoplankton and heterotrophic bacteria, FCM FLS and SSC only were binned, because CHL was not measured for these particles.

FCM-Mie Method

A combination of flow cytometric measurements and Mie theory were used to determine particle properties (D, n, and n') and optical cross-sections at 488 nm (σ_a, σ_b, and σ_{bb}) (referred to as the "FCM-Mie method"). I applied the FCM-Mie method (described in Chapter 2) to the analysis of eukaryotic phytoplankton, *Synechococcus*, heterotrophic bacteria, and non-phytoplankton in each sample. FCM-Mie analysis

was limited to particles less than 10 μm in diameter, because solutions are often not unique for larger particles. Particle properties were determined from the FCM-Mie method by comparison of FCM FLS and SSC and particle absorption to values in a Mie-based lookup table.

In order to apply Mie theory to FCM measurements, an optimization was performed between theory and measurements using calibration particles of known refractive index and /or size (for details see Chapter 2). Particles used in the optimization included polydisperse oil suspensions of heptane, nonane, and dodecane, polystyrene beads, and a silica bead. A single optimization was used for phytoplankton and non-phytoplankton analyzed on both the summer and spring CMO cruises. Using this optimization, a 3-dimensional lookup table of Mie theory-based solutions for particle FLS, SSC, and σ_a was created over the expected ranges of particle $\overline{D}$ (0-10 μm), n (1-1.30), and n' (0-0.030) for the marine particles of interest. A separate optimization was determined for heterotrophic bacteria, because FCM settings were changed in order to enumerate smaller particles (see Appendix 2). Using this optimization, a 3-dimensional lookup table of Mie theory-based solutions for particle FLS, SSC, and σ_a was created over the expected ranges of bacteria D (0.06-1 μm), n (1-1.20), and n' (set to an assumed value, see below).

The FCM-Mie method was applied to flow cytometric measurements of FLS, SSC, and CHL for phytoplankton cells to determine particle properties (D, n, and n') and optical cross-sections (σ_a, σ_b, and σ_{bb}). For phytoplankton, FCM FLS, SSC, and

an initial value of absorption cross-section (σ_a) were input to the FCM-Mie method. An initial value of σ_a for each cell was determined from FCM CHL based on an empirical calibration with spectrophotometric σ_a previously determined in the laboratory (see Chapter 2). Corrections were applied to values of FLS and SSC for phytoplankton before they were compared to values in the Mie-based lookup table; FLS and SSC corrections were previously determined using laboratory cultures as described in Chapter 2. All eukaryotic phytoplankton in a sample were analyzed using the FCM-Mie method. Analysis of *Synechococcus* was limited to 20,000 cells per sample, because the cumulative sums for FLS, SSC, and CHL were found to not vary significantly by including more cells. Using the FCM-Mie method, I analyzed each particle in a sample and created distributions of D, n, n', σ_a, σ_b, and σ_{bb} for eukaryotic phytoplankton and *Synechococcus*. Mean values of each property were calculated by considering all particles in a sample.

The FCM-Mie method was applied to flow cytometric measurements of FLS and SSC for non-phytoplankton and heterotrophic bacteria to determine particle properties (D and n) and optical cross-sections (σ_a, σ_b, and σ_{bb}). For non-phytoplankton and heterotrophic bacteria, FCM FLS and SSC were input to the FCM-Mie method, assuming a constant value of n'. Absorption by non-phytoplankton and heterotrophic bacteria could not be determined directly from FCM measurements. For heterotrophic bacteria, n' was assumed to be 5×10^{-4} at 488nm based on previously published values (Morel and Ahn 1990; Stramski and Mobley 1997). For non-

phytoplankton, n′ was determined by iteratively changing its value until total absorption by non-phytoplankton (detritus + minerals), a_{dm}, was approximately equal to spectrophotometric a_{dm}. All non-phytoplankton in a sample were analyzed using the FCM-Mie method. As for *Synechococcus*, analysis of heterotrophic bacteria was limited to 20,000 particles in a sample, because the cumulative sums for both FLS and SSC were found to not vary significantly by including more particles. Using the FCM-Mie method, I analyzed each non-phytoplankton and heterotrophic bacteria particle in a sample and calculated distributions and mean values of D, n, σ_a, σ_b, and σ_{bb}.

Calculation of Particle Contributions to Inherent Optical Properties

Particle contributions to inherent optical properties were calculated as a sum of contributions from particles analyzed using the FCM-Mie method and contributions from particles outside the diameter range of the FCM-Mie method, which were analyzed using different methodology. Particle absorption, a_p, scattering, b_p, and backscattering, bb_p, were determined for each particle group. Using the FCM-Mie method, the optical cross-sections, σ_a, σ_b, and σ_{bb}, were determined for each particle (as previously described), and total a_p, b_p, and b_{bp} at 488 nm were calculated by summing over all particles in a known volume. Additionally, for eukaryotic phytoplankton and non-phytoplankton, contributions to IOPs were estimated for particles outside the range of FCM measurement (i.e. < 0.75 μm in diameter) and the

FCM-Mie method (i.e. particles > 10 μm in diameter and detritus < 1.2 μm in diameter).

Using the FCM-Mie values of real refractive index, n, non-phytoplankton were separated into detrital and mineral components. Based on previous measurements (Aas 1996), I defined detritus (organic particles) as non-phytoplankton with $n \leq 1.10$ and minerals (inorganic particles) as non-phytoplankton with $n > 1.10$. The lower diameter limit for FCM measurement (0.75 μm) was used for minerals. However, a higher lower diameter limit of 1.2 μm was used for detritus, because detrital particles smaller than this size were in a region of FCM measurements that were not well fit by the Mie theory calibration.

The contribution of small detritus (0.1-1.20 μm) and minerals (0.1-0.75 μm) was determined using Mie theory with inputs of extrapolated size distributions and mean values of n and n' from particles measured with the FCM-Mie method. Junge (differential) size distributions were created separately for detritus and minerals in the diameter range of the FCM-Mie method. A segmented distribution was found to best describe particle size spectra, in concurrence with previous findings (Harris 1977; McCave 1983; Risovic 1993). Two different slopes were used to describe power function fits to each distribution, one slope calculated from the lower diameter limit for minerals (0.75 μm) and detritus (1.20 μm) to 3.5 μm and the other slope from 3.5-10 μm. These slopes will be referred to as the <3.5 and >3.5 slopes. The split at 3.5 μm was determined by finding the minimum of the root mean square difference

between the log-log size distributions and two linear fits to the distributions using a split at each diameter in the distribution. Contributions to IOPs of small detritus and minerals were calculated using Mie theory with inputs of the size distribution extrapolated using the < 3.5 μm slopes, a mean value of n based on particles measured with the FCM-Mie method, and the same n' as determined for all non-phytoplankton based on comparison with spectrophotometric a_{dm}. It is possible that heterotrophic bacteria were included in the detrital group of particles by using an extrapolation for particle concentration between 0.1 and 1.20 μm which was based on the size distribution of larger particles.

The contributions of larger particles (between 10μm and ~50μm) to IOPs was calculated using Mie theory with inputs of empirically derived D and mean values of n and n' from particles measured with the FCM-Mie method. For both eukaryotic phytoplankton and non-phytoplankton, D was determined from FCM FLS using an empirical fit with Coulter Counter diameter determined in the laboratory (Chisholm 1992). For eukaryotic phytoplankton, n' was calculated from D and σ_a obtained from an empirical fit between FCM CHL and spectrophotometric σ_a determined in the laboratory (described in Chapter 2). For detritus and minerals, n' was the same as the value determined for all non-phytoplankton based on comparison with spectrophotometric a_{dm}. For eukaryotic phytoplankton and non-phytoplankton, n was assumed to be the same as the mean value determined for each group from the FCM-Mie method. The ratio of non-phytoplankton assumed to be detritus and minerals for

diameters >10 μm was assumed to be the same as determined for FCM-Mie non-phytoplankton. Diameter, n, and n' were used as inputs to Mie theory to determine the contributions to a, b, and b_b of particles >10 μm in diameter. The contributions to IOPs of eukaryotic phytoplankton of 10-50 μm, non-phytoplankton of 10-50 μm, minerals of 0.1-0.75 μm, and detritus of 0.1-1.20 μm were added to the contributions determined for particles from the FCM-Mie method.

RESULTS AND DISCUSSION

Comparison of Particle Sum and Bulk Approaches

I compared phytoplankton absorption, a_{ph}, estimated from the particle sum method to spectrophotometric values of a_{ph}. Particle sum a_{ph} was calculated as a sum of absorption by eukaryotic phytoplankton and *Synechococcus*. In comparison to spectrophotometric a_{ph}, particle sum a_{ph} were on average 87% of measured values in both the summer and the spring (Fig. 1A-B), and a high percentage of the variance was explained in both cases (r^2=0.83 and 0.90, respectively). Particle sum a_{ph} may be a slight underestimate because of absorption by larger cells (>50 μm) that were not considered. Phytoplankton cells within the range of FCM-Mie analysis (0.75-10 μm in diameter) accounted for the majority of particle sum a_{ph} in both the summer (95%) and spring (80%).

I evaluated the particle sum determination of absorption by non-phytoplankton by comparing values with independent measurements of non-phytoplankton absorption. As described above, non-phytoplankton absorption, a_{dm}, was determined

by assuming a constant n′ for all non-phytoplankton particles which gave the best fit between particle sum and spectrophotometric a_{dm}. For the summer cruise, I limited the comparison to the top 30 m, because a significantly higher n′ was needed to fit specrophotometric a_{dm} below the mixed layer. This was done because I was most interested in the properties of particles in the upper ocean, and as well, it was determined from Mie calculations that errors in the choice of n′ for non-phytoplankton below 30 m should have little effect on their contribution to scattering. For the spring cruise, all depths were used in the comparison. Assuming a value for n′ of 0.001 gave the best fit between particle sum and spectrophotometric a_{dm} on both cruises with slopes close to 1, but regressions were not significant (Figs. 2A-B). Non-phytoplankton within the range of FCM-Mie analysis accounted for 80% and 42% of particle sum a_{dm} in the summer and spring, respectively. Unexplained variance in the fit between particle sum and spectrophotometric a_{dm} is likely caused by variability in the absorption properties of non-phytoplankton due to their complex composition (e.g. as heterotrophs, dead cells, fecal pellets, or minerals). My value for non-phytoplankton n′ is significantly higher than a previously proposed value of 3×10^{-5} at 488 nm (Stramski et al. 2001), determined from analysis of the microphotometric data of Iturriaga and Siegel (1989) for particles between ~9 and 27 μm in diameter. The difference between these two estimates may reflect a difference in the composition of non-phytoplankton particles between my study site and the Sargasso Sea.

Total scattering by all particles, b_p, was compared to bulk (ac-9) measurements of b_p. The particle groups of eukaryotic phytoplankton, *Synechococcus*, heterotrophic bacteria, detritus, and minerals were included in the particle sum. For the summer cruise, the comparison was limited to the top 30m, because particle sum b_p was significantly lower than bulk b_p below the mixed layer, presumably because I did not account for non-phytoplankton >50 μm in diameter. For the spring cruise, all depths were used in the comparison. All comparisons were made for in situ bulk measurements collected not more than 5 hours apart from the time of water sampling for FCM measurements, but on average collected ~1.7 hours apart. The linear regressions between particle sum and bulk b_p had slopes of 1.13 ($r^2=0.45$) and 1.25 ($r^2=0.51$) in the summer and spring, respectively (Fig. 3A-B). Given that particles greater than 50 μm in diameter were not considered in the particle sum estimates, I expected the FCM-Mie b_p to account for a slightly lower percentage of the ac-9-measured bulk b_p. Reasons for the overestimate of b_p with the particle sum methods include potential errors in ac-9 measurements and the need for a scattering correction for heterotrophic bacteria and non-phytoplankton such as was applied to phytoplankton to account for deviation of particles from homogenous spheres. In spite of the differences between particle sum and measured b_p, the generally good comparison between the two methods gave me confidence in applying the particle sum approach to interpretation of variability in IOPs for the CMO cruises.

Particle Properties and Seasonal Variability

The water columns of the summer and spring cruises exhibited different physical and bulk optical properties, and these differences were reflected in particle properties determined from the FCM-Mie method. During the late summer cruise, the water column was well stratified during the first two weeks of the sampling period, after which conditions were drastically disrupted by the passage of Hurricane Edouard through the study site, resulting in a well mixed water column and a decrease in phytoplankton abundance. Before the passage of the hurricane, the summer sampling period was characterized by stratified conditions, including depleted nutrient levels in the surface mixed layer, a subsurface chlorophyll maximum between 20 and 30 m, and mid-water column maxima in IOPs (Sosik et al. 2001). During the spring cruise, the water column was more weakly stratified, however, stratification did increase with time over the three week sampling period leading to a phytoplankton increase in surface waters, an associated decrease in nutrient levels, and increased IOPs. In the spring, the highest values of chlorophyll *a* and IOPs consistently occured in the top 25 m of the water column. Particle properties were significantly different in the top of the water column (0-40 m) versus below in both the summer and spring. Between seasons, differences included decreased abundance of *Synechococcus* in the spring, more variability in n′ for phytoplankton cells with depth in the summer, and a higher concentration of detritus in the summer.

Important differences were observed in eukaryotic phytoplankton properties both seasonally and vertically. Mean distributions of D, n, and n′ were unimodal, and

cells occurred most frequently in the ranges for D of 1 μm to 3 μm, for n of 1.02 to 1.10, and n′ of 0 to 0.015 (Figs. 4A-C). Mean property values were calculated by first averaging replicates from the same sample, followed by averaging all samples from the same day and the same depth bin (0-20 m, 20-40 m, and 40-65 m). Based on a comparison of mean property values, eukaryotic phytoplankton in summer surface waters (0-20 m), compared to the spring, were significantly less abundant (1.84×10^4 ml^{-1} vs. 2.46×10^4 ml^{-1}; $p < 0.05$), smaller (2.05 μm vs. 2.31 μm; $p < 0.01$), and had higher values of n (1.066 vs. 1.059; $p < 0.01$), however, values of n′ were not significantly different (0.0051 and 0.0057) (Fig. 4A-C; Table 1). In the summer, cells increased in size with depth, in contrast to the spring when cells decreased in size with depth. This difference may have been caused by vertical differences in nutrient availability. In the summer, high nutrient levels below the mixed layer may have allowed larger cells to grow versus in the spring during which similar nutrient levels existed throughout the water column and light level may have determined cell size. In agreement with my finding in the spring, previous studies using phytoplankton cultures have suggested that cells are generally larger at high light levels than at low light levels for similar nutrient levels (Falkowski et al. 1985; Sakshaug et al. 1987; Sosik et al. 1989). Also, species differences within and below the mixed layer could have contributed to differences in diameter. Values of both n and n′ increased with depth in both seasons, but the variation in n′ with depth was greater in summer than in spring (~3- vs. 2-fold). Lower values of n′ are expected in surface waters where cells

have less photosynthetic pigment per cell under conditions of high light and low nutrients (e.g. Mitchell and Kiefer 1988; Sosik et al. 1989; Sosik and Mitchell 1991). This would then suggest that lower values of n′ should have been observed in summer surface waters than in the spring which was not the case, presumably because of absorption by accessory pigments in summer surface waters. The increase in n for eukaryotes with depth suggests that cells have higher intracellular carbon content below the mixed layer, which may be caused by changes in species composition, acclimation of the same species to higher carbon per cell, and/or rearrangements in internal structures.

Seasonal differences were observed in the properties of *Synechococcus* which, in contrast to eukaryotes, were less abundant in the spring. Mean distributions of D, n, and n′ for *Synechococcus* were peaked, and cells occurred most frequently in the ranges for D of 0.6 μm to 1.6 μm, for n of 1.03 to 1.10, and n′ of 0 to 8×10^{-3} (Figs. 4D-F). Distributions of *D*, n, and n′ had a more narrow range for *Synechococcus* than for eukaryotes, as expected, because the eukaryotes contain a broad range of taxa. Based on a comparison of mean property values, *Synechococcus* in the top 20 m of the water column in the summer, compared to the spring, were significantly more abundant (5.9×10^4 ml^{-1} vs. 0.78×10^4 ml^{-1}; p<0.001) and smaller (1.09 μm vs. 1.38 μm; p<0.001), and had higher values of n (1.067 vs. 1.054; p<0.001), however, n′ was not significantly different (0.0022 vs 0.0024) (Fig. 4D-F; Table 2). Distributions of n and n′ were broader in range for *Synechococcus* in the summer (when cells were more

abundant) than in the spring. Lower *Synechococcus* concentrations measured in the spring compared to summer agree with previous measurements of Waterbury et al. (1986) who documented a relationship between water temperature and *Synechococcus* abundance. As with eukaryotic phytoplankton, *Synechococcus* increased in size with depth in summer, and decreased in size with depth in spring. Values of n changed little with depth, however, n' did change with depth, increasing by 4-fold and 2-fold for the summer and spring, respectively. Real refractive index distributions for *Synechococcus* and eukaryotic phytoplankton were in the range expected for phytoplankton (1.01-1.10), and mean n was approximately the same for the two groups in summer and slightly lower for *Synechococcus* in spring. Imaginary refractive index distributions for *Synechococcus* and eukaryotes were in the range expected for phytoplankton (generally from 0.002-0.02; Stramski et al. 2001); the mean values of n' for *Synechococcus* were lower than for eukaryotes, presumably because the major accessory pigment in *Synechococcus* is phycoerythrin (assuming low phycourobilin concentration) which does not absorb as well as the accessory pigments of eukaryotes at 488 nm (Olson et al. 1990).

Variability was observed in the properties of heterotrophic bacteria, including seasonal differences in the shape of size distributions and decreasing abundance with depth in both seasons. Mean distributions of D for heterotrophic bacteria were peaked in the summer and bimodal in the spring, and values occurred most frequently in the range of 0.2-0.7 μm (Fig. 4G). The bimodal distribution in the spring was most likely

caused by the presence of different species of heterotrophic bacteria (Zubkov et al. 2001). Mean distributions of n were peaked in both seasons, and values were most frequently in the range of 1.03-1.15, a broader range than observed for phytoplankton (Fig. 4C, F, and I). Based on a comparison of mean property values, heterotrophic bacteria in the summer water column, compared to the spring, were significantly less abundant ($1.1x10^6$ ml^{-1} vs. $1.5x10^6$ ml^{-1}; $p<0.005$) and had lower values of n (1.079 vs. 1.081; $p<0.05$), however, D was not significantly different (both 0.46 μm) (Figs. 4G-I; Table 3). Concentrations were highest in surface waters where the creation of dissolved organic materials due to phytoplankton growth and grazing would have been the highest. Previous studies have documented decreasing bacterial concentrations with depth, and concentrations similar to ours on the order of 10^6 for the upper ocean (Cho and Azam 1990; Koike et al. 1990; Sieracki and Viles 1992; Noble and Fuhrman 1998; Kuipers et al. 2000). Values of D and n changed little with depth, except following increased stratification in the spring when n was higher in surface waters. My values of mean D of ~0.45 μm are within range of findings of Stramski and Kiefer (1990) who reported cells occuring most frequently between 0.3 and 0.6 μm in diameter with an average cell diameter of 0.55 μm. My values of mean n of ~1.079 are slightly higher than their values which were between 1.042 and 1.068.

Non-phytoplankton particles were generally more abundant in summer surface waters, compared to the spring because of higher concentrations of detritus in the summer. Non-phytoplankton concentration increased with decreasing size, and Junge

slopes of size distributions were within the range of values (2-5, with 3-4 typical) previously reported for marine particle size distributions (Fig. 4J; refs. in Mobley (1994)). In both seasons, Junge slopes for <3.5 μm non-phytoplankton, detritus, and minerals were in the range of 3.5-4.9 and were higher than Junge slopes for >3.5 μm non-phytoplankton, detritus, and minerals which were in the range of 1.6-3.2 (Tables 4-6). The highest Junge slopes observed were for small (<3.5 μm) detrital particles in summer surface waters. Based on a comparison of mean values, non-phytoplankton were significantly more abundant in summer surface waters (0-20 m), compared to the spring (1.7×10^8 ml^{-1} vs. 1.7×10^7 ml^{-1}; p<0.001), because detritus were significantly more abundant (1.6×10^8 vs. 0.87×10^7; p<0.001). In contrast, minerals were not significantly different in concentration in surface waters between summer and spring (1.1×10^7 ml^{-1} vs. 0.87×10^7 ml^{-1}). Submicron detrital particles were primarily responsible for higher abundances of non-phytoplankton in the summer. One hypothesis for the higher concentrations of small detritus in the late summer is that the preceding several months of increased productivity lead to the accumulation of a type of organic particulate which is not readily useable by grazers. The idea of a biological source for small detrital particles has been previously suggested (Koike et al. 1990; Sieracki and Viles 1992; Yamasaki et al. 1998) and may be a result of flagellate grazing of bacteria and/or viral lysis of bacteria (Koike et al. 1990; Nagata and Kirchman 1996; Shibata et al. 1997). The percent of non-phytoplankton that was detritus in the FCM-Mie diameter range (1.2-10 μm) generally decreased with depth

on both cruises, and the difference between the mixed layer and below the mixed layer was greater in the summer (Fig. 5A-B). Percentages averaged 77% above 20 m and 58% below 20 m in summer, and 46% and 39%, respectively, in spring (Table 4). Similar to findings of a depth dependence in summer, Meade et al. (1975) reported that in the Middle Atlantic Bight in September an average of 80% of suspended matter (by weight) was combustible organic matter in surface waters, whereas 40% was organic near bottom.

Variability was observed in the real refractive index, n, of non-phytoplankton between seasons and vertically with depth within a season. Distributions of n for non-phytoplankton were peaked at around 1.065, and values occurred most frequently in the range for n of 1.02 to 1.25 (Fig. 4K). As previously discussed, n' was assumed constant with a value of 1×10^{-3} (Fig. 4L). Detritus on both cruises had mean n in the range of 1.064-1.072, similar to values determined for phytoplankton and heterotrophic bacteria. In comparison to detritus, minerals had higher mean n in the range of 1.16-1.19, similar to values previously assumed for minerals (Stramski et al. 2001; Twardowski et al. 2001). Non-phytoplankton in summer surface waters, compared to the spring, had significantly lower values of n (1.081 vs. 1.10; p<0.001), because detritus were more abundant in summer surface waters. As well, the high contribution of detritus in summer surface waters, compared to the spring and to deeper waters in the summer, was reflected in non-phytoplankton values of n which increased with depth in the summer (1.081-1.10) and were relatively constant with depth in the spring (1.10-1.11).

Constituent Contributions to Inherent Optical Properties

Mean depth profiles of absorption, a, scattering, b, and backscattering, b_b, at 488 nm were computed for seawater constituents to determine their contributions in the summer and spring. Values of IOPs for seawater (assumed constant) were based on Pope and Fry (1997) and Morel (1974), and a_g was measured with the filtered ac-9. Total IOPs for each particle group were computed by summing the respective optical cross-sections for all particles in the group. In surface waters, the largest particle contributors to a and b were eukaryotic phytoplankton in both seasons (Figs. 6-7). The largest particle contributors to b_b were detritus in the summer and minerals in the spring (Fig. 9).

The main contributors to total absorption in surface waters were phytoplankton and dissolved materials in both seasons (Figs. 6A-B). In the case of absorption by detritus and minerals, spectrophotometric measurements of a_{dm} were used, because there was high uncertainty in the determination of a_{dm} from the particle sum method. Dissolved materials were the most important contributor to absorption in surface waters in the summer, and eukaryotic phytoplankton were the most important contributor in the spring. In surface waters (0-20 m) on the summer cruise, mean contributions to absorption were 31% by dissolved materials, 27% by eukaryotic phytoplankton, 22% by water, 12% by non-phytoplankton, and 7% by *Synechococcus*. In surface waters on the spring cruise, mean contributions to absorption were 39% by eukaryotic phytoplankton, 28% by dissolved materials, 20% by waters, 11% by non-phytoplankton, and a negligible 1% by *Synechococcus*. Absorption by heterotrophic

bacteria was not important in either season, with contributions of $\leq 1\%$. Between particle groups, values of σ_a, diameter, and n' were more important than concentration in determining contributions to a_p. For example, eukaryotic phytoplankton were the most important contributors to a_p but were the lowest in abundance of all groups considered, and heterotrophic bacteria were the least important contributors to a_p but were higher in abundance than the phytoplankton groups. Similar to the findings for summer and spring, Stramski et al. (2001) reported that microbes were the dominant particulate component in absorption in simulations of oligotrophic waters.

All particle groups were important contributors to total scattering on both cruises, except for *Synechococcus* in the spring (Figs. 7A-B). In surface waters on the summer cruise, mean contributions to b_p were 40% by eukaryotic phytoplankton, 25% by detritus, 12% each by minerals and *Synechococcus*, and 10% by heterotrophic bacteria. In surface waters on the spring cruise, mean contributions to b_p were 53% by eukaryotic phytoplankton, 20% by minerals, 12% each by detritus and heterotrophic bacteria, and only 2% by *Synechococcus*. Scattering by water was not important in either season, contributing $\leq 1\%$. Ratios of the optical cross-sections, σ_b/σ_a, explain differences in particle group contributions to b_p compared to a_p. Notably, heterotrophic bacteria were more important contributors to b_p than to a_p, because their mean σ_b/σ_a is ~31 considering both cruises, whereas the ratio for eukaryotic phytoplankton and *Synechococcus* is ~6. This was a direct result of heterotrophic bacteria having lower values of n' than phytoplankton, but similar values of n. In

agreement with findings in the equatorial Pacific (DuRand and Olson 1996; Claustre et al. 1999), eukaryotic phytoplankton and non-phytoplankton were the most important contributors to beam attenuation by particles, c_p (a_p+b_p), in New England shelf surface waters, with *Synechococcus* and heterotrophic bacteria being relatively less important optically. In contrast to the present results, Stramski et al. (2001) reported that non-phytoplankton were relatively more important to scattering than were phytoplankton in simulations of oligotrophic waters. The difference was caused by higher concentrations of phytoplankton in continental shelf waters than were simulated for the open ocean.

Seasonal variability in the particulate scattering to absorption ratio, $b_p(488):a_p(488)$, was explained mainly by differences in the contributions of non-phytoplankton. Measurements of $b_p(488):a_p(488)$ are routinely made in the ocean, and a better understanding can be gained of variability in this quantity through individual particle analysis, as in the present study. A ratio of $b_p(488):a_p(488)$ of ~14 was observed in summer surface waters, higher than a value of ~9 which was observed in spring surface waters (Fig. 8). Vertical changes in $b_p(488):a_p(488)$ were approximately the same as vertical changes in $b_{np}(488):a_p(488)$ for non-phytoplankton, such that the higher ratio in summer surface waters was caused by the increased contribution of non-phytoplankton, and specifically detritus, compared to the spring. Eukaryotic phytoplankton also contributed to high ratios in summer surface waters, because of decreased cellular absorption as a result of photoacclimation. Sosik et al. (2001) conjectured that high surface values in the summer could not be explained

solely on the basis of phytoplankton and were more likely caused by weakly absorbing particles such as heterotrophic bacteria. Heterotrophic bacteria did have the highest ratios of $b_x(488){:}a_x(488)$, where x denotes individual particle groups, with a mean value of ~31 for both cruises compared to values of ~5 for eukaryotic phytoplankton, ~6 for *Synechococcus*, and ~13 for non-phytoplankton. However, their contribution to total scattering was low compared to non-phytoplankton (Fig. 7).

The main contributors to total backscattering were detritus in the summer and minerals in the spring (Figs. 9A-B). Non-plankton contributed $\geq 50\%$ to total b_b on both cruises. In surface waters on the summer cruise, mean contributions to total b_b were 36% by detritus, 30% by minerals, 23% by water, 7% by heterotrophic bacteria, and 2% each by eukaryotic phytoplankton and *Synechococcus*. In surface waters on the spring cruise, mean contributions to total b_b were 49% by minerals, 30% by water, 12% by heterotrophic bacteria, 6% by detritus, 3% by eukaryotic phytoplankton, and <1% by *Synechococcus*. Notably, minerals were more important contributors to backscattering than to scattering in both seasons because of their high values of n, which lead to higher backscattering ratios, b_b/b (or σ_{bb}/σ_b), than for other particles (Tables 1-6). The mean ratio of b_b/b in surface waters was 3.5% for minerals, 1.1% for heterotrophic bacteria, 0.2% for *Synechococcus*, and 0.07% for eukaryotic phytoplankton. The backscattering ratio for detritus was higher in summer surface waters (2.3%) than in the spring (0.6%) because of the higher concentration of submicron detritus in the summer. Thus, detritus was an important contributor to backscattering in summer surface waters, because of its higher abundance and smaller

size. In concurrence with the present findings, it has previously been conjectured that microbes were of little importance in determining backscattering (Morel and Ahn 1991; Stramski and Kiefer 1991; Stramski et al. 2001). In contrast to the present study, Stramski et al. (2001) found that minerals were by far the most important backscattering component, which was the case in spring surface waters, but in the summer detritus was more important. The difference between the results of the present study and Stramski et al.'s simulation was caused by differences in measured versus assumed size distributions for detritus and minerals. For example, in summer surface waters, minerals were 2.5x less abundant and detritus was 1.2x more abundant than assumed concentrations in the simulation.

Particle group contributions to IOPs exhibit variability with depth, reflecting the degree of water column stratification in each season (Figs. 6-9). For all microbial groups (eukaryotic phytoplankton, heterotrophic bacteria, and *Synechococcus*), profiles of a_p and b_p exhibit subsurface maxima in the summer at ~25 m and surface maxima (0-25 m) in the spring. The contributions to IOPs of microbial groups decreased below 20-30 m in both seasons, mainly due to a decrease in microbial concentrations with depth. The contribution of eukaryotic phytoplankton to absorption and scattering in the top 30 m of the water column, versus below, changed by ~4.5-fold and 2.5-fold in the summer and spring, respectively. Similarly, the concentrations of eukaryotic phytoplankton changed by ~9-fold and 4-fold in the summer and spring, respectively (Table 1). The larger change in the concentration and contribution to IOPs of eukaryotic phytoplankton in the summer was caused by a

higher degree of water column stratification. In contrast to microbes, the contribution to IOPs of minerals generally increased below 20-30 m in both seasons, and the contribution of detritus to IOPs was relatively constant with depth. The increased contribution of minerals with depth was most evident in the summer, caused by mineral particles which were larger in size and had higher real refractive indices (Table 6), indicating the effects of sediment resuspension (Boss et al. 2001).

Sensitivity of IOPs to Changes in Particle Properties

For the three microbial groups, intragroup variability in inherent optical properties was determined mainly by variability in particle concentration. The sensitivity of IOPs to changes in particle properties was determined using Mie theory and inputs of three of the properties (concentration, D, n, and/or n′) which were allowed to change over their normal values and one property which was held constant at its mean value. For eukaryotic phytoplankton in the spring, the correlation coefficients between modeled and expected a_{euk} and modeled and expected b_{euk} indicated that holding concentration constant had the largest effect ($r^2 \leq 0.2$), diameter had some effect ($r^2 \approx 0.5$), and n and n′ had little effect ($r^2 \geq 0.86$) (Figs. 10 A-H). Concentration was the major determinant of variability in IOPs for eukaryotic phytoplankton, *Synechococcus* and heterotrophic bacteria. Diameter and n′ had secondary effects in determining IOP variability in eukaryotic phytoplankton and *Synechococcus*, however, n never had a major effect on the determination of IOPs for the microbial groups. In contrast, variability between groups (e.g. eukaryotic

93

phytoplankton versus minerals) is highly dependent on not only concentration, but n,

n', and diameter as well. For example, when the mean n for minerals was assumed for

eukaryotic phytoplankton, backscattering was on average 25x higher than expected

values, and when the mean n' of non-phytoplankton was assumed for eukaryotic

phytoplankton, absorption was 7x too low.

For non-phytoplankton, changes in submicron detrital concentrations and both

submicron and >1 μm mineral concentrations were important determinants of

backscattering. In the summer, backscattering by detritus, $b_{b,det}$, was well correlated

with submicron detrital concentrations ($r^2 = 0.92$ for a linear fit of logarithmic values)

but not with >1 μm detrital concentrations (Fig. 11 A and D). Detritus in the spring

was not considered, because it was not an important contributor to b_b. In the summer,

mineral backscattering, $b_{b,min}$, was correlated with both submicron and >1 μm mineral

concentrations ($r^2 = 0.76$ and 0.58, respectively; Fig. 11 B and E). In contrast, in the

spring, mineral backscattering, $b_{b,min}$, was better correlated with >1 μm mineral

concentrations (0.62) than with submicron mineral concentrations ($r^2 = 0.29$; Fig. 11 E

and F). The low real refractive index, n, of detritus means that they can only be

important contributors to b_b when they are high in concentration, as occurs at

submicron sizes. In contrast, high values of n for minerals means that they are

important contributors to b_b at all sizes, without the need to invoke high concentrations

at submicron sizes. Considering both seasons, comparisons with $b_{b,det}$ and $b_{b,min}$

showed that submicron detritus and mineral particles played a role in determining

variability in particle backscattering, emphasizing the need for better measurements of this size fraction in the ocean.

CONCLUSIONS

The application of Mie theory and individual particle measurements to analysis of IOPs in New England continental shelf waters provided important insights into the roles of particles in determining variability in IOPs in natural samples. An important step in the approach was the validation of particle sum methods by comparison with concurrently measured bulk optical properties. This comparison showed that the sum contribution to scattering of particle groups accounted for approximately all of the scattering measured independently on bulk samples. Variability was observed both seasonally and vertically with depth in the contribution of particles to absorption, scattering, and backscattering. Eukaryotic phytoplankton were the most important particle contributor to both absorption and scattering in surface waters, because of their larger diameters and higher n' than other particle groups. As well, eukaryotic phytoplankton contributed relatively more to IOPs in the spring when their concentration was higher. In both seasons, minerals were the most important contributor to scattering below ~30 m and were significant contributors to backscattering at all depths. Their concentration was similar between seasons, implying that minerals may play an important role in determining scattering and backscattering throughout the year. The concentration of detritus was higher

throughout the water column in the summer, compared to spring, and in surface waters in the summer contributed the most to backscattering.

The type of particle budgets presented in this study, which include both microbes and non-phytoplankton, have previously only been attempted in simulations of open ocean conditions. Stramski et al. (2001) used Mie theory and expected mean values of concentration, n, and n' for particle groups to calculate their contributions to IOPs in oligotrophic waters. Their example simulations showed that the use of Mie theory and particle measurements could be a powerful research tool permitting analysis of IOPs. However, the simulations could not provide generalized conclusions about the roles played by various particles in ocean optics, because they were not based on actual measurements. The difference between the results of the present study and Stramski et al.'s simulations, which predicted that minerals were the most important contributor to both scattering and backscattering, was caused by differences in measured and assumed particle concentrations for eukaryotic phytoplankton, detritus, and minerals.

The size distributions and real refractive indices of non-phytoplankton were important determinants of variability in scattering and backscattering in New England shelf waters. The contribution of detritus to backscattering in summer surface waters was a result of their high concentrations at small sizes, compared to the spring. Small detritus was presumably more abundant in the summer because of the preceding several months of increased productivity. The contribution of detritus to IOPs with depth in the summer was relatively constant. In contrast, minerals increased in

importance with depth, even though their concentration changed little, because of an increase in mineral particle size, presumably due to sediment resuspension. As well, the higher refractive index of minerals caused them to be relatively more important contributors to backscattering than detritus at the same particle concentrations. For example, in the spring, minerals had similar or lower abundances than detritus, but contributed significantly to backscattering, whereas the contribution by detritus was small. It is clear that measurements of the size distributions and optical properties of detritus and minerals are necessary to explain changes in IOPs, especially scattering and backscattering, in the ocean.

Table 1. Mean Property Values for Eukaryotic Phytoplankton

	0-20 m	Summer 20-40 m	40-65 m	0-20 m	Spring 20-40 m	40-65 m
Conc. (#/ml)	1.84×10^4	1.44×10^4	0.180×10^4	2.46×10^4	1.60×10^4	0.532×10^4
D (μm)	2.05	2.26	2.28	2.31	2.23	2.05
n	1.066	1.073	1.073	1.059	1.064	1.067
n'	0.0051	0.0139	0.0165	0.0057	0.0089	0.0100
σ_a (m^2)	1.07×10^{-12}	2.85×10^{-12}	2.85×10^{-12}	1.44×10^{-12}	1.67×10^{-12}	1.32×10^{-12}
σ_b (m^2)	9.01×10^{-12}	9.25×10^{-12}	8.14×10^{-12}	1.05×10^{-11}	0.93×10^{-11}	0.67×10^{-11}
σ_{bb} (m^2)	6.58×10^{-15}	7.20×10^{-15}	7.63×10^{-15}	5.53×10^{-15}	5.40×10^{-15}	5.67×10^{-15}

Values of n, n', σ_a, σ_b, and σ_{bb} were determined at 488 nm in Tables 1-6.

Table 2. Mean Property Values for *Synechococcus*

	0-20 m	Summer 20-40 m	40-65 m	0-20 m	Spring 20-40 m	40-65 m
Conc. (#/ml)	5.94×10^4	9.14×10^4	0.847×10^4	0.776×10^4	0.672×10^4	0.515×10^4
D (μm)	1.09	1.16	1.23	1.38	1.35	1.34
n	1.067	1.068	1.069	1.054	1.056	1.057
n'	0.0022	0.0071	0.0093	0.0024	0.0033	0.0043
σ_a (m^2)	0.59×10^{-13}	2.24×10^{-13}	3.19×10^{-13}	1.17×10^{-13}	1.53×10^{-13}	1.86×10^{-13}
σ_b (m^2)	0.67×10^{-12}	0.89×10^{-12}	1.11×10^{-12}	1.16×10^{-12}	1.16×10^{-12}	1.08×10^{-12}
σ_{bb} (m^2)	1.76×10^{-15}	1.91×10^{-15}	2.62×10^{-15}	1.87×10^{-15}	1.93×10^{-15}	1.84×10^{-15}

Table 3. Mean Property Values for Bacteria

	0-20 m	Summer 20-40 m	40-65 m	0-20 m	Spring 20-40 m	40-65 m
Conc. (#/ml)	1.06×10^6	1.22×10^6	0.94×10^6	1.48×10^6	1.30×10^6	1.18×10^6
D (μm)	0.46	0.45	0.45	0.46	0.45	0.45
n	1.079	1.077	1.077	1.081	1.081	1.078
σ_a (m^2)	1.14×10^{-15}	1.09×10^{-15}	1.11×10^{-15}	1.15×10^{-15}	1.09×10^{-15}	1.08×10^{-15}
σ_b (m^2)	3.82×10^{-14}	3.33×10^{-14}	3.39×10^{-14}	3.83×10^{-14}	3.49×10^{-14}	3.21×10^{-14}
σ_{bb} (m^2)	4.27×10^{-16}	3.79×10^{-16}	3.79×10^{-16}	4.45×10^{-16}	4.18×10^{-16}	3.77×10^{-16}

Table 4. Mean Property Values for Non-phytoplankton (Detritus + Minerals)

	Summer			Spring		
	0-20 m	20-40 m	40-65 m	0-20 m	20-40 m	40-65 m
Conc. (#/ml)	1.73×10^8	1.01×10^8	0.58×10^8	1.74×10^7	1.26×10^7	2.83×10^7
Junge slope: <3.5 μm	4.85	4.66	4.23	4.06	3.96	4.07
Junge slope: >3.5 μm	3.21	3.10	2.57	3.10	3.07	3.04
n	1.081	1.088	1.10	1.10	1.10	1.11
Detrital % (1.2-10 μm)	77	68	48	46	45	33

Table 5. Mean Property Values for Detritus

	Summer			Spring		
	0-20 m	20-40 m	40-65 m	0-20 m	20-40 m	40-65 m
Conc. (#/ml)	1.62×10^8	0.88×10^8	0.49×10^8	0.87×10^7	0.44×10^7	2.16×10^7
Junge slope: <3.5 μm	4.82	4.58	4.36	3.61	3.45	4.08
Junge slope: >3.5 μm	1.93	2.24	2.22	2.22	2.25	2.42
n	1.064	1.064	1.067	1.070	1.072	1.072
σ_a (m^2)	0.98×10^{-15}	1.64×10^{-15}	2.74×10^{-15}	6.09×10^{-14}	8.30×10^{-14}	0.57×10^{-14}
σ_b (m^2)	1.22×10^{-15}	1.56×10^{-15}	2.36×10^{-15}	4.21×10^{-14}	6.26×10^{-14}	0.52×10^{-14}
σ_{bb} (m^2)	2.17×10^{-17}	2.50×10^{-17}	3.34×10^{-17}	3.12×10^{-16}	4.39×10^{-16}	0.56×10^{-16}

Table 6. Mean Property Values for Minerals

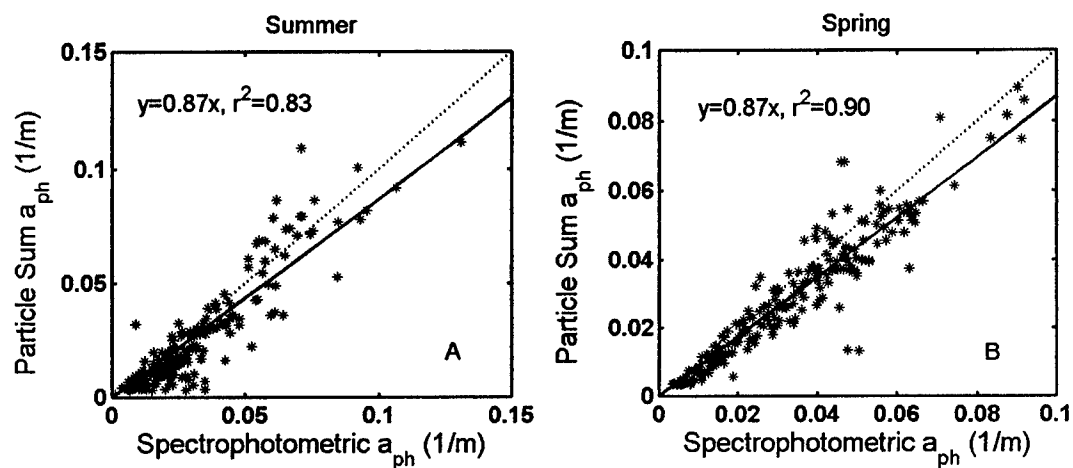|	Summer			Spring		
	0-20 m	20-40 m	40-65 m	0-20 m	20-40 m	40-65 m
Conc. (#/ml)	1.12×10^7	1.28×10^7	0.92×10^7	0.87×10^7	0.82×10^7	0.67×10^7
Junge slope: <3.5 μm	4.37	4.25	3.81	4.00	3.98	3.68
Junge slope: >3.5 μm	1.62	1.61	1.67	2.54	2.58	2.52
n	1.16	1.18	1.19	1.19	1.19	1.19
σ_a (m^2)	0.70×10^{-15}	0.73×10^{-15}	3.66×10^{-15}	0.98×10^{-15}	0.95×10^{-15}	2.44×10^{-15}
σ_b (m^2)	4.06×10^{-15}	3.95×10^{-15}	8.74×10^{-15}	0.95×10^{-14}	0.70×10^{-14}	1.27×10^{-14}
σ_{bb} (m^2)	1.82×10^{-16}	1.89×10^{-16}	3.55×10^{-16}	2.45×10^{-16}	2.47×10^{-16}	3.81×10^{-16}

Figure 1. Comparison of particle sum and spectrophotometric phytoplankton absorption, a_{ph}, at 488 nm in the (A) summer and (B) spring. Particle sum a_{ph} is a sum of absorption by eukaryotic phytoplankton and *Synechococcus*.
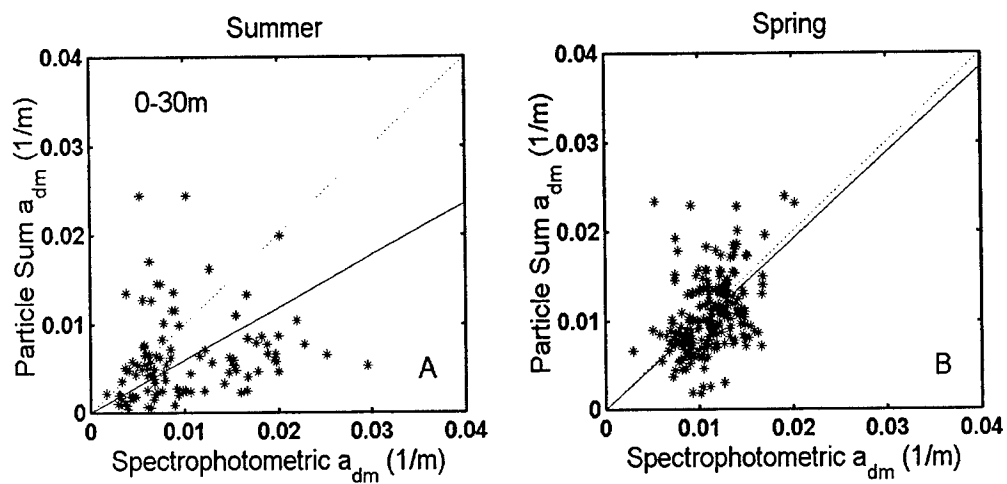
Figure 2. Comparison of particle sum and spectrophotometric non-phytoplankton (detritus+mineral) absorption, a_{dm}, at 488 nm in the (A) summer and (B) spring. In the summer, only points above 30 m were included in the comparison, and in the spring, points from throughout the water column were included.
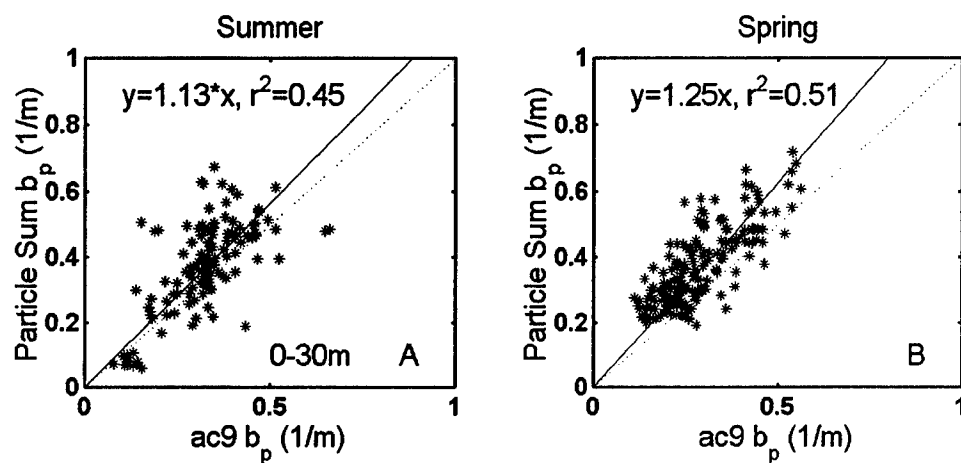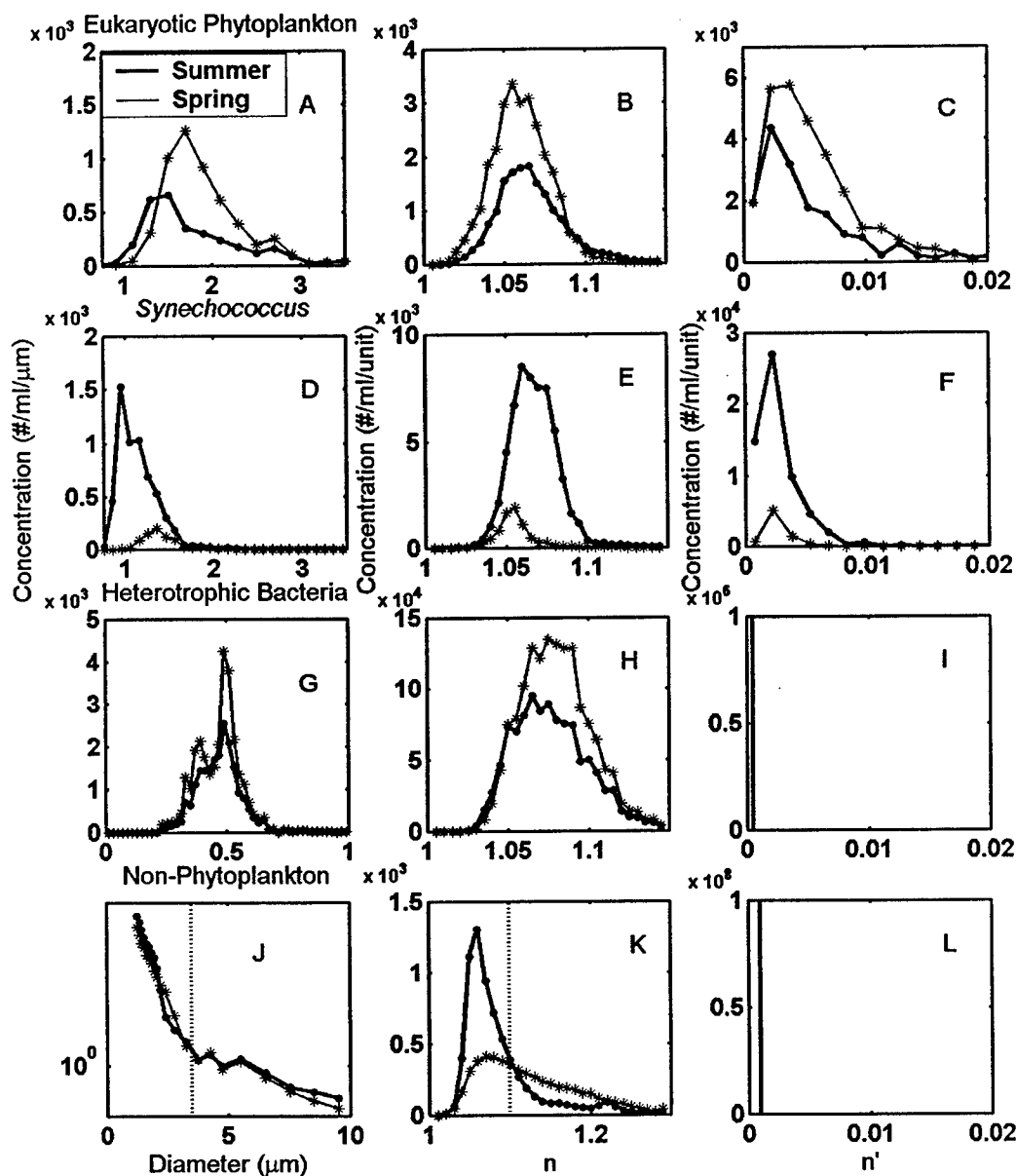
Summer

$y=1.13{*}x, r^2=0.45$

Particle Sum b_p (1/m)

0-30m   A

ac9 b_p (1/m)

Spring

$y=1.25x, r^2=0.51$

Particle Sum b_p (1/m)

B

ac9 b_p (1/m)

Figure 3. Comparison of particle sum and bulk (ac-9) scattering, b_p, at 488 nm in the (A) summer and (B) spring. Particle sum scattering is a sum of scattering by all particles, including eukaryotic phytoplankton, *Synechococcous*, heterotrophic bacteria, detritus, and minerals, from 0.1-50 μm in diameter. In the summer, only points above 30 m were included in the comparison, and in the spring, points from throughout the water column were included.

Figure 4. Mean property distributions of D, n, and n′ in summer and spring surface waters (0-20m) for eukaryotic phytoplankton (A-C), Synechococcus (D-F), heterotrophic bacteria (G-I), and non-phytoplankton (J-L). Values of n′ for heterotrophic bacteria (I) and non-phytoplankton (L) have been assumed constant at the values 5×10^{-4} and 1×10^{-3}, respectively. A dotted line was drawn at 3.5 µm on non-phytoplankton size distributions (J) to mark the cutoff between >3.5 µm and <3.5 µm Junge slopes. A dotted line was also drawn at 1.10 on non-phytoplankton n distributions (K) to mark the cutoff between detritus and minerals. Note the change in x-axes in (G), (J), and (K).
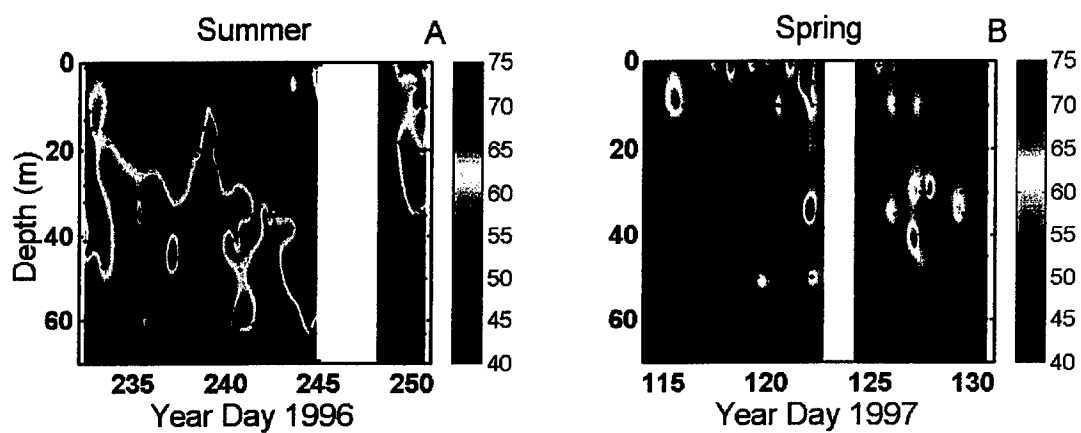
Figure 5. Percent organic composition of non-phytoplankton for the (A) summer and (B) spring. Results are based on non-phytoplankton particles analyzed with the FCM-Mie method in the range of 1.2-10 μm. Higher values of organic composition and more variability with depth were observed in the summer than in the spring.

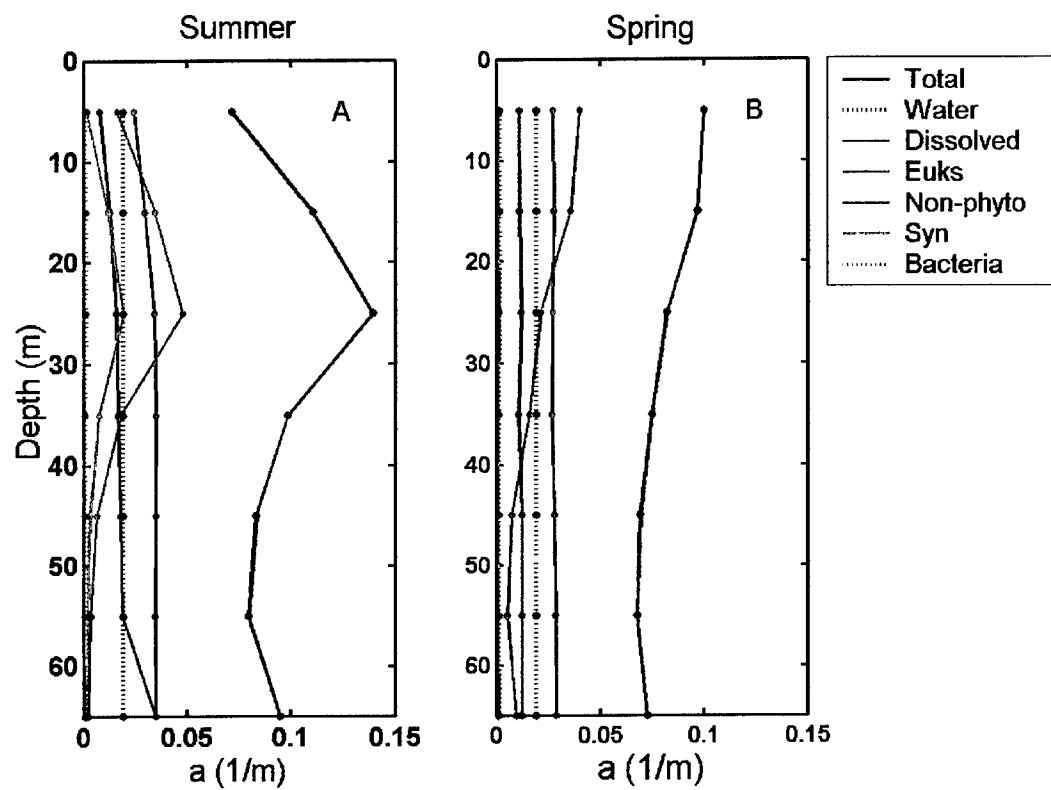Figure 6. Depth profiles of constituent contributions to absorption, a, at 488 nm in the summer (A) and spring (B).
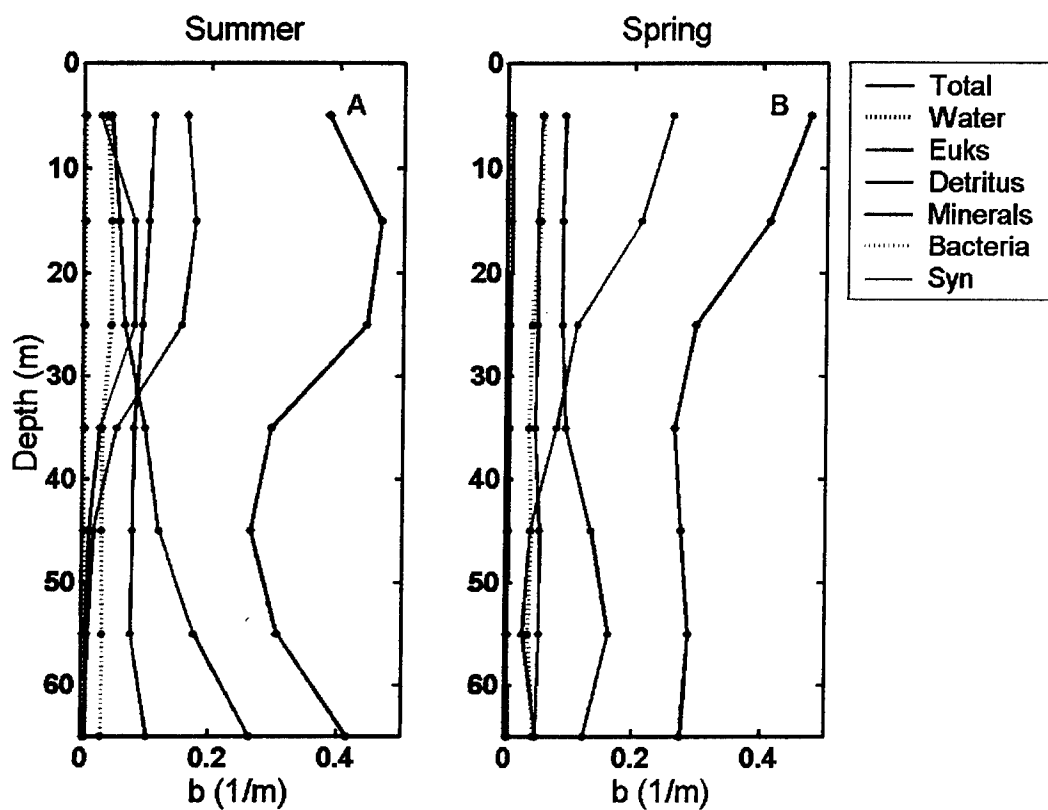
Figure 7. Depth profiles of constituent contributions to scattering, b, at 488 nm in the summer (A) and spring (B).
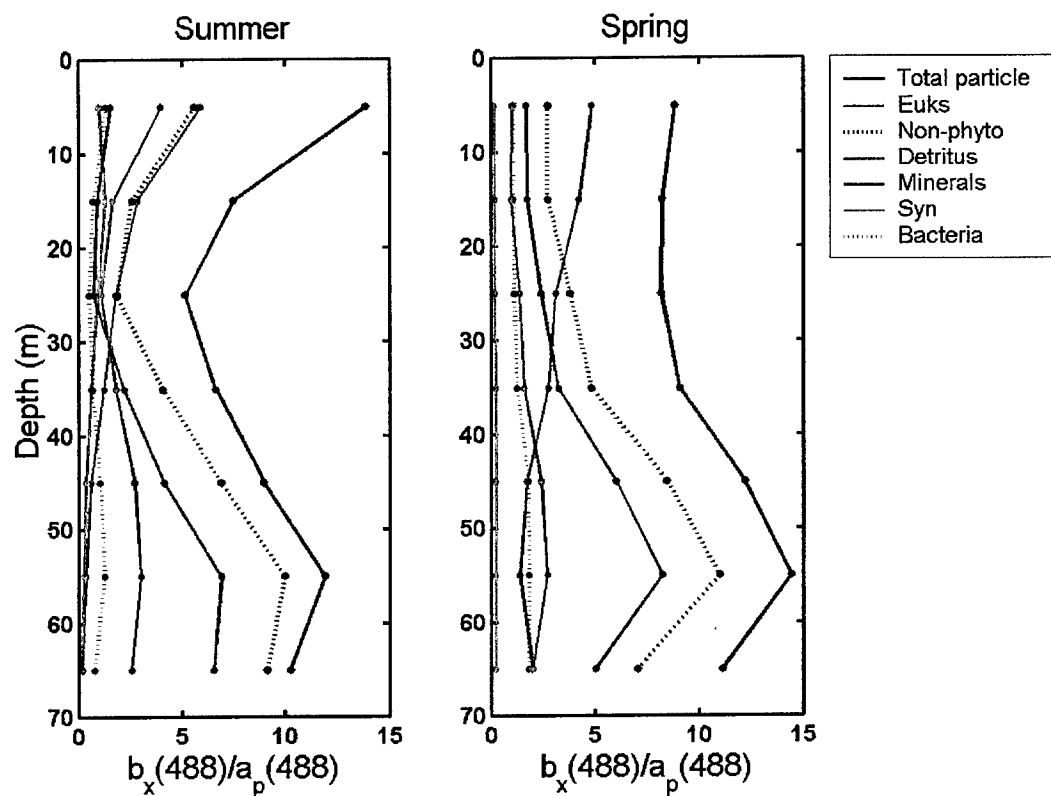
Figure 8. Depth profiles of constituent contributions to the ratio of constituent scattering to particle absorption, $b_x(488):a_p(488)$ in the summer (A) and spring (B) where x denotes each particle group and "total particle" is the sum of all particle groups. The sum of contributions by detritus and minerals (non-phytoplankton) has been plotted to emphasize the similarity with depth of the ratio for total particles and non-phytoplankton.
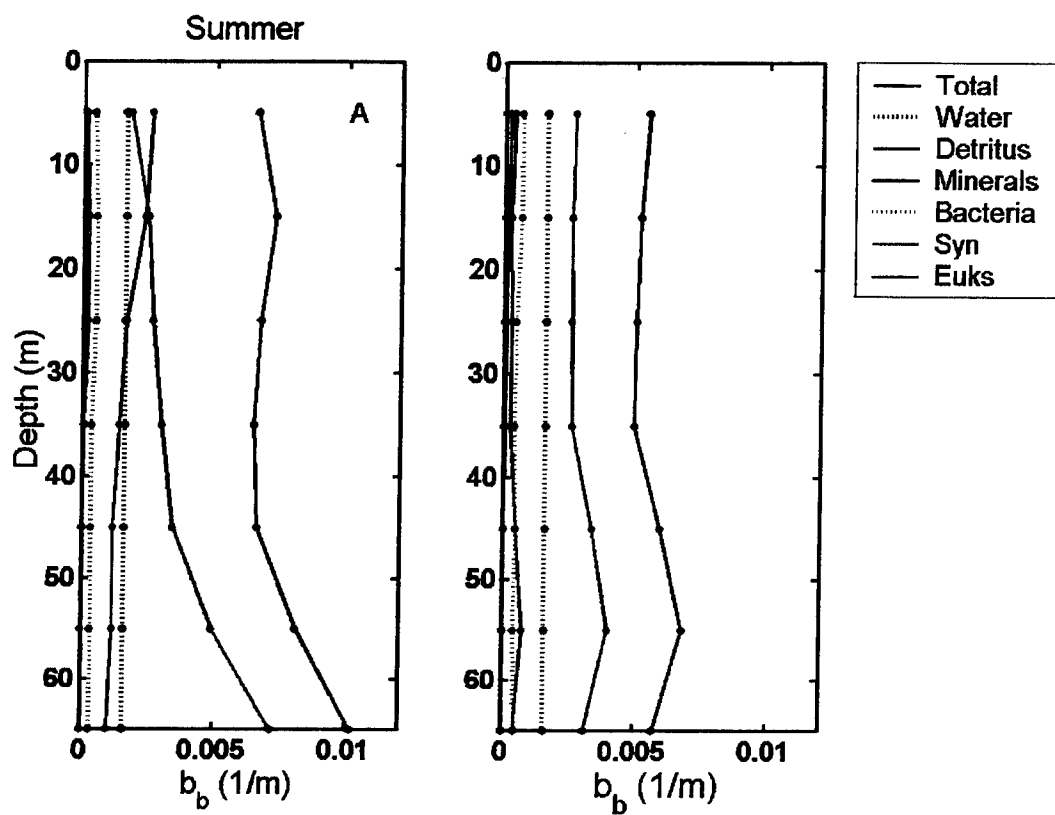
Figure 9. Depth profiles of constituent contributions to backscattering, b_b, at 488 nm in the summer (A) and spring (B).
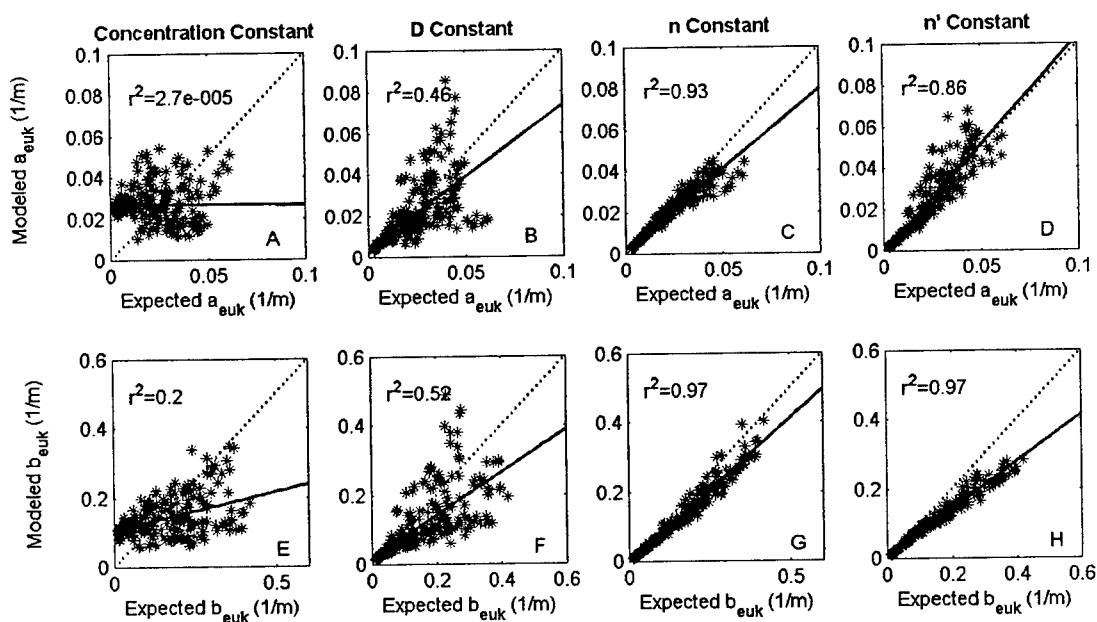
Figure 10. Sensitivity of (A-D) eukaryotic phytoplankton absorption, a_{euk}, and (E-H) scattering, b_{euk}, in the spring to variability in concentration, D, n, and n'. Expected values of a_{euk} and b_{euk} were calculated using Mie theory and inputs of all four properties (concentration, D, n, or n') which were allowed to vary over their normal values. Modeled a_{euk} and b_{euk} were calculated using Mie theory and inputs of three of the properties which were allowed to vary over their normal values and one property which was held constant at its mean value. The effects of variability on backscattering were not included, because eukaryotic phytoplankton were not important contributors to b_b.

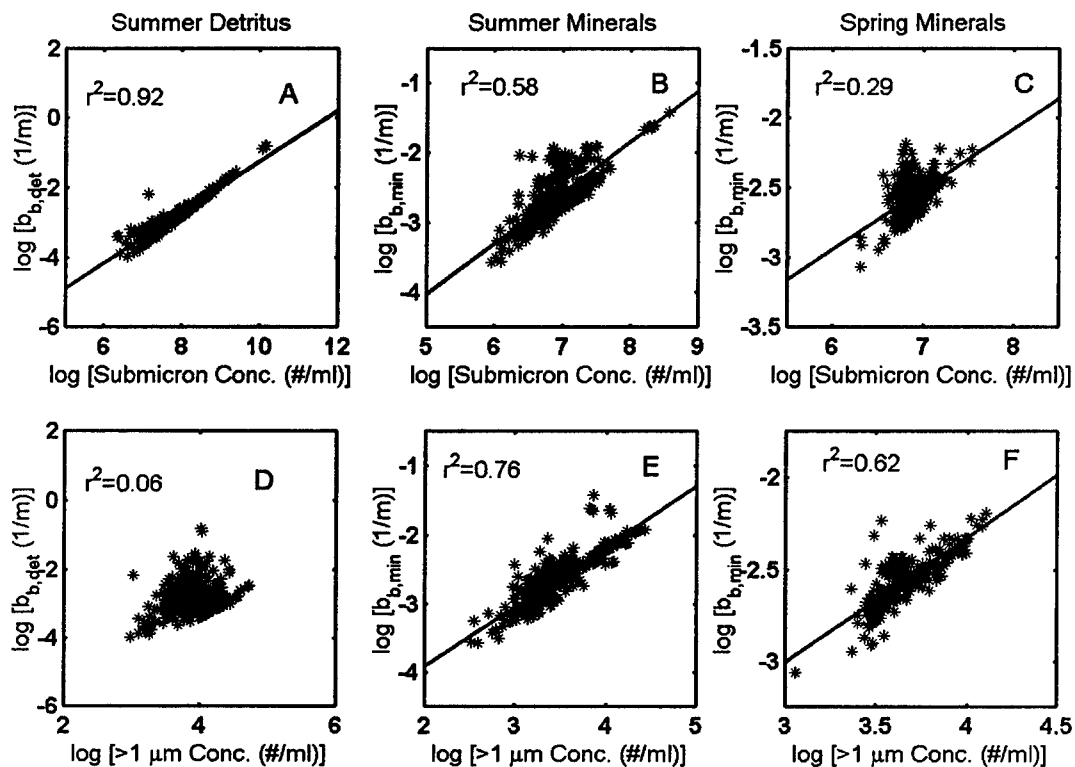Figure 11. Comparisons of backscattering by detritus, $b_{b,det}$, and minerals, $b_{b,min}$, and submicron particle concentrations (A-C) and >1 µm particle concentrations (D-F). Comparisons are included for detritus in the summer (A and D), minerals in the summer (B and E), and minerals in the spring (C and F). However, detritus in the spring was not considered, because it was not an important contributor to total b_b.

REFERENCES

Aas, E. 1996. Refractive index of phytoplankton derived from its metabolite composition. J. Plankton Res. **18**: 2223-2249.

Ackelson, S.G., and R.W. Spinrad. 1988. Size and refractive index of individual marine particulates: a flow cytometric approach. Appl.Optics **27**: 1270-1277.

Boss, E., W.S. Pegau, W.D. Gardner, J.R.V. Zaneveld, A.H. Barnard, M.S. Twardowski, G.C. Change, and T.D. Dickey. 2001. Spectral particulate attenuation and particle size distribution in the bottom boundary layer of a continental shelf. J. Geophys. Res. **106**: 9509-9516.

Chisholm, S.W. 1992. Phytoplankton size, p. 213-237. *In* P. G. Falkowski and A. D. Woodhead, [eds.]. Primary productivity and biogeochemical cycles in the sea. Plenum.

Cho, B.C., and F. Azam. 1990. Biogeochemical significance of bacterial biomass in the ocean's euphotic zone. Mar. Ecol. Prog. Ser. **63**: 253-259.

Claustre, H., A. Morel, M. Babin, C. Cailliau, D. Marie, J.C. Marty, D. Tailliez, and D. Vaulot. 1999. Variability in particle attenuation and chlorophyll fluorescence in the tropical Pacific: Scales, patterns, and biogeochemical implications. J. Geophys. Res. **104**: 3401-3422.

DuRand, M.D., and R.J. Olson. 1996. Contributions of phytoplankton light scattering and cell concentration changes to diel variations in beam attenuation in the equatorial Pacific from flow cytometric measurements of pico-, ultra- and nanoplankton. Deep-Sea Res. II **43**: 891-906.

DuRand, M.D., and R.J. Olson. 1998. Diel patterns in optical properties of the chlorophyte Nannochloris sp.: relating individual-cell to bulk measurements. Limnol.Oceanogr. **43**: 1107-1118.

Falkowski, P.G., Z. Dubinsky, and K. Wyman. 1985. Growth-irradiance relationships in phytoplankton. Limnol. Oceanogr. **30**: 311-321.

Harris, J.E. 1977. Characterization of suspended matter in the Gulf of Mexico - II, particle size analysis of suspended matter from deep water. Deep-Sea Res. **24**: 1055-1061.

Iturriaga, R., and D.A. Siegel. 1989. Microphotometric characterization of phytoplankton and detrital absorption properties in the Sargasso Sea. Limnol. Oceanogr. **34**: 1706-1726.

Kirk, J.T.O. 1983. Light and photosynthesis in aquatic ecosystems. Cambridge University Press.

Koike, I., S. Hara, K. Terauchi, and K. Kogure. 1990. Role of sub-micrometre particles in the ocean. Nature **345**: 242-244.

Kuipers, B., G.J. van Noort, J. Vosjan, and G.J. Herndl. 2000. Diel periodicity of bacterioplankton in the euphotic zone of the subtropical Atlantic Ocean. Mar. Ecol. Prog. Ser. **201**: 13-25.

Lewis, M.R., and J.J. Cullen. 1991. From cells to the ocean: Satellite ocean color, p. 325-337. *In* S. Demers, [eds.]. Particle Analysis in Oceanography. Springer-Verlag.

Marie, D., F. Partensky, S. Jacquet, and D. Vaulot. 1997. Enumeration and cell cycle analysis of natural populations of marine picoplankton by flow cytometry using the nucleic acid stain SYBR Green I. Appl. Environ. Microbiol. **63**: 186-193.

McCave, I.N. 1983. Particulate size spectra, behavior, and origin of nepheloid layers over the Nova Scotian continental rise. J. Geophys. Res. **88**: 7647-7666.

Meade, R.H., P.L. Sachs, F.T. Manheim, J.C. Hathaway, and D.W. Spencer. 1975. Sources of suspended matter in waters of the Middle Atlantic Bight. J. Sed. Petrol. **45**: 171-188.

Mitchell, B.G., and D.A. Kiefer. 1988. Chlorophyll *a* specific absorption and fluorescence excitation spectra for light-limited phytoplankton. Deep-Sea Res. **35**: 639-663.

Mobley, C.D. 1994. Light and water; radiative transfer in natural waters. Academic Press, Inc.

Mobley, C.D., and D. Stramski. 1997. Effects of microbial particle on oceanic optics: Methodology for radiative transfer modeling and example simulations. Limnol.Oceanogr. **42**: 550-560.

Morel, A. 1974. Optical properties of pure water and pure seawater, p. 1-24. *In* N. G. Jerlov and E. S. Nielsen, [eds.]. Optical aspects of oceanography. Academic.

Morel, A., and Y.H. Ahn. 1990. Optical efficiency factors of free-living marine bacteria: Influence of bacterioplankton upon the optical properties and particulate organic carbon in oceanic waters. J. Mar. Res. **48**: 145-175.

Morel, A., and Y.H. Ahn. 1991. Optics of heterotrophic nanoflagellates and ciliates: A tentative assessment of their scattering role in oceanic waters compared to those of bacterial and algal cells. J. Mar. Res. **49**: 177-202.

Morel, A., and A. Bricaud. 1986. Inherent optical properties of algal cells including picoplankton: Theoretical and experimental results, p. 521-559. *In* T. Platt and W. K. W. Li, [eds.]. Photosynthetic picoplankton. Can. Bull. Fish. Aquat. Sci. 214.

Nagata, T., and D.L. Kirchman. 1996. Roles of submicron particles and colloids in microbial food webs and biogeochemical cycles within marine environments. Adv. Microb. Ecol.. **15**: 81-103.

Noble, R.T., and J.A. Fuhrman. 1998. Use of SYBR Green I for rapid epifluorescence counts of marine viruses and bacteria. Aquatic Microbial Ecology **14**: 113-118.

Olson, R.J., S.W. Chisholm, E.R. Zettler, M.A. Altabet, and J.A. Dusenberry. 1990. Spatial and temporal distributions of prochlorophyte picoplankton in the North Atlantic Ocean. Deep-Sea Res. **37**: 1033-1051.

Olson, R.J., E.R. Zettler, and O.K. Anderson. 1989. Discrimination of eukaryotic phytoplankton cell types from light scatter and autofluorescence properties measured by flow cytometry. Cytometry **10**: 636-643.

Olson, R.J., E.R. Zettler, and M.D DuRand. 1993. Phytoplankton Analysis Using Flow Cytometry, p. 175-186. *In* P. F. Kemp, B. F. Sherr, E. B. Sherr and J. J. Cole, [eds.]. Aquatic Microbial Ecology. Lewis Publishers.

Perry, M.J., and S.M. Porter. 1989. Determination of the cross-section absorption coefficient of individual phytoplankton cells by analytical flow cytometry. Limnol.Oceanogr. **34**: 1727-1738.

Pope, R.M., and E.S. Fry. 1997. Absorption spectrum (380-700 nm) of pure water. II Integrating cavity measurements. Appl. Opt. **36**: 8710-8723.

Risović, D. 1993. Two-component model of sea particle size distribution. Deep-Sea Res. I **40**: 1459-1473.

Sakshaug, E., S. Demers, and C.M. Yentsch. 1987. *Thalassiosira oceanica* and *T. pseudonana*: two different photoadaptational responses. Mar. Ecol. Prog. Ser. **41**: 275-282.

Shibata, A., K. Kogure, I. Koike, and K. Ohwada. 1997. Formation of submicron colloidal particles from marine bacteria by viral infection. Mar. Ecol. Prog. Ser. **155**: 303-307.

Sieracki, M., and C. Viles. 1992. Distributions and fluorochrome-staining properties of sub-micrometer particles and bacteria in the North Atlantic. Deep-Sea Res. **39**: 1919-1929.

Sosik, H.M., S.W. Chisholm, and R.J. Olson. 1989. Chlorophyll fluorescence from single cells: Interpretation of flow cytometric signals. Limnol. Oceanogr. **34**: 1749-1761.

Sosik, H.M., R.E. Green, W.S. Pegau, and C.S. Roesler. 2001. Temporal and vertical variability in optical properties of New England shelf waters during late summer and spring. J. Geophys. Res. **106**: 9455-9472.

Sosik, H.M., and B.G. Mitchell. 1991. Absorption, fluorescence and quantum yield for growth in nitrogen limited *Dunaliella tertiolecta*. Limnol. Oceanogr. **36(5)**: 910-921.

Stramski, D., A. Bricaud, and A. Morel. 2001. Modeling the inherent optical properties of the ocean based on the detailed composition of the planktonic community. Appl. Optics **40**: 2929-2945.

Stramski, D., and D.A. Kiefer. 1990. Optical properties of marine bacteria, p. 250-268. *In* M. A. Blizard, [eds.]. Ocean Optics X. Society of Photo-Optical Instrumentation Engineers.

Stramski, D., and D.A. Kiefer. 1991. Light scattering by microorganisms in the open ocean. Prog. Oceanogr. **28**: 343-383.

Stramski, D., and C.D. Mobley. 1997. Effects of microbial particles on oceanic optics: A database of single-particle optical properties. Limnol. Oceanogr. **42**: 538-549.

Stramski, D., and A. Morel. 1990. Optical properties of photosynthetic picoplankton in different physiological states as affected by growth irradiance. Deep-Sea Res. **37**: 245-266.

Twardowski, M.S., E. Boss, J.B. Macdonald, W.S. Pegau, A.H. Barnard, and J.R.V. Zaneveld. 2001. A model for estimating bulk refractive index from the optical backscattering ratio and the implications for understanding particle composition in case I and case II waters. J. Geophys. Res. **106**: 14129-14142.

Waterbury, J.B., S.W. Watson, F.W. Valois, and D.G. Franks. 1986. Biological and ecological characterization of the marine unicellular cyanobacterium *Synechococcus*, p. 71-120. *In* W. K. W. L. T.Platt, [eds.]. Photosynthetic Picoplankton, Can. Bull. Fish. Aquat. Sci. 214

Yamasaki, A., H. Fukuda, R. Fukuda, T. Miyajima, T. Nagata, H. Ogawa, and I. Koike. 1998. Submicrometer particles in northwest Pacific coastal environments: Abundance, size distribution, and biological origins. Limnol. Oceanogr. **43**: 536-542.

Zaneveld, J.R.V., D.R. Roach, and H. Pak. 1974. The determination of the index of refraction distribution of oceanic particulates. J. Geophys. Res. **79**: 4091-4095.

Zubkov, M.V., B.M. Fuchs, P.H. Burkill, and R. Amann. 2001. Comparison of cellular and biomass specific activities of dominant bacterioplankton groups in stratified waters of the Celtic Sea. Appl. Environ. Microbiol. **67**: 5210-5218.

CHAPTER 4:

PARTICLE CONTRIBUTIONS TO VARIABILITY IN APPARENT OPTICAL

PROPERTIES OF THE UPPER OCEAN

ABSTRACT

Apparent optical properties (AOPs) of surface waters were modeled using a radiative transfer model (Hydrolight) and budgets of absorption, scattering and backscattering based on measurements of individual particles and dissolved materials for continental shelf waters sampled in two seasons. Budgets of spectral absorption, scattering, and backscattering were determined using Mie theory and measurements of optically important seawater constituents, including dissolved materials, eukaryotic pico/nanophytoplankton, *Synechococcus*, heterotrophic bacteria, detritus, and minerals. Good agreement was reached between modeled and measured values of diffuse attenuation (K_d) and remote sensing reflectance (R_{rs}) in New England surface waters in the late summer and spring. Modeled values of K_d and R_{rs} were within 15% of measurements, considering all wavelengths and both seasons, and this agreement allowed for the interpretation of variability in AOPs using the contributions of different seawater constituents. Higher values of K_d in the spring compared to summer were explained by higher values of absorption by eukaryotic phytoplankton (a_{euk}) and dissolved materials (a_g) in the spring, consistent with higher nutrient levels in surface waters and less stratified conditions than in the summer. Within the summer, variability in K_d was caused by variability in both a_{euk} and a_g, in contrast to the spring during which variability in K_d was determined by a_{euk} alone. Differences in the spectral shape of R_{rs} between the seasons were contributed to approximately equally by differences in a_{euk}, a_g, and backscattering by non-phytoplankton (the sum of backscattering by minerals, $b_{b,min}$, and backscattering by detritus, $b_{b,det}$). The main difference in backscattering by non-phytoplankton between the two seasons was a higher inverse wavelength dependence of spectral backscattering in the summer due to the contribution of small organic detritus. Although *Synechococcus* and heterotrophic bacteria were included in the absorption, scattering, and backscattering budgets, they were not important contributors to AOP magnitude or variability. Bio-optical models based on chlorophyll concentrations underestimated b_b and R_{rs} in the summer and overestimated $R_{rs}(443):R_{rs}(555)$ in both seasons.

INTRODUCTION

Typical ocean color algorithms are based on the parameterization of apparent optical properties (AOPs), such as diffuse attenuation (K_d) and remote sensing reflectance (R_{rs}), as a function of inherent optical properties (IOPs) and other factors such as chlorophyll concentration. To first order, K_d is related to absorption ($K_d \propto a$), and R_{rs} is proportional to the ratio of backscattering and absorption ($R_{rs} \propto b_b/a$) (Gordon et al. 1975; Morel and Prieur 1977). Two uncertainties related to describing absorption in bio-optical algorithms include the effects of phytoplankton community structure (Sathyendranath et al. 2001) and variability in the ratio between algal absorption and nonalgal absorption (Garver and Siegel 1997; Morel and Maritorena 2001; Sathyendranath et al. 2001). The difficulty arises because there is not a reliable relationship between nonalgal absorption and chlorophyll concentration. Relationships between chlorophyll and scattering have significantly more unexplained variance than do relationships between chlorophyll and absorption (Gordon and Morel 1983), and no reliable relationship exists between particle backscattering and chlorophyll. Perhaps the most uncertainty in current bio-optical models is associated with the modeling of backscattering by particles, since the main contributors are thought to be small nonalgal particles of less than 1 μm in size for which few measurements have been made (Stramski and Kiefer 1991). In a recent review, Morel and Maritorena (2001) concluded that purely analytical approaches to ocean color algorithms, ideally based on radiative transfer calculations, remain problematic

because of the insufficient knowledge of the phase function and backscattering efficiency of oceanic particles.

A major source of particulate backscattering in the oceans is thought to be small (<1 μm), numerically abundant detrital and/or mineral particles. Little is known about this fraction of particles, but Stramski and Kiefer (1991) conjectured based on Mie calculations that two groups of particles may be responsible: (1) fine particles of diameter near 0.3 μm, and (2) high refractive index (n $\approx$ 1.15-1.20) particles ranging between 2 and 10 μm in diameter. A potential group of particles that fits the former group was measured by Koike et al. (1990) using epifluorescence microscopy and particle counting; they were described as small (<0.6 μm), nonliving particles with high water and organic material content. An association of submicron detrital particles with biological activity was suggested by Sieracki and Viles (1992) who measured a decrease in concentration below the sub-surface chlorophyll maximum. In addition, correlations have been observed between submicron particle concentrations and the concentrations of chlorophyll, bacteria, and heterotrophic nanoflagellates (Koike et al. 1990; Yamasaki et al. 1998). It has been hypothesized that submicron particles are directly produced by biological processes, including flagellates grazing on bacteria and viral lysis of bacteria (Koike et al. 1990; Nagata and Kirchman 1996; Shibata et al. 1997), and by physical forces contributing to disaggregation, flocculation and adsorption on surfaces (refs. in Stramski and Kiefer, 1991; reviewed by Nagata and Kirchman 1996). In contrast, Stramski et al. (2001) suggested the role

of a different group of particles of high refractive index in determining backscattering in the open ocean. In their simulations of oligotrophic waters, minerals were the most important determinant of backscattering, contributing ~80% to total b_b.

The roles of seawater constituents in determining AOPs can be better understood through simulations using radiative transfer theory. Radiative transfer numerical models provide a means to understand the effects of different seawater constituents on oceanic light fields. Hydrolight is a software package for solving the time-independent, depth-dependent radiative transfer equation and has been used in studies of spectral radiance distributions within and leaving natural water bodies (e.g. Mobley 1994; Mobley and Stramski 1997; Berwald et al. 1998; Lee et al. 1998; Mobley et al. 2002). Using Hydrolight and expected mean values for microbial properties, Mobley and Stramski (1997) simulated the effects of various particulate components on the quantities K_d and R_{rs}. They found that different microbial compositions in two water bodies can give considerably different optical properties, even for the same chlorophyll concentrations.

To interpret variability in AOPs of New England shelf waters, I have used Hydrolight and measurements to constrain the IOPs of optically important seawater constituents. Seawater constituents included in the analysis were water, dissolved materials, eukaryotic pico/nanophytoplankton, *Synechococcus*, heterotrophic bacteria, detritus, and minerals. Spectral absorption, scattering, and backscattering were determined for each particle group using Mie theory with inputs of size distribution and spectral n and n'. Absorption by eukaryotic phytoplankton and dissolved

118

materials accounted for most of the variability in K_d both within and between the summer and spring seasons. Differences in R_{rs} were explained by a combination of changes in absorption by eukaryotic phytoplankton, absorption by dissolved materials, backscattering by minerals, and backscattering by detritus. Improved techniques are needed for the measurement of submicron detrital and mineral particles, because these particles appear to be the main contributors to backscattering.

METHODS

Bulk Optical Measurements

Vertical profiles for water sampling and measurements of IOPs and AOPs were made as part of the CMO Experiment (Sosik et al. 2001). The CMO site is located on the southern New England shelf, south of Martha's Vineyard (40° 30' N, 70° 30' W), in a region known as the "Mud Patch" and has a water depth of ~70 m. Data was collected during two 3 week cruises in the late summer of 1996 aboard the R/V *Seward Johnson* (cruise SJ9610, 17 August - 7 September) and spring of 1997 aboard the R/V *Knorr* (cruise KN150, 24 April - 13 May). Profiles were carried out approximately three times per day during daylight hours at the main CMO site. Measurement of bulk IOPs, during in situ profiles using ac-9 meters and in the laboratory on discrete water samples using a spectrophotometer, was previously described in Chapter 3. Measurements of chlorophyll a and phaeopigment concentrations were made on discrete samples by collecting material on glass fiber filters (GF/F, Whatman), extracting for 24 hours in cold 90% acetone, and measuring

fluorometrically using a Turner Designs Model 10 fluorometer calibrated spectrophotometrically with pure chlorophyll a (Sigma Chemical Co.).

Apparent optical properties were measured with a tethered free-fall spectral radiometer (SPMR system, Satlantic, Inc.) at seven spectral wavelengths (412, 443, 490, 510, 555, 665, and 683 nm; spectral bandwidth, 10 nm) (for experimental details see Sosik et al., 2001). The SPMR system consisted of a profiler that measures downwelling irradiance (E_d), upwelling radiance (L_u), conductivity, temperature, pressure, and instrument tilt, as well as a reference sensor (SMSR) which floated just below the water surface (30 cm depth) and measured spectral E_d. Data from the spectral radiometers were processed using software provided by Satlantic, Inc. (ProSoft version 3.5d). All casts were edited to remove bad data at the top and bottom of the water column which could be recognized by high tilt and low velocity of the sensors, and were calibrated and averaged to 1-m bins over depth (z). Typically the top 5-6 m of data were eliminated from profiles based on these criteria (mean over both cruises was 5.8 m with standard deviation of 1.7 m). Depth-dependent diffuse attenuation coefficients for downwelling irradiance (K_d) were computed for each wavelength as $d\{\ln[E_d(z)]\}/dz$ (Smith and Baker 1984; Smith and Baker 1986) over 8 1-m depth bins; diffuse attenuation coefficients for upwelling radiance (K_u) were computed in an analogous manner with L_u substituted for E_d. Remote sensing reflectance (R_{rs}) was estimated as the ratio of water-leaving radiance to E_d just above the sea surface ($z = 0^+$); values at $z = 0^+$ were estimated by extrapolating from the top of the measured vertical L_u and E_d profiles to $z = 0^-$ using the shallowest K_d and K_u

estimates available for each cast, and then assuming Fresnel reflectance for the sea surface of 0.021 for L_u and 0.043 for E_d (Gordon et al. 1988; Mueller and Austin 1995).

Individual Particle Measurements and Theory

The contribution of particles (0.1-50 μm in size) to IOPs, including absorption, a, scattering, b, and backscattering, b_b, at 488 nm were computed using a combination of flow cytometry, Mie theory, and the extrapolation of size distributions for small particles (for details see Chapter 3). Five particle groups were measured in water samples using flow cytometry, including eukaryotic pico/nanophytoplankton ("eukaryotic phytoplankton"), *Synechococcus*, heterotrophic bacteria, detritus, and minerals. The FCM-Mie method was used to determine the particle properties (D, n, and n′) and optical cross-sections (σ_a, σ_b, and σ_{bb} at 488 nm) for particles in the diameter range of 0.75-10 μm, except for detritus which was measured in the size range of 1.2-10 μm. In addition, a combination of Mie theory, FCM measurements, and the extrapolation of size distributions for small particles were used to determine the contributions to IOPs by detritus and minerals in the size range of 0.1-0.75 and 0.1-1.2 μm, respectively, and by eukaryotic phytoplankton, detritus, and minerals in the size range of 10-50 μm. Particle sum contributions to a, b, and b_b at 488 nm were calculated by summing over the optical cross-sections, σ_a, σ_b, and σ_{bb}, of all particles (0.1-50 μm in size) in a known volume.

Radiative Transfer Modeling

The numerical model, Hydrolight version 4.1, was used to solve the radiative transfer equation and to generate values of diffuse attenuation, K_d, and remote sensing reflectance, R_{rs}. User-defined input to Hydrolight includes sea surface and bottom boundary conditions and the spectral IOPs of the water (Mobley 1994; Mobley and Stramski 1997). For all calculations, the same boundary conditions were used, including a wind speed of 5 m/s, a semi-empirical sky model (irradiances based on Gregg and Carder (1990) and radiances based on Harrison and Coombes (1988)), a solar zenith angle of 0° (sun directly overhead), and a bottom depth of 70 m. Calculations were made at 412, 440, 488, 510, 532, and 555 nm and at depth intervals of 10 m. Modeling was not performed at the higher wavelengths corresponding to SPMR measurements (i.e., 650, 676, and 715 nm), because the effects of chlorophyll and CDOM fluorescence were not included in the Hydrolight simulations. Total spectral IOPs for a, b, and b_b were input to Hydrolight, and spectral b and b_b were used by Hydrolight to determine the phase function. Values of IOPs were specified for the top 20 m of the water column (at 1, 10, and 20 m depth) and not below this depth, because my goal was to model AOPs for surface waters. Three examples were chosen from each season to exemplify within and between season differences in optical properties. All single particle and bulk optical data for each example was collected within two hours of local noon.

Total IOPs were defined as sums over the constituents of a natural sample. The total spectral absorption coefficient, $a_{total}(\lambda)$, was calculated as a sum of the

absorption by each of the constituents of water ($a_w(\lambda)$), dissolved materials ($a_g(\lambda)$), eukaryotic phytoplankton ($a_{euk}(\lambda)$), *Synechococcus* ($a_{syn}(\lambda)$), heterotrophic bacteria ($a_{bact}(\lambda)$), and non-phytoplankton ($a_{dm}(\lambda)$; detritus+minerals). Values of $a_w(\lambda)$ (assumed constant) were based on Pope and Fry (1997), and a_g was measured with the filtered ac-9. The total scattering and backscattering coefficients, $b_{total}(\lambda)$ and $b_{b,total}(\lambda)$, were defined as sums of the contributions by pure seawater and each particle group. Values of $b_w(\lambda)$ were based on Morel (1974), and $b_{b,w}(\lambda)$ were assumed to be half of $b_w(\lambda)$.

The spectral contributions of particles to IOPs were calculated using properties at 488 nm combined with Mie theory. Inputs to Mie theory included the particle size distribution from 0.1 μm to 50 μm, a wavelength-independent n equal to the FCM-Mie mean n for each particle group, and a wavelength-dependent n'. Mean values of n' at 488 nm for eukaryotic phytoplankton and *Synechococcus* were determined from the FCM-Mie method, and the value of n' at 488 nm for detritus and minerals was assumed to be 1×10^{-3}. The spectral shape of n' for phytoplankton and non-phytoplankton was based on average spectrophotometric measurements of $a_{ph}(\lambda)$ and $a_{dm}(\lambda)$ for the depth range of 0-20 m (Sosik et al. 2001) and was calculated using the equation $n'(\lambda) = a_s * \lambda / (4 * \pi * 1.339)$, where a_s is the absorption coefficient of the substance and λ is the wavelength of light in a vacuum. Spectral n' for heterotrophic bacteria was assumed equal to values presented in Stramski and Mobley (1997). Total absorption, scattering, and backscattering for each particle group was calculated using

the above inputs to Mie theory, with the exception of values for a_{dm}, for which

spectrophotometric measurements were used, because there was high uncertainty in

the determination of a_{dm} from the particle sum method (see Chapter 3).

RESULTS AND DISCUSSION

Spectral Variations in Measured K_d and R_{rs}

Differences in the magnitude and spectral shape of near-surface (<15 m) K_d

were evident between the seasons. At blue and green wavelengths, mean K_d values in

surface waters were higher in the spring (Fig. 1A-C). Because K_d is highly dependent

on absorption, an initial interpretation of variability in K_d can be made based on bulk

ac9 measurements of absorption. Higher total absorption, a_{total}, in the spring

accounted for values of K_d that were larger than in the summer at all wavelengths.

Compared to summer, spring surface waters had chlorophyll concentrations that were

~4x higher (mean of 1.8 mg m^{-3} vs. 0.50 mg m^{-3}) and particulate absorption, $a_p(440)$,

that was ~2x higher (mean of 0.085 m^{-1} vs. 0.035 m^{-1}). The standard errors for K_d

were also higher in the spring, due to more variability in a_{total} in spring surface waters

than in the summer. Absorption was less variable in summer surface waters, because

the water column was highly stratified, nutrient levels were low in the mixed layer,

and elevated phytoplankton concentrations were evident mid-water column but not in

surface waters. In comparison, in the spring, the water column was relatively well

mixed, nutrient levels were high in surface waters, and the onset of stratification was

associated with a phytoplankton bloom in surface waters. On April 30 (lowest spring

K_d) the water column was well mixed compared to on May 6 and 9, which followed the onset of stratification (Fig. 1C). May 6 (highest spring K_d) showed peak chlorophyll concentrations in surface waters, and by May 9 chlorophyll concentrations had begun to decrease again. There was a small but significant spectral shift toward enhanced blue relative to green attenuation in spring compared to summer. Mean ratios of $K_d(443):K_d(555)$ of 1.20 in the summer and 1.43 in the spring were reported by Sosik et al. (2001).

Differences in the magnitude and spectral shape of R_{rs} were also evident between the seasons. In the spring, surface waters were generally darker and greener, exemplified by R_{rs} values that were lower at blue wavelengths but slightly higher at 555 nm compared to the summer (Fig. 1D-F). Given that R_{rs} is determined primarily by the ratio of backscattering to absorption, $b_{b,total}:a_{total}$, it is difficult to make an initial interpretation of variability in R_{rs} based on bulk optical measurements, because bulk backscattering was not measured on the CMO cruises. Mean ratios of $R_{rs}(443):R_{rs}(555)$ of 1.62 in the summer and 0.90 in the spring were reported by Sosik et al. (2001), and the standard deviation of this ratio was ~2x higher in the spring. The greater variation observed in R_{rs} spectral shape in the spring was exemplified by the large difference among the April 30, May 6, and May 9 spectra (Fig. 1F). Despite these spectral differences, $R_{rs}(550)$ was always greater than $R_{rs}(412)$ in the spring, whereas in the summer $R_{rs}(550)$ was always less than $R_{rs}(412)$.

Constituent Inherent Optical Properties

Differences in the contributions of eukaryotic phytoplankton and dissolved materials were the main determinants of variability in a_{total} between seasons (Fig. 2A-F). Water was an important contributor to absorption in both seasons at wavelengths ≥ 488 nm. The contribution of a_w to a_{total} was more important in the summer when a_{total} was lower. Considering both seasons, a_{euk} was the most variable contributor to a_{total}, followed by a_g. Values of a_{total} were always higher in the spring than in the summer, due primarily to a_{euk} which was ~5x higher and secondarily to a_g which was ~1.5x higher. Values of a_{euk} were maximal at 440 nm in all cases, as expected for phytoplankton based on previous studies (e.g. Sathyendranath et al. 1987). In the summer examples, the contribution of a_{euk} to a_{total} decreased with time and was the lowest on August 26. In the spring, the contribution of a_{euk} to a_{total} increased following the onset of stratification and was the highest on May 6 when a_{euk} was an important contributor to a_{total} at all wavelengths. Absorption by dissolved materials, a_g, decreased with increasing wavelength and was a larger fraction of a_{total} in the summer when values of a_{total} were lower than in the spring. The absolute magnitude of a_g was smaller in summer surface waters compared to the spring ($a_g(412) = 0.073$ vs. 0.11), however, most likely because of photooxidation of dissolved materials in summer surface waters as has previously been suggested for this region (Vodacek et al. 1997; Boss et al. 2001). Absorption by non-phytoplankton, a_{dm}, increased with decreasing wavelength, as expected for particulate detritus (Roesler et al. 1989), and contributions to a_{total} at 412 nm ranged from 9-14% in both seasons. The absorption contributions of

heterotrophic bacteria and *Synechococcus* were negligible in both seasons, with each group contributing ≤1% at all wavelengths.

Eukaryotic phytoplankton were the most important contributor to b_{total} in both seasons (Fig. 3A-F). The contribution of b_{euk} to b_{total} was 45-69%, considering both seasons and all wavelengths. The spectral shape of b_{euk} was generally the inverse of the spectral shape of a_{euk}, as expected based on previous work (Ahn et al. 1992). This was a direct outcome of the calculation of b_{euk} from Mie theory using inputs of n' with the spectral shape of a_{euk} and n assumed spectrally constant. Detritus was more important to b_{total} in the summer than in the spring, with contributions of 16-23% in the summer and 9-18% in the spring, considering all wavelengths. In contrast, minerals were more important to b_{total} in the spring than in the summer, with contributions of 9-15% in the summer and 15-24% in the spring. Heterotrophic bacteria contributed ≤12% to b_{total} in both seasons. *Synechococcus* and water were minor contributors to b_{total}, contributing <5% and <3%, respectively in either season and at all wavelengths.

Differences in the contributions of detritus and minerals were the main determinants of variability in $b_{b,total}$ between seasons (Fig. 4 A-F). The magnitudes of $b_{b,total}$ were similar for both seasons, betweeen 0.003-0.008, and were within the range of 0.001-0.02 previously reported for bulk optical measurements of natural samples (Stramski et al. 1999; Balch et al. 2001; Reynolds et al. 2001; Twardowski et al. 2001). Total backscattering, $b_{b,total}$, increased with decreasing wavelength, mainly due

to the importance of $b_{b,w}$ at blue wavelengths. Water contributed ~50% to $b_{b,total}$ at 412 nm and ~25% to $b_{b,total}$ at 555 nm in both seasons. Detritus was more important in the summer than in the spring, contributing 20-45% to $b_{b,total}$ in the summer and ≤12% in the spring. Minerals were equal to or less important than detritus in the summer and contributed 15-35% to $b_{b,total}$. In contrast, in the spring, minerals were the most important particulate contributor to $b_{b,total}$ and their contribution increased with time, contributing 30-60% overall. Spectral $b_{b,det}$ in the summer increased with decreasing wavelength, and spectral $b_{b,min}$ in both the summer and spring was relatively flat compared to results of Stramski et al (2001) showing both $b_{b,min}$ and $b_{b,det}$ increasing with decreasing wavelength. The contributions of microbes were generally small with eukaryotic phytoplankton and heterotrophic bacteria each contributing ≤9% to $b_{b,total}$ in both seasons, and *Synechococcus* contributing <1%.

The size distributions of detritus and minerals exemplify the relative importance of the different non-phytoplankton types and size classes to backscattering. Detritus were important contributors to $b_{b,total}$ in the summer but not in the spring, because small detritus (≤1.2 µm) were more abundant in the summer (Fig. 5A-D). Small detritus contributed >50% to $b_{b,total}$ in the summer, whereas larger detritus contributed only 3%. The abundance of small detritus in the spring was higher on April 30 than on May 6 or 9, though not as high as in the summer. Correspondingly, small detritus contributed a higher percentage to $b_{b,total}$ on April 30 (~16%) compared to the other spring examples (~1%). The importance of small detritus in the summer

caused spectral $b_{b,det}$ and particle backscattering, $b_{b,p}$, to increase with decreasing wavelength (Figs. 4A-C, 6A). In contrast to detritus, minerals were important contributors to $b_{b,total}$ in both seasons, due to the abundances and contributions of both small (≤ 0.75 μm) and large (0.75-50 μm) minerals. Small and large minerals contributed 29% and 14%, respectively, to $b_{b,total}$ in the summer and 43% and 43%, respectively, to $b_{b,total}$ in the spring. The contribution of large minerals was the cause of spectral $b_{b,min}$ that were relatively flat in both seasons (Fig. 4) and $b_{b,p}$ that was relatively flat in the spring (Fig. 6A). Higher backscattering ratios, $b_{b,p}/b_p$, were observed in the summer (Fig. 6B) and were the result, not of differences in the magnitude of $b_{b,p}$, but of lower total scattering, b_{total}, in the summer, mainly caused by lower values of b_{euk} than in the spring. Higher summer ratios of $b_{b,p}/b_p$ when chlorophyll concentrations were lower is consistent with previous findings of an inverse relationship between $b_{b,p}/b_p$ and chlorophyll concentration (e.g. Sathyendranath et al. 1989; Ulloa et al. 1994).

Comparison of Modeled and Measured K_d and R_{rs}

Modeled values of K_d, using Hydrolight with spectral IOPs as input, compared well with measured values of K_d in both magnitude and spectral shape (Fig. 6 A-F). Modeled values were slightly higher than measurements by a mean of 0.013 in the summer (considering all wavelengths), a difference of 15% from measurements, and were slightly lower by a mean of 0.018 in the spring, a difference of 10% from measurements. The modeled spectral K_d were similar in shape to measured K_d.

Values of $K_d(440){:}K_d(555)$ were always higher in the summer than in the spring with

mean ratios of 1.29 and 1.07 for modeled and measured values in the summer,

respectively, and 1.58 and 1.43 for modeled and measured values in the spring,

respectively. Modeled ratios of $K_d(440){:}K_d(555)$ tended to be higher than measured

values, possibly because values of a_{euk} at 488 nm underestimated actual values by

about 13% as reported in Chapter 3, and higher a_{euk} would be relatively higher at blue

relative to green wavelengths.

Modeled values of R_{rs}, using Hydrolight with spectral IOPs as input, were

similar to measured values of R_{rs} in both magnitude and spectral shape (Fig. 7 A-F).

In the summer, modeled values differed from measurements by a mean of 2.4×10^{-4}

(considering all wavelengths and absolute values of differences), a difference of 11%

from measurements, and in the spring, modeled values were different from

measurements by a mean of 3.1×10^{-4}, a difference of 15% from measurements. The

modeled spectral R_{rs} were similar in shape to measured R_{rs}. Both the modeled and

measured R_{rs} exhibited the same trends of higher values of $R_{rs}(440){:}R_{rs}(550)$ in the

summer than in the spring, with values >1 in the summer and <1 in the spring. Values

of modeled and measured $R_{rs}(440){:}R_{rs}(550)$ were 1.31 and 1.84, respectively, in the

summer and 0.80 and 0.90, respectively, in the spring. The generally lower modeled

ratios of R_{rs} compared to measured ratios, especially in the summer, might also be

attributed to the slightly underestimated values of a_{euk} and/or to errors in the modeling

of small detrital and mineral particles. However, the generally good agreement

between modeled and measured magnitudes and spectral shapes for both R_{rs} and K_d

justifies applying the Hydrolight analyses with inputs of constituent IOPs to the interpretation of variability in AOPs measured during both seasons.

Sources of Variability in K_d and R_{rs}

Differences in K_d between seasons was caused by variability in absorption by eukaryotic phytoplankton and dissolved materials. As discussed above, a_{euk} and a_g were the most important contributors to variability in a_{total}. The roles of a_{euk} and a_g in determining variability in K_d between seasons were determined by performing two Hydrolight substitution simulations for the spring examples with: (1) a_{euk} replaced by mean summer values, and (2) both a_{euk} and a_g replaced by mean summer values. From this analysis, it is clear that the higher magnitude of K_d at all wavelengths in the spring was caused primarily by higher values of a_{euk} and secondarily by higher values of a_g especially at 412 nm (Fig. 9). This is consistent with the finding of Sosik et al. (2001) that absorption by particles, a_p, was more important than a_g in determining variability in K_d in both seasons but that a_g was significant in magnitude, especially at 412 nm. There was a spectral shift toward enhanced blue relative to green attenuation in the spring primarily because phytoplankton absorb more at blue than at green wavelengths. Substitution of a_{euk} by its mean value removed most of the difference in spectral shape between seasons, resulting in a ratio of $K_d(440):K_d(555)$ in the spring of 1.34, similar to the summer value of 1.29. The residual difference in K_d at 412 nm, after substitution with summer a_{euk}, was due to higher values of a_g in the spring compared to summer.

Variations in K_d during the summer were caused by changes in both a_{euk} and a_g, and variations during the spring were mainly caused by changes in a_{euk}. During the summer, values of a_g and a_{euk} were approximately equally variable, with standard deviations of 0.01 and 0.006, respectively, at 412 nm for the three samples. Values of K_d were highest on August 22, because both a_{euk} and a_g were the highest of the three samples. Values of K_d on August 20 and 26 were approximately the same, because a_{total} was about the same. However, a_{euk} comprised relatively more of a_{total} on August 20, and a_g comprised relatively more of a_{total} on August 26. Variability in a_g in the summer was most likely related to both the periodic intrusions of oceanic warm salty water, as occurred on August 22, and to vertical displacements of the pycnocline by Rossby or Kelvin waves as suggested by Boss et al. (2001). In contrast to the summer, spring values of a_g were less variable than a_{euk}, with standard deviations of 0.008 and 0.03, respectively, at 412 nm for the three samples. Changes in K_d in the spring were directly related to changes in a_{euk}. Values of K_d and a_{euk} measured on April 30 (prior to the onset of stratification) were the lowest of the three examples (Figs. 2D-F and 7D-F). Higher values of K_d were measured following the onset of stratification with the highest value on May 6 when chlorophyll concentrations and a_{euk} were the highest, and lower values of K_d were measured on May 9 when chlorophyll concentrations and a_{euk} had begun to decrease.

Differences in R_{rs} between seasons were caused by variability in constituent contributions to spectral absorption and backscattering. As described above, a_{euk}, a_g, $b_{b,min}$, and $b_{b,det}$ were the most important contributors to variability in a_{total} and $b_{b,total}$.

The roles of a_{euk}, a_g, $b_{b,det}$, and $b_{b,min}$ in determining variability in R_{rs} between seasons were determined by performing three Hydrolight substitution simulations for the spring examples with: (1) a_{euk} replaced by mean summer values, (2) both a_{euk} and a_g replaced by mean summer values, and (3) all of a_{euk}, a_g, $b_{b,det}$, and $b_{b,min}$ replaced by mean summer values (Fig. 10A). Each substitution accounted for ~1/3 of the difference in the ratio of $R_{rs}(440):R_{rs}(555)$ between seasons, with ratios of 1.00, 1.14, and 1.32 following each substitution, respectively (Fig. 10B). The ratio for the third simulation was nearly the same as the summer value of 1.31. Notably, higher values of both a_{euk} and a_g in the spring compared to summer were enough to account for a ratio of $R_{rs}(440):R_{rs}(555)$ which was <1 in spring and >1 in summer. Spectral differences in particle backscattering, $b_{b,p}$, also contributed to summer values of R_{rs} which were higher at blue wavelengths and lower at green wavelengths. The magnitudes of $b_{b,p}$ were similar between seasons, however, spectral $b_{b,p}$ had a higher inverse wavelength dependence in the summer than in the spring (Fig. 6A). This result is consistent with the prediction of Sosik et al. (2001) that $b_{b,p}$ had to differ between the two seasons in order to account for the larger difference observed between $R_{rs}(443)/R_{rs}(555)$ and $K_d(555)/K_d(443)$ in the summer than in the spring. Specifically, the authors predicted that a steeper inverse wavelength dependence and/or higher backscattering efficiency existed for smaller particles in the summer. In concurrence with both predictions, a steeper inverse wavelength dependence of $b_{b,p}$ and higher ratios of $b_{b,p}/b_p$ were observed in the summer (Fig. 6A-B).

Spectral variations in R_{rs} were small in the summer and higher in the spring caused mainly by variability in a_{euk} and $b_{b,min}$. The spectral shape of R_{rs} on April 30 was significantly different than on May 6 and May 9, with ratios of $R_{rs}(443){:}R_{rs}(555)$ of 1.00, 0.71, and 0.67, respectively. Values of a_{total} and $b_{b,min}$ were the lowest on April 30. The roles of a_{euk} and $b_{b,min}$ in determining variability between April 30 and May 6/9 was determined by performing two Hydrolight simulations for April 30 with: (1) a_{euk} replaced by mean May 6/9 values, and (2) both a_{euk} and $b_{b,min}$ replaced by mean May 6/9 values. Substitution of a_{euk} lowered the ratio of $R_{rs}(443){:}R_{rs}(555)$ from 1.00 to 0.85, and substitution of both a_{euk} and $b_{b,min}$ resulted in a ratio of 0.75, which is similar to the ratios for May 6/9. Thus, changes in both a_{euk} and $b_{b,min}$ were responsible for variability in the spectral shape of R_{rs} in the spring.

Application of Bio-Optical Models

The magnitude of b_b in the summer in New England shelf waters was underestimated by current bio-optical models, however, the spectral shape in both the summer and spring generally agreed with model estimates. Use of a typical bio-optical model for b_b for case 1 waters (Morel and Maritorena 2001) resulted in the underestimation of b_b by ~40% at 488 nm in the summer and the slight overestimation of b_b by 16% in the spring (Fig. 11A). Higher values of b_b in the summer compared to model estimates were caused both by higher backscattering efficiencies and higher scattering for non-phytoplankton than were assumed by the model. Concentrations of small detrital particles in the summer were higher than modeled concentrations of non-

phytoplankton, which is not unreasonable considering the differences between continental shelf and Case 1 waters. Typically, bio-optical models of R_{rs} consider ratios of b_b at two wavelengths, $b_b(443):b_b(555)$, thus avoiding errors in magnitude at one wavelength. In fact, ratios of $b_b(443):b_b(555)$ in both the summer and spring compared fairly well with modeled values (Fig. 11B). The modeled increase in the backscattering ratio with decreasing chlorophyll concentration, reflected in the summer and spring data, is based on the observation that particles are relatively smaller in low chlorophyll waters (Sathyendranath et al. 1989; Ulloa et al. 1994).

Ratios of $R_{rs}(443):R_{rs}(555)$ estimated from a bio-optical model were higher than measured ratios in the spring and summer, mainly because of the underestimation of the contributions by dissolved materials. Using a typical bio-optical model for Case 1 waters (Prieur and Sathyendranath 1981; Morel and Maritorena 2001) resulted in mean overestimates in $R_{rs}(443):R_{rs}(555)$ of 45 and 20% for the spring and summer, respectively (Fig. 12). The differences between measured and modeled values of this R_{rs} ratio were caused by assumptions about absorption by dissolved materials. In the present bio-optical model, $a_g(440)$ was assumed to be a constant fraction (0.2) of the absorption due to both water and particles (Prieur and Sathyendranath 1981). In contrast, measured values of this fraction were higher during both seasons, with means of 1.32 in the summer and 0.67 in the spring. When the measured ratio for each season was substituted into the model of $a_g(440)$, the measured relationships between chlorophyll concentration and $R_{rs}(440):R_{rs}(555)$ in both seasons were close to modeled values (Fig. 12). The finding that differences in the relationship between a_g and

absorption by phytoplankton were a source of significant error in bio-optical models of R_{rs} has been emphasized in recent reviews (Morel and Maritorena 2001; Sathyendranath et al. 2001). With measured ratios for $a_g(440)$ substituted into the models, the magnitude of $R_{rs}(440)$ was well estimated in the spring but was underestimated in the summer by ~40%, a direct result of the underestimate of b_b for non-phytoplankton in the summer.

CONCLUSIONS

Based on the present modeling, spectral eukaryotic phytoplankton absorption, dissolved absorption, mineral backscattering, and detrital backscattering were the most important contributors to variability in AOPs both within and between seasons at our study site in New England continental shelf waters. Surface water values of K_d, a_{euk}, and a_g were higher in the spring due to less stratification than in the summer, with higher nutrients in spring surface waters available for phytoplankton growth and greater mixing minimizing the effects of photooxidation on a_g. In addition to differences in absorption, values of R_{rs} were impacted by differences in the spectral shape of $b_{b,total}$, due to the high abundance of submicron detritus in the summer and the abundance at all size ranges of minerals in both seasons. Of the four important IOPs, a_{euk} and a_g were known with the most confidence, given that a_{euk} compared well with measured spectrophotometric values (see Chapter 3) and a_g was directly measured using an ac-9. In contrast, my method for measuring the contributions of detritus and minerals to backscattering were dependent on the extrapolation of their submicron size

distributions, a size range that was important to backscattering. Future modeling of detrital and mineral backscattering would benefit from concurrent measurements of bulk backscattering (Maffione and Dana 1997), improved methods for optical characterization of submicron non-phytoplankton particles, and spectral Mie modeling to include the distributions of n for particles, especially for minerals which have a broader range of n than do organic particles. In spite of these suggestions for future research, my results strongly suggest that seasonal differences in the spectral shape of R_{rs} in New England coastal waters are affected by differences in the size distributions, abundance, and type of non-phytoplankton particles. An important example of this was the effect of a higher abundance of submicron detrital particles in the late summer surface waters.

The type of modeling presented in this chapter using Hydrolight and constituent IOPs provides a powerful means for separating and understanding the effects of the different seawater constituents on oceanic light fields, of particular importance to bio-optical (or ocean color) algorithms. Recently, revised bio-optical algorithms have been proposed for the determination of chlorophyll concentration from remote sensing reflectance (Morel and Maritorena 2001; Sathyendranath et al. 2001). These algorithms rely on the modeling of phytoplankton absorption, non-phytoplankton absorption, dissolved absorption, and particulate backscattering in terms of chlorophyll concentration. In application of the Morel and Maritorena (2001) model, $b_b(443)$ and $R_{rs}(443)$ were underestimated in the summer in New England shelf waters, and $R_{rs}(443):R_{rs}(555)$ was overestimated in both the summer and the spring.

The work presented here shows that, particularly for coastal waters, the greatest improvements to such models are needed in the modeling of dissolved absorption, and more importantly in the determination of particulate backscattering which remains poorly characterized for marine particles.
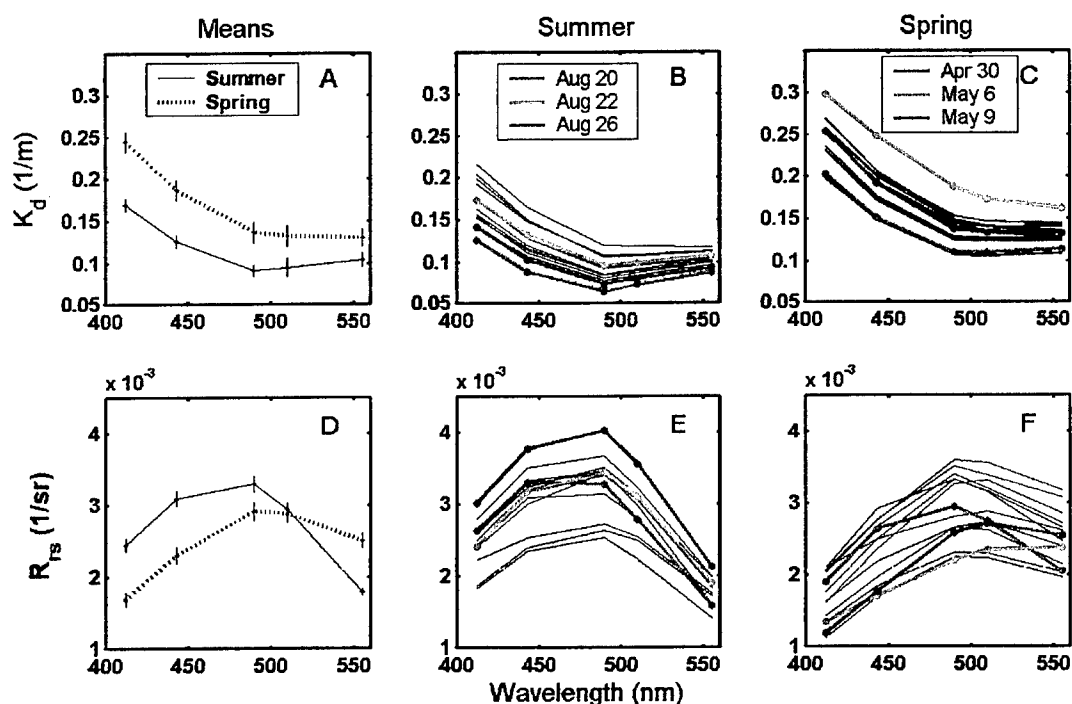
Figure 1. Measured values of near-surface (<15 m) diffuse attenuation, K_d, (A) spectral means for each season, (B) summer spectra, and (C) spring spectra, and measured values of remote sensing reflectance, R_{rs}, (D) spectral means for each season, (E) summer spectra, and (F) spring spectra. Standard errors are plotted for each mean spectrum. Three example spectra were chosen from each of the summer and spring season to exemplify within and between season differences in optical properties and have been highlighted.
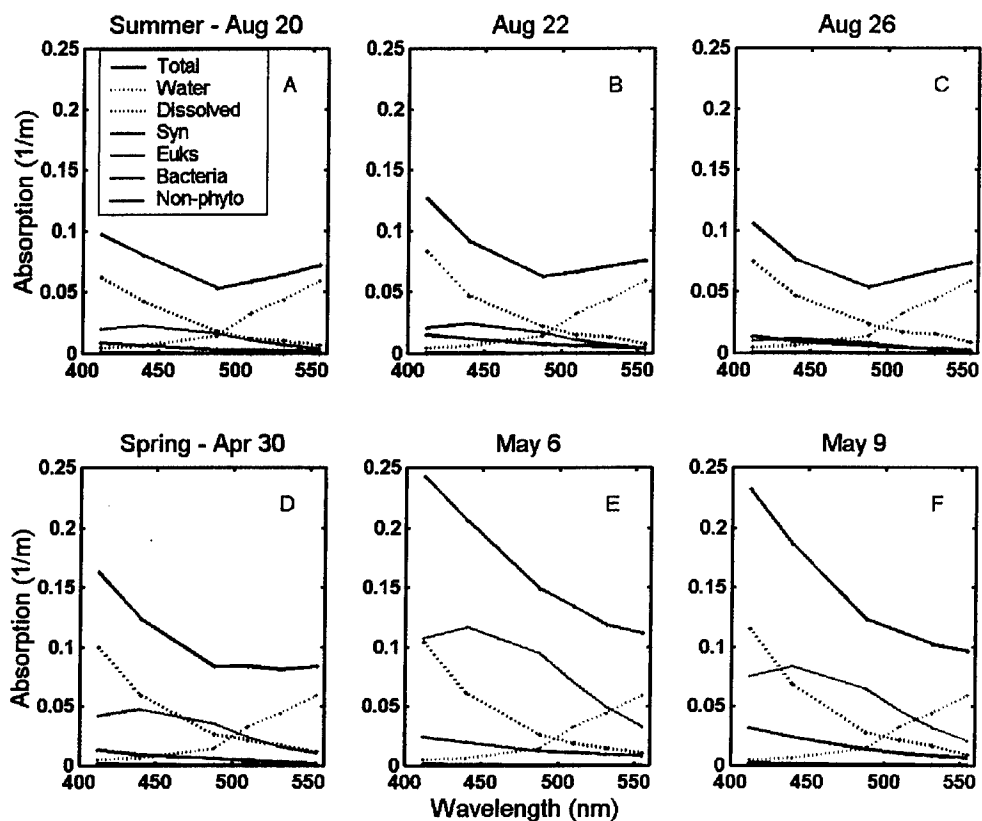
Figure 2. Total and constituent absorption spectra for (A-C) each of the three summer examples and (D-F) each of the three spring examples. Notably, there is a significant difference in absorption by eukaryotic phytoplankton, a_{euk}, between the two seasons.
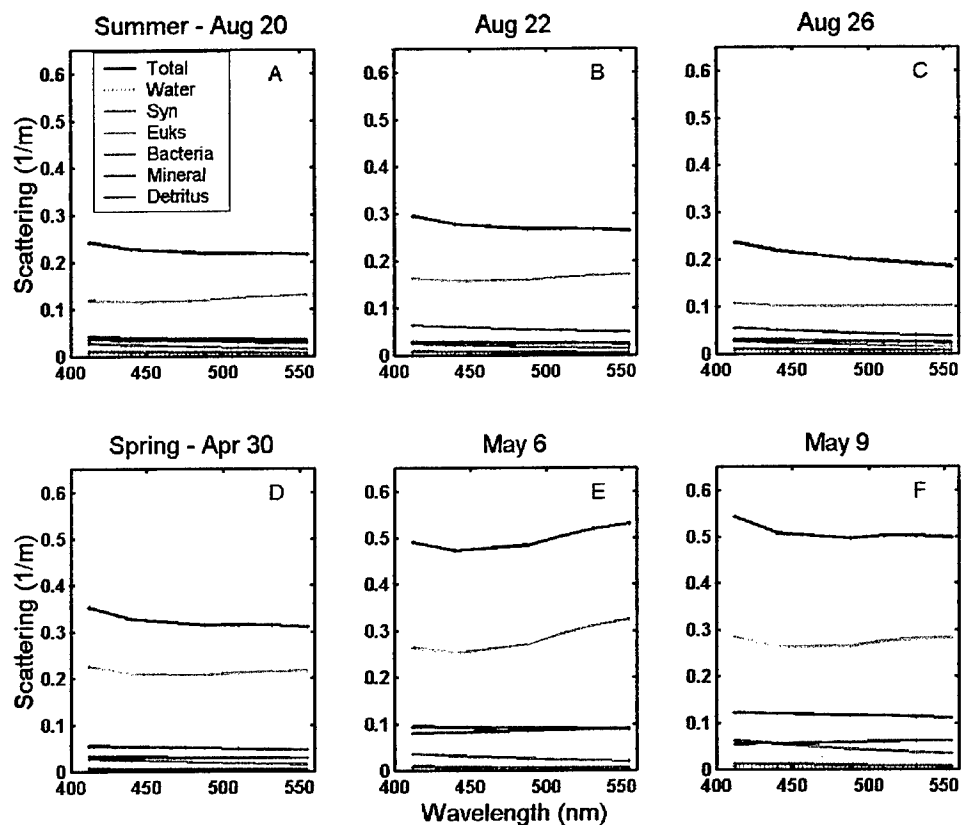
Figure 3. Total and constituent scattering spectra for (A-C) each of the three summer examples and (D-F) each of the three spring examples. Eukaryotic phytoplankton, detritus, and minerals were generally the most important contributors to b_{total}.
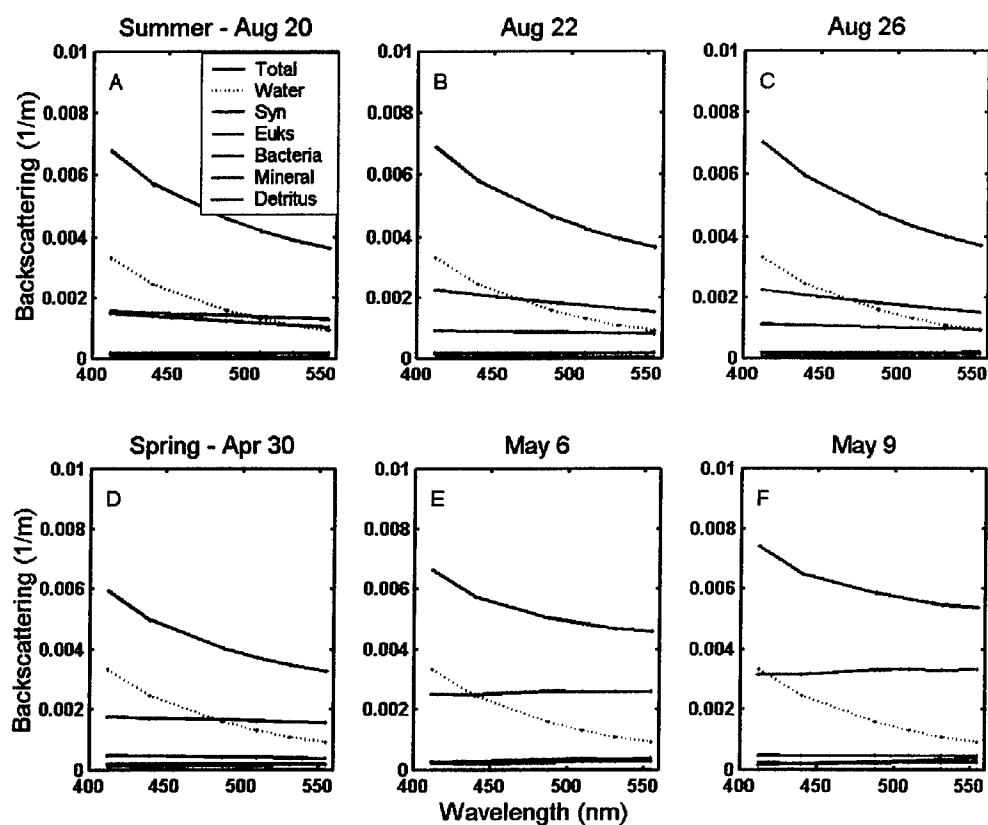
Figure 4. Total and constituent backscattering spectra for (A-C) each of the three summer examples and (D-F) each of the three spring examples. Minerals and detritus are the most important contributors to backscattering in the summer, in comparison to the spring during which minerals were most important.
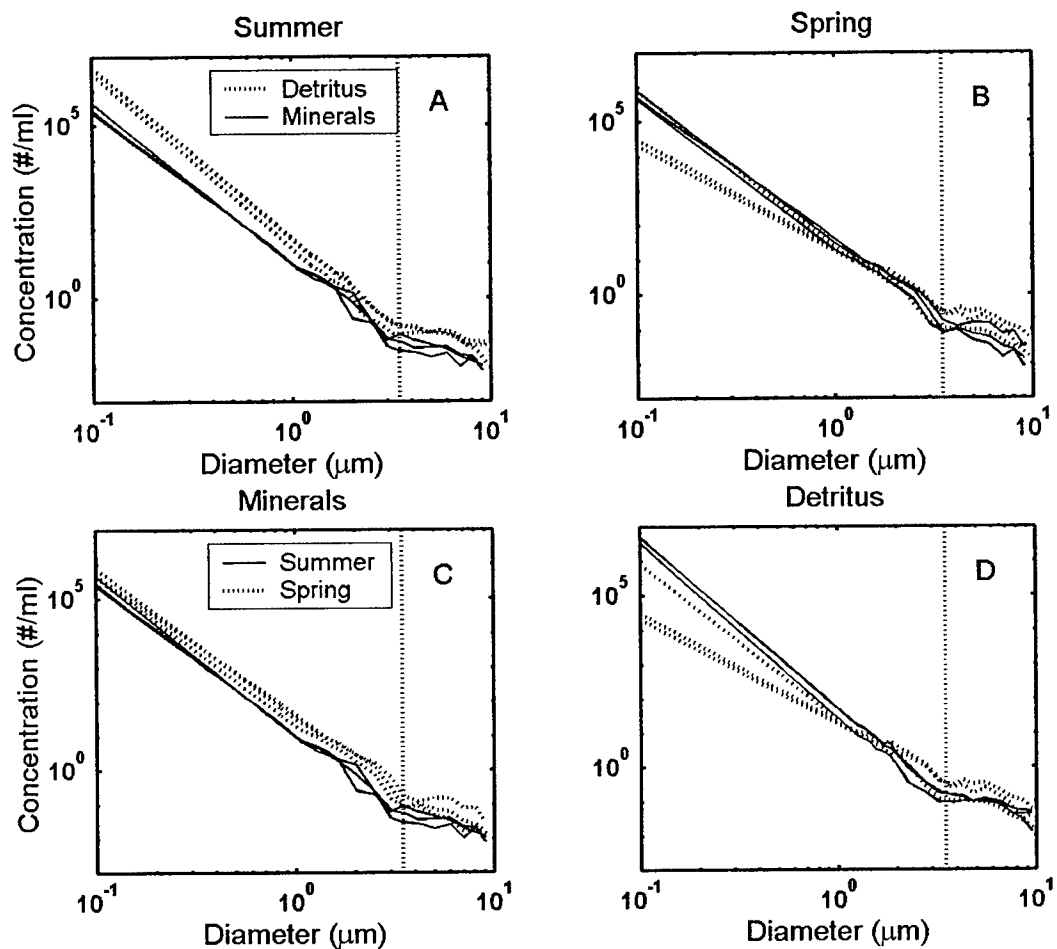
Figure 5. Size distributions of detritus and minerals for the (A) summer examples and (B) spring examples, and size distributions for both seasons of (C) minerals and (D) detritus. Total size distributions contain the portion determined from the FCM-Mie method and the portion extrapolated using the <3.5 μm Junge slopes. Note that the small detrital slope on April 30 is higher than on May 6 and May 9 but is not as high as in the summer.
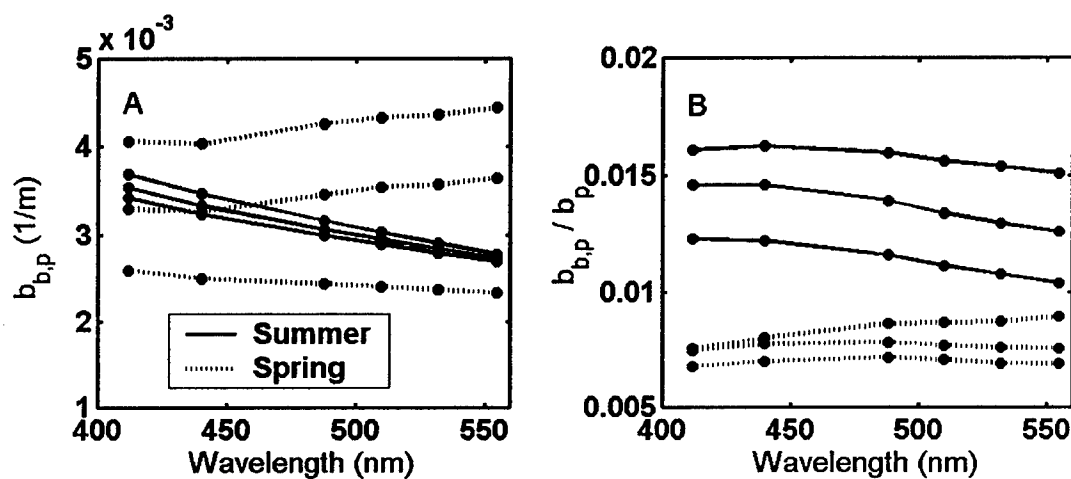
Figure 6. Summer and spring spectra of (A) particle backscattering, $b_{b,p}$, and (B) the ratio of particle backscattering to particle scattering, $b_{b,p}/b_p$. Steeper negative slopes of $b_{b,p}$ are caused by size distributions with relatively more small particles, as occurred in the summer relative to the spring. Higher ratios of $b_{b,p}/b_p$ in the summer were caused by lower values of b_p in the summer, with values of $b_{b,p}$ similar between the two seasons.
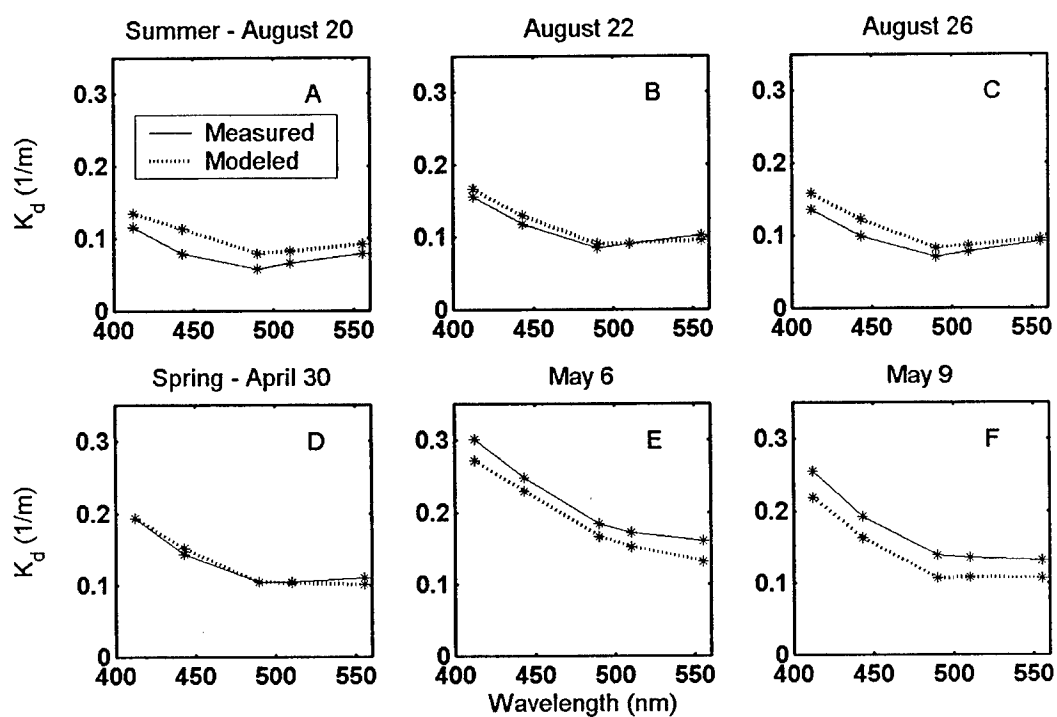
Figure 7. Spectra of measured and modeled diffuse attenuation, K_d, for (A-C) the summer examples and (D-F) the spring examples.
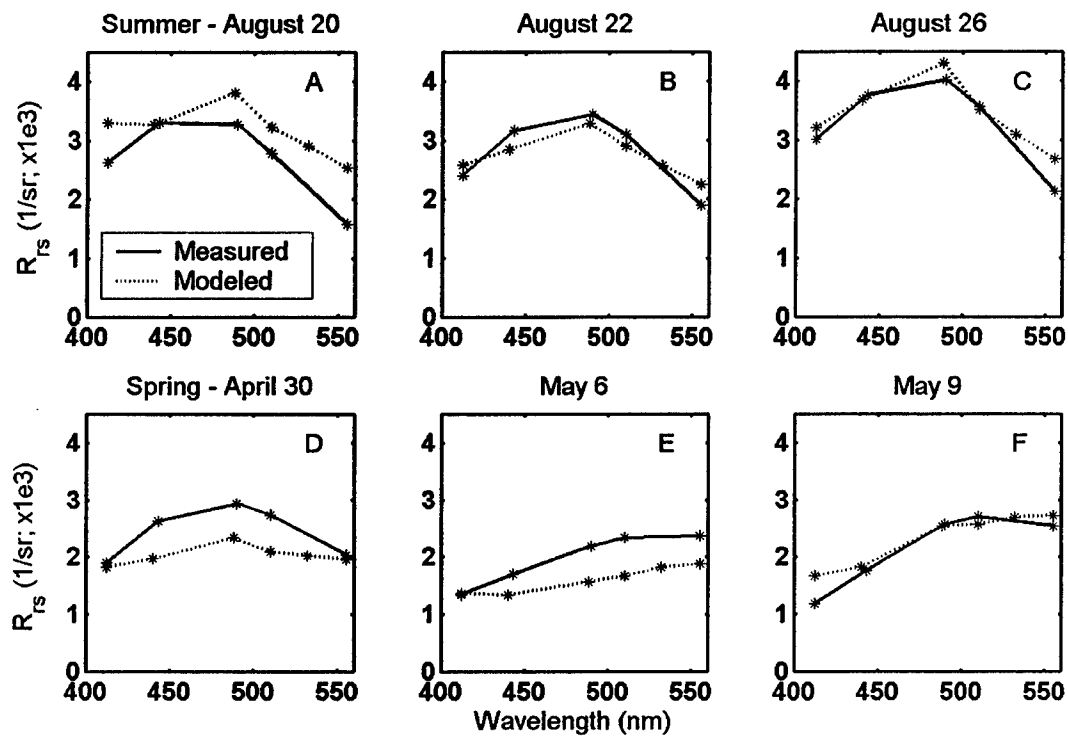
Figure 8. Spectra of measured and modeled remote sensing reflectance, R_{rs}, for (A-C) the summer examples and (D-F) the spring examples.
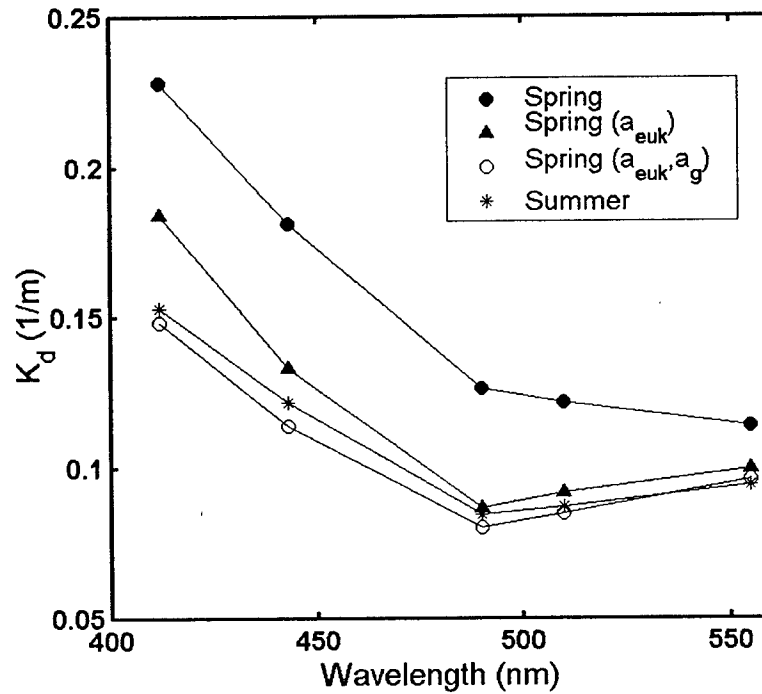
Figure 9. Mean spectra of modeled diffuse attenuation, K_d, for the summer and spring examples. Cases are shown for the actual mean K_d spectra for each season and for substitution simulations for the spring examples (noted in parantheses in legend) with spring eukaryotic phytoplankton absorption, a_{euk}, replaced by mean summer values, and both of spring a_{euk} and dissolved absorption, a_g, replaced by mean summer values. Notably, the ratio $K_d(440):K_d(555)$ is more similar between the summer and spring cases when spring a_{euk} is substituted with the mean summer value. The residual difference at 412 nm after substitution of a_{euk} is accounted for by a_g with higher values in the spring than in the summer.
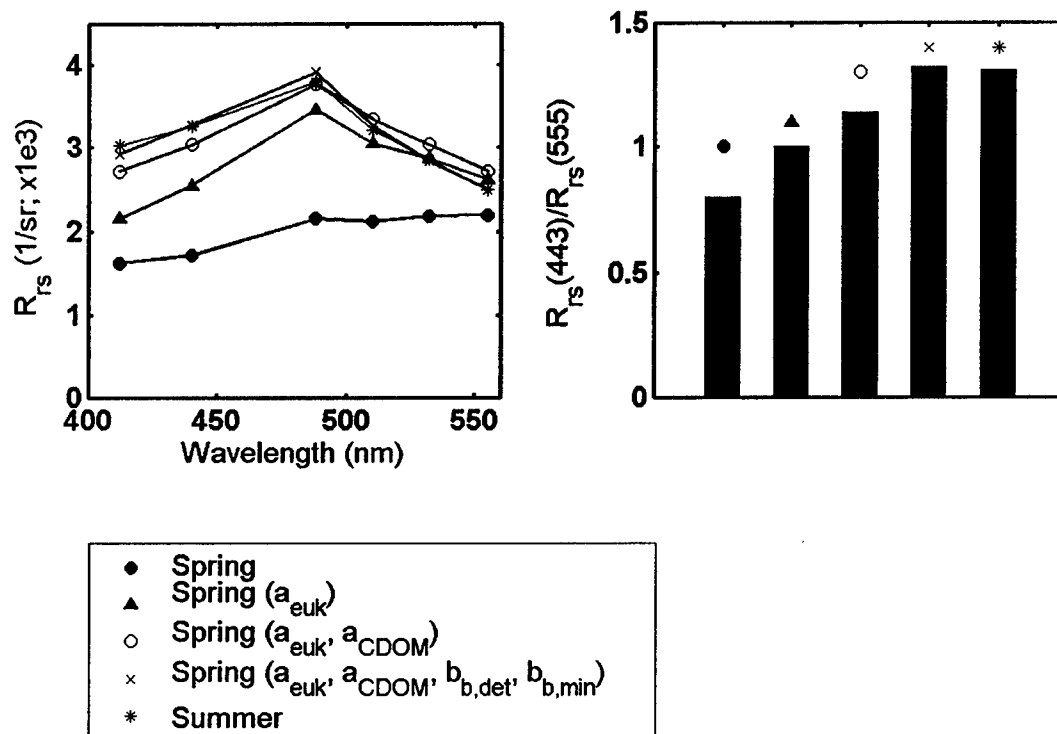
147

Figure 10. Mean spectra of (A) modeled remote sensing reflectance, R_{rs}, and mean ratios of (B) $R_{rs}(443){:}R_{rs}(555)$ for summer and spring examples. In panel A, cases are shown for the actual mean R_{rs} spectra for each season and for substitution simulations for the spring examples (noted in parantheses in legend) with spring a_{euk} replaced by mean summer values, both spring a_{euk} and a_g replaced by mean summer values, and all of spring a_{euk}, a_g, $b_{b,det}$, and $b_{b,min}$ replaced by mean summer values.
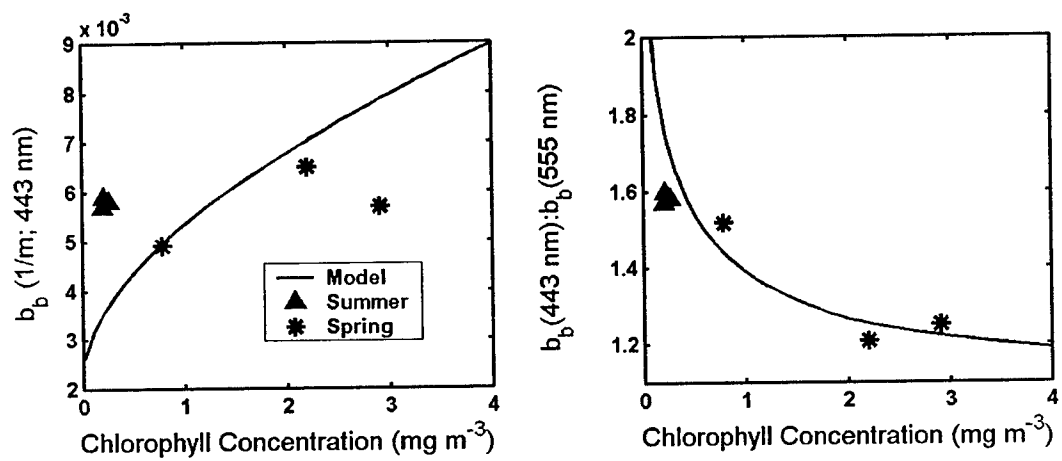
Figure 11. Comparison of bio-optical estimates and summer and spring values of (A) $b_b(443)$ and (B) $b_b(443):b_b(555)$.
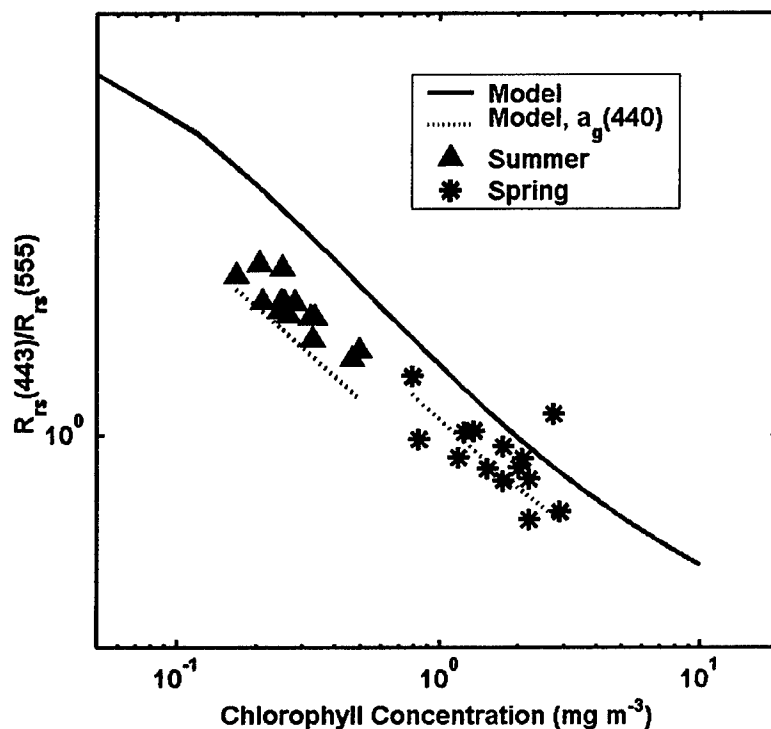
Figure 12. Comparison of the reflectance ratio, $R_{rs}(443):R_{rs}(555)$, at different chlorophyll concentrations measured during the summer and spring and estimated using a bio-optical model. Results are shown both for the typical bio-optical model ("Model"), with its assumption of $a_g(440)$ equal to 20% of the sum of absorption by water and particles, and for the bio-optical model with the measured percentages of $a_g(440):(a_w(440)+a_p(440))$ in the summer and spring substituted into the model ("Model, $a_g(440)$").

REFERENCES

Ahn, Y.H., A. Bricaud, and A. Morel. 1992. Light backscattering efficiency and related properties of some phytoplankters. Deep-Sea Res. **39**: 1835-1855.

Balch, W.M., D.T. Drapeau, J.J. Fritz, B.C. Bowler, and J. Nolan. 2001. Optical backscattering in the Arabian Sea - continuous underway measurements of particulate inorganic and organic carbon. Deep-Sea Res. I **48**: 2423-2452.

Berwald, J., D. Stramski, C. Mobley, and D. Kiefer. 1998. Effect of Raman scattering on the average cosine and diffuse attenuation coefficient of irradiance in the ocean. Limnol. Oceanogr. **43**: 564-576.

Boss, E., W.S. Pegau, J.R.V. Zaneveld, and A.H. Barnard. 2001. Spatial and temporal variability of absorption by dissolved material at a continental shelf. J. Geophys. Res. **106**: 9499-9507.

Garver, S., and D. Siegel. 1997. Inherent optical property inversion of ocean color spectra and its biogeochemical interpretation 1. Time Series from the Sargasso Sea. J. Geophys. Res. **102**: 18607-18625.

Gordon, H.R., O.B. Brown, R.H. Evans, J.W. Brown, R.C. Smith, K.S. Baker, and D.K. Clark. 1988. A semianalytic radiance model of ocean color. J. Geophys. Res. **93**: 10909-10924.

Gordon, H.R., O.B. Brown, and M.M. Jacobs. 1975. Computed relationships between the inherent and apparent optical properties of a flat homogeneous ocean. Appl. Opt. **14**: 417-427.

Gordon, H.R., and A. Morel. 1983. Remote assessment of ocean color for interpretation of satellite visible imagery - A review. Springer-Verlag.

Gregg, W.W., and K.L. Carder. 1990. A simple spectral solar irradiance model for cloudless maritime atmospheres. Limnol. Oceanogr. **35**: 1657-1675.

Harrison, A.W., and C.A. Coombes. 1988. An opaque cloud cover model of sky short wavelength radiance. Solar Energy **41**: 387-392.

Koike, I., S. Hara, K. Terauchi, and K. Kogure. 1990. Role of sub-micrometre particles in the ocean. Nature **345**: 242-244.

Lee, Z., K. Carder, C. Mobley, R. Steward, and J. Patch. 1998. Hyperspectral remote sensing for shallow waters. I. A semianalytical model. Appl. Opt. **37**: 6329-6338.

Maffione, R.A., and D.R. Dana. 1997. Instruments and methods for measuring the backward-scattering coefficient of ocean waters. Appl. Opt. **36**: 6057-6067.

Mobley, C.D. 1994. Light and water; radiative transfer in natural waters. Academic Press, Inc.

Mobley, C.D., and D. Stramski. 1997. Effects of microbial particle on oceanic optics: Methodology for radiative transfer modeling and example simulations. Limnol. Oceanogr. **42**: 550-560.

Mobley, C.D., L.K. Sundman, and E. Boss. 2002. Phase function effects on oceanic light fields. Appl. Opt. **41**: 1035-1050.

Morel, A. 1974. Optical properties of pure water and pure seawater, p. 1-24. *In* N. G. Jerlov and E. S. Nielsen, [eds.]. Optical aspects of oceanography. Academic.

Morel, A., and S. Maritorena. 2001. Bio-optical properties of oceanic waters: A reappraisal. J. Geophys. Res. **106**: 7163-7180.

Morel, A., and L. Prieur. 1977. Analysis of variations in ocean color. Limnol. Oceanogr. **22**: 709-722.

Mueller, J.L., and R.W. Austin. 1995. Ocean optics protocols for SeaWiFS validation, revision 1. In *NASA Technical Memorandum*.

Nagata, T., and D.L. Kirchman. 1996. Roles of submicron particles and colloids in microbial food webs and biogeochemical cycles within marine environments. Adv. Microb. Ecol. **15**: 81-103.

Pope, R.M., and E.S. Fry. 1997. Absorption spectrum (380-700 nm) of pure water. II Integrating cavity measurements. Appl. Opt. **36**: 8710-8723.

Prieur, L., and S. Sathyendranath. 1981. An optical classification of coastal and oceanic waters based on the specific spectral absorption curves of phytoplankton pigments, dissolved organic matter, and other particulate materials. Limnol. Oceanogr. **26**: 671-689.

Reynolds, R.A., D. Stramski, and B.G. Mitchell. 2001. A chlorophyll-dependent semianalytical reflectance model derived from field measurements of absorption and backscattering coefficients within the Southern Ocean. J. Geophys. Res. **106**: 7125-7138.

Roesler, C.S., M.J. Perry, and K.L. Carder. 1989. Modeling in situ phytoplankton absorption from total absorption spectra in productive inland marine waters. Limnol. Oceanogr. **34**: 1510-1523.

Sathyendranath, S., G. Cota, V. Stuart, H. Maass, and T. Platt. 2001. Remote sensing of phytoplankton pigments: a comparison of empirical and theoretical approaches. Internat. J. Remote Sensing **22**: 249-273.

Sathyendranath, S., L. Lazzara, and L. Prieur. 1987. Variations in the spectral values of specific absorption of phytoplankton. Limnol. Oceanogr. **32**: 403-415.

Sathyendranath, S., L. Prieur, and A. Morel. 1989. A three-component model of ocean colour and its application to remote sensing of phytoplankton pigments in coastal waters. Internat. J. Remote Sensing **10**: 1373-1394.

Shibata, A., K. Kogure, I. Koike, and K. Ohwada. 1997. Formation of submicron colloidal particles from marine bacteria by viral infection. Mar. Ecol. Prog. Ser. **155**: 303-307.

Sieracki, M., and C. Viles. 1992. Distributions and fluorochrome-staining properties of sub-micrometer particles and bacteria in the North Atlantic. Deep-Sea Res. **39**: 1919-1929.

Smith, R.C., and K.S. Baker. 1984. The analysis of ocean optical data, p. 119-126. *In* [eds.]. Ocean optics VII. SPIE.

Smith, R.C., and K.S. Baker. 1986. Analysis of ocean optical data II, p. 95-107. *In* M.Blizard, [eds.]. Ocean Optics VIII. SPIE.

Sosik, H.M., R.E. Green, W.S. Pegau, and C.S. Roesler. 2001. Temporal and vertical variability in optical properties of New England shelf waters during late summer and spring. J. Geophys. Res. **106**: 9455-9472.

Stramski, D., A. Bricaud, and A. Morel. 2001. Modeling the inherent optical properties of the ocean based on the detailed composition of the planktonic community. Appl. Opt. **40**: 2929-2945.

Stramski, D., and D.A. Kiefer. 1991. Light scattering by microorganisms in the open ocean. Prog. Oceanogr. **28**: 343-383.

Stramski, D., and C.D. Mobley. 1997. Effects of microbial particles on oceanic optics: A database of single-particle optical properties. Limnol. Oceanogr. **42**: 538-549.

Stramski, D., R.A. Reynolds, M. Kahru, and B.G. Mitchell. 1999. Estimation of particulate organic carbon in the ocean from satellite remote sensing. Science **285**: 239-242.

Twardowski, M.S., E. Boss, J.B. Macdonald, W.S. Pegau, A.H. Barnard, and J.R.V. Zaneveld. 2001. A model for estimating bulk refractive index from the optical backscattering ratio and the implications for understanding particle composition in case I and case II waters. J. Geophys. Res. **106**: 14129-14142.

Ulloa, O., S. Sathyendranath, and T. Platt. 1994. Effect of the particle-size distribution on the backscattering ratio in seawater. Appl. Opt. **33**: 7070-7077.

Vodacek, A., N.V. Blough, M.D. DeGranpre, E.T. Peltzer, and R.K. Nelson. 1997. Seasonal variations of CDOM and DOC in the Middle Atlantic Bight: Terrestrial inputs and photooxidation. Limnol. Oceanogr. **42**: 674-686.

Yamasaki, A., H. Fukuda, R. Fukuda, T. Miyajima, T. Nagata, H. Ogawa, and I. Koike. 1998. Submicrometer particles in northwest Pacific coastal environments: Abundance, size distribution, and biological origins. Limnol. Oceanogr. **43**: 536-542.

CHAPTER 5:

CONCLUSIONS

I utilized a combination of Mie theory and flow cytometric measurements of individual particles to interpret variability in concurrently measured bulk optical properties in natural waters. There were two major components to this research: (1) to accurately determine particle properties from individual particle measurements, and (2) to use particle group optical properties to explain variability in measured bulk optical properties. In order to accomplish these goals, I helped to collect concurrent measurements of individual particle and bulk optical properties during two seasons (late summer and spring) in New England continental shelf waters. In addition, I have performed laboratory experiments to investigate the use of Mie theory in application to flow cytometry for accurately determining particle properties. I then applied methodology determined from the laboratory experiments to the measurements of natural samples to interpret observed patterns.

The accurate determination of particle diameter and complex refractive index $(n+n'i)$ was achieved from laboratory experiments with calibration particles (oils and beads) and ten phytoplankton cultures using Mie theory and flow cytometry. Individual particle estimates of diameter, n, and n' were compared with estimates from bulk optical methods. For the ten phytoplankton cultures, ranging in size from *Synechococcus* at ~1 μm to *Dunaliella tertiolecta* at ~8 μm, diameter was initially underestimated, and n and n' were initially overestimated. Corrections were

developed for forward angle light scattering and side angle light scattering to obtain more accurate estimates of cell properties; resulting diameter, n, and n′ were determined to within 13, 28, and 36% of independent estimates and n′ was correlated with intracellular chlorophyll concentration (r^2=0.60). The method initially developed by Ackleson and Spinrad (1988) for the application of Mie theory to flow cytometry was improved in this study to describe the deviation of phytoplankton cells from homogenous spheres and to determine phytoplankton n′, knowledge of which is necessary for quantifying the contribution of phytoplankton to absorption. Validation of the individual particle approach with independent measurements was important, because it has previously been shown that phytoplankton scattering deviates from that estimated by Mie theory (Quinby-Hunt et al. 1989; Volten et al. 1998). This was the first study to quantify the deviation from Mie theory of individual particle measurements using flow cytometry.

Interpretation of variability in bulk optical properties has been considerably improved by measurements of the individual particle properties of both microbes and non-phytoplankton. For surface waters in the equatorial Pacific, DuRand and Olson (1996) and Claustre et al. (1999) determined particle contributions to beam attenuation at 660 nm and reported that phytoplankton of ≤20 microns in size accounted for 30-45% of total beam attenuation, *Prochlorococcus* and heterotrophic bacteria accounted for ~10% each, and *Synechococcus* contributed a negligible amount (≤5%). Non-plankton (which by definition here include microzooplankton) were not measured but

were inferred to account for 50-60% of beam attenuation. In the present study, individual particle measurements were made of three microbial groups (eukaryotic phytoplankton, *Synechococcus*, and heterotrophic bacteria) and two non-phytoplankton groups (detritus and minerals). The summed contribution to scattering of these groups accounted for approximately the entire scattering coefficient measured independently using bulk methods. In agreement with findings for the equatorial Pacific, eukaryotic phytoplankton and non-phytoplankton were the most important particle contributors to total attenuation in New England shelf surface waters, with *Synechococcus* and heterotrophic bacteria being relatively less important optically. Seasonal differences in optical properties were explained by changes in individual particles. Eukaryotic phytoplankton had higher n in summer surface waters and similar values of n′ in both the spring and summer. However, they contributed more to absorption and scattering in surface waters in the spring, because they were ~2x higher in concentration. Of the non-phytoplankton components, detritus contributed more to attenuation than minerals in the summer because of their higher abundance. In contrast, minerals were more important contributors than detritus in the spring, even though their concentrations were approximately the same, because of their higher real refractive indices, n.

Advances in our understanding of scale closure in ocean optics relies on the concurrent measurement of bulk optical properties and individual particles, perhaps most importantly to elucidate the role of small non-phytoplankton particles. Recent simulations of open ocean waters by Stramski et al. (2001) were based on estimates of

particle concentrations for numerous groups of microbes, detritus, and minerals. In their simulations, microbes were less important than both detritus and minerals in contributing to scattering, and they contributed negligibly to backscattering; minerals were the most important contributor to both scattering and backscattering. Similar to the findings for Stramski et al. (2001), I found that microbes were of little importance in determining backscattering in New England shelf waters. Eukaryotic phytoplankton, however, were the most important contributors to scattering in both the summer and spring because of higher concentrations in continental shelf waters than were assumed for the open ocean. Additionally, although minerals were important contributors to backscattering in both seasons, detritus was the most important backscatterer in summer surface waters. For detritus and minerals, the difference between the results of the present study and the simulations of Stramski et al. was caused by differences in measured versus assumed size distributions. The shape of these size distributions directly determines the slope of spectral backscattering and was responsible in New England shelf waters for non-phytoplankton backscattering which increased with decreasing wavelength in the summer and backscattering which was relatively flat spectrally in the spring. It is clear that measurement of the detrital and mineral size distributions in natural samples, including the submicron size range, is necessary for accurate understanding of optical properties, especially backscattering, and for understanding the role of these particles in ecosystems.

Variability in the spectral shape of remote sensing reflectance (R_{rs}) in New England shelf waters was determined by eukaryotic phytoplankton absorption,

dissolved absorption, and non-phytoplankton backscattering. Values of R_{rs} were higher at blue wavelengths and lower at green wavelengths in the summer compared to the spring. These general spectral differences in R_{rs} between seasons were to first order related to chlorophyll concentration (low in summer and high in spring), an observation consistent with the original basis for bio-optical models (e.g. Gordon and Morel (1983)). Using Hydrolight simulations and spectral IOPs for seawater constituents, the difference in R_{rs} spectral shape (i.e. $R_{rs}(490):R_{rs}(550)$) between seasons was contributed to approximately equally by differences in absorption by eukaryotic phytoplankton, absorption by dissolved materials, and backscattering by non-phytoplankton. In concurrence with these findings, Reynolds et al. (2001) reported that ~80% of the change in $R_{rs}(490):R_{rs}(550)$ they measured in the Southern Ocean was caused by differences in absorption and that ~20% was caused by differences in backscattering. The main cause of variability in R_{rs} in New England surface waters was lower absorption by eukaryotic phytoplankton and dissolved materials in the summer, compared to spring, and a higher inverse wavelength dependence of spectral backscattering in the summer because of the contribution of small detrital particles.

Important insights into current bio-optical models are likely to be gained through the combined use of radiative transfer modeling and the measurement of the inherent optical properties of seawater constituents. In the spring and summer in New England shelf surface waters, deviations from chlorophyll-based bio-optical models were primarily caused by differences in scattering and backscattering by non-

phytoplankton and absorption by dissolved materials. Values of a_g in the summer and spring were ~3 and 7x higher, respectively, than values based on bio-optical models and were the main cause of differences between measured and modeled $R_{rs}(440):R_{rs}(555)$. A better understanding of the relationship between a_g and a_p is clearly needed for continental shelf waters. In my data, this relationship varied with season, primarily caused by variability in absorption by particles, especially eukaryotic phytoplankton. The accurate representation of the magnitudes of b_b and R_{rs} in bio-optical models was sensitive to assumptions regarding the backscattering efficiencies and scattering of non-phytoplankton. The magnitudes of both b_b and R_{rs} at 440 nm were underestimated by ~40% in the summer because of higher backscattering efficiencies and scattering by non-phytoplankton than were estimated by the models. If b_b and R_{rs} are to be accurately represented in bio-optical models, then an improved understanding is needed of the relationship between chlorophyll concentration and backscattering by non-phytoplankton in continental shelf waters. With respect to development of these models, individual particle measurements provide a powerful tool for understanding the relationship between the optical properties of different particle groups, chlorophyll concentration, and ecosystem functioning.

In the study of scale closure between individual particle and bulk optical measurements, there are several areas of future research which would improve our understanding of marine ecosystems. In coastal regions, significant variability can be expected in the types of seawater constituents which affect remote sensing reflectance,

because of such complex factors as riverine inputs, anthropogenic nutrient inputs, and sediment resuspension. The application of studies of scale closure to these highly productive regions will be important for developing regional models for accurately interpreting ocean color. In addition to bulk measurements of absorption and scattering, measurements of bulk backscattering would allow for validation of individual particle estimates of backscattering. Because small particles play an important role in determining backscattering, and thus remote sensing reflectance, improved methods need to be developed for their measurement. For example, the routine use of two flow cytometers may be necessary in studies of scale closure, one of low sensitivity for measuring large particles (>1 μm) and one of high sensitivity for measuring small (submicron) particles. Studies of scale closure will improve the monitoring of ecosystem change by allowing us to determine the contributions of different seawater constituents to ocean color, including the contributions of different species of phytoplankton, dissolved materials, and non-phytoplankton groups, such as heterotrophic bacteria, detritus, and minerals.

REFERENCES

Ackleson, S.G., and R.W. Spinrad. 1988. Size and refractive index of individual marine particulates: a flow cytometric approach. Appl. Opt. **27**: 1270-1277.

Claustre, H., A. Morel, M. Babin, C. Cailliau, D. Marie, J.C. Marty, D. Tailliez, and D. Vaulot. 1999. Variability in particle attenuation and chlorophyll fluorescence in the tropical Pacific: Scales, patterns, and biogeochemical implications. J. Geophys. Res. **104**: 3401-3422.

DuRand, M.D., and R.J. Olson. 1996. Contributions of phytoplankton light scattering and cell concentration changes to diel variations in beam attenuation in the equatorial Pacific from flow cytometric measurements of pico-, ultra- and nanoplankton. Deep-Sea Res. II **43**: 891-906.

Gordon, H.R., and A. Morel. 1983. Remote assessment of ocean color for interpretation of satellite visible imagery - A review. Springer-Verlag.

Quinby-Hunt, M.S., A.J. Hunt, L. Lofftus, and D. Shapiro. 1989. Polarized-light scattering studies of marine *Chlorella*. Limnol. Oceanogr. **34**: 1587-1600.

Reynolds, R.A., D. Stramski, and B.G. Mitchell. 2001. A chlorophyll-dependent semianalytical reflectance model derived from field measurements of absorption and backscattering coefficients within the Southern Ocean. J. Geophys. Res. **106**: 7125-7138.

Stramski, D., A. Bricaud, and A. Morel. 2001. Modeling the inherent optical properties of the ocean based on the detailed composition of the planktonic community. Appl. Opt. **40**: 2929-2945.

Volten, H., J.F. de Haan, J.W. Hovenier, R. Schreurs, W. Vassen, A.G. Dekker, H.J. Hoogenboom, F. Charlton, and R. Wouts. 1998. Laboratory measurements of angular distributions of light scattered by phytoplankton and silt. Limnol. Oceanogr. **43**: 1180-1197.

APPENDIX 1

Cultures and Calibration Particles Used in FCM-Mie Method Development

The methodology for applying Mie theory to FCM measurements was developed using a calibration dataset from measurements for ten species of phytoplankton ("FCM-Mie Calibration") and was then evaluated by applying it to a larger evaluation dataset. The evaluation dataset included four experiments ("MicroDiel", "Roof Calibration", "CMO1 Calibration", and "NannoDiel") consisting of measurements for 21 cultures, with thirteen species each of phytoplankton grown at low-light levels and high-light levels (Table 1). The experiments contained in the two datasets were performed over several years, from 1994-2000, and by several different researchers. A more detailed table than that contained in Chapter 2 has been created to include experiment dates, light levels, light:dark cycles, temperature of growth, and optical measurements which were made (Table 1).

Particle shape, size, and homogeneity all affect how a particle scatters light. These characteristics for particles and the sources from which particles were obtained have been tabulated for oil suspensions, beads, and FCM-Mie Calibration cultures (Table 2). Oil droplets and beads are spherical in shape, and most cells included in the calibration dataset were coccoid (spherical). Cultures which deviated the most from spherical were *Dunaliella tertiolecta* (3x10 µm), *Thalassiosira pseudonana* (2x4 µm), and *Monochrysis lutheri* (6-10 µm). Phytoplankton cells which were far from spherical (e.g., pennate diatoms or chains of cells) or contained gas vacuoles were not

included in measurements. These cells have scattering properties which are difficult

to model by Mie theory.

Table 1. Experimental conditions for phytoplankton cultures analyzed in five different experiments. For each experiment, the date, species analyzed, light level, and instrumentation used to measure spectral absorption (a) and attenuation (c) are indicated. Natural sunlight for the FCM-Mie Calibration and Roof Calibration datasets corresponds to cultures acclimated for growth during July-September, 1999 and June-August, 1998, respectively, in Woods Hole, Massachusetts. The NannoDiel was performed under natural sunlight with an average integrated light level of 1,500 μmol m^{-2} s^{-1} for the day.

Experiment	Date	Phytoplankton Species	Light Level (μmol photons m^{-2} s^{-1})	L:D Period	Temp (°C)	Spectral a and c
FCM-Mie Calibration	Sept-Oct 99	*Dunaliella tertiolecta*	Natural sunlight, 90	constant	20	spectro-photometer; ac-9
		unidentified eukaryote (t6)	90			
		unidentified eukaryote (islow1)	Natural sunlight, 90			
		Nannochloris sp.	Natural sunlight, 90			
		Isochrysis sp.	Natural sunlight, 90			
		Emiliania huxleyi (no coccoliths)	90			
		Thalassiosira pseudonana	Natural sunlight, 90			
		Monochrysis lutheri	90			
		unidentified eukaryote (isb)	90			
		Synechococcus sp. (7D95m)	Natural sunlight, 90			
MicroDiel	Apr 00	*Micromonas pusilla*	120	12:12	24	spectro-photometer; ac-9
Roof Calibration	Jul-Aug 98	*Dunaliella tertiolecta*	Natural sunlight, 70	constant	20	Not measured
		Isochrysis sp.	Natural sunlight, 70			
		Emiliania huxleyi	Natural sunlight			
		Nannochloris sp.	Natural sunlight, 70			
		Minutocellus polymorphous (13DT11)	Natural sunlight			
		unidentified eukaryote (t6)	Natural sunlight, 70			
		Platymonas sp.	Natural sunlight			

164

Table 1 cont'd.

Experiment	Date	Phytoplankton Species	Light Level (μmol photons m^{-2} s^{-1})	L:D Period	Temp (°C)	Spectral a and c
Roof Calibration (cont'd.)		*Synechococcus* sp. (7d95m)	Natural sunlight, 70			
		Olisthodiscus	Natural sunlight			
		Monochrysis lutheri	Natural sunlight			
		unidentified eukaryote (t11)	Natural sunlight			
		unidentified coccolithophorid, with coccoliths (clone 12-1)	Natural sunlight			
CMO1 Calibration	Sept 96	unidentified eukaryote (islow1)	Natural sunlight 50-100	constant	20-22	spectro-photometer
		Synechococcus sp. (WH8012)				
		Synechococcus sp. (WH7803)				
		Nannochloris sp.				
		Pycnococcus provasolii				
		Isochrysis galbana				
		Monochrysis lutheri				
NannoDiel	Aug 94	*Hymenomonas carterae*		constant	22	spectro-photometer; SeaTech transmisso-meter
		Nannochloris sp.	Natural sunlight			

Table 2. Specifications for the different particle types (oil suspensions, beads, and FCM-Mie Calibration cultures) measured on the FCM. Refractive indices for oils and beads are reported relative to water.

Particle Type	Characteristics (Shape, Diameter (µm), etc.)	Source
Heptane Oil Suspension, n = 1.0325	Spherical; Polydisperse	Sigma Chemical, Co.
Nonane Oil Suspension, n = 1.0467	Spherical; Polydisperse	Sigma Chemical, Co.
Dodecane Oil Suspension, n = 1.0590	Spherical; Polydisperse	Sigma Chemical, Co.
Polystyrene Beads, n = 1.19	Spherical; 0.66, 2.14, 2.9, 3.79, 5.2, 6.2	Polysciences, Inc.
Silica Beads, n = 1.09	Spherical; 1.58	Duke Scientific, Inc.
Dunaliella tertiolecta (clone Dun)	Flattened oval; 3x10	CCMP[1]
Emiliania huxleyi (clone EH12-1)	Coccoid; 4	CCMP
Nannochloris sp.	Oblong round; 3-4; chl *b*	CCMP
Isochrysis sp.	Oblong round; 5	CCMP
Emiliania huxleyi (no coccoliths)	Ovoid; 5	CCMP
Thalassiosira pseudonana	Cylindrical; 2x4; silica outer shell; water vacuoles	CCMP
Micromonas pusilla	Coccoid; 1-2	CCMP
Monochrysis lutheri	Flattened triangle; 6-10	CCMP
Platymonas sp.	Ovoid; 10	CCMP
Olisthodiscus	Flattened ovoid; 10	CCMP
Synechococcus sp. (7D95m)	Coccoid; 1-2	Carribean isolate (21°N, 67°W)
Minutocellus polymorphous (13DT11)	Coccoid; 3	Carribean isolate (37°N, 75°W)
unidentified eukaryote (islow1)	Coccoid; 2-3; chl *b*	Sargasso Sea isolate
unidentified eukaryote (isb)	Coccoid; 1-2; chl *b*	Sargasso Sea isolate
unidentified eukaryote (t6)	Coccoid; 2-3	Equatorial Pacific isolate
unidentified eukaryote (T-11)	Coccoid; 4-5	Equatorial Pacific isolate

[1] Provasoli-Guillard National Center for Culture of Marine Phytoplankton (CCMP), Bigelow Laboratory.

APPENDIX 2

Flow Cytometry and Mie Theory Optimization for Heterotrophic Bacteria

An optimization was performed between Mie theory calculations of scattering and flow cytometric (FCM) measurements, for particles in the size range of heterotrophic bacteria, using calibration particles of known refractive index and /or size. A separate optimization from that used for phytoplankton and non-phytoplankton was determined for heterotrophic bacteria, because the FCM configuration was changed (i.e. the laser beam focusing lens) in order to enumerate smaller particles. Particles used in the optimization included polydisperse oil suspensions of heptane, nonane, and dodecane and polystyrene beads of 0.28, 0.46, and 0.57 μm in diameter. A close fit was observed between theoretical and measured FLS and SSC in the size range for heterotrophic bacteria, between 0.25 and 0.75 μm (Fig. 1). Similar trends between the measured and modeled oils are observed, such as the inflection at an FLS of ~7x10^{-3}.

Using this optimization, a 3-dimensional lookup table of Mie theory-based solutions for particle FLS, SSC, and σ_a was created over the expected ranges of heterotrophic bacteria D (0.06-1 μm), n (1-1.20), and n' set to an assumed value of 5x10^{-4}. The mean n' for polystyrene beads of 6x10^{-4} was similar to that used for heterotrophic bacteria, and the same lookup table was used for both. Comparison between FCM-Mie estimates of D and n and measured values for all polystryrene

beads analyzed, resulted in the FCM-Mie method overestimating D by an average of
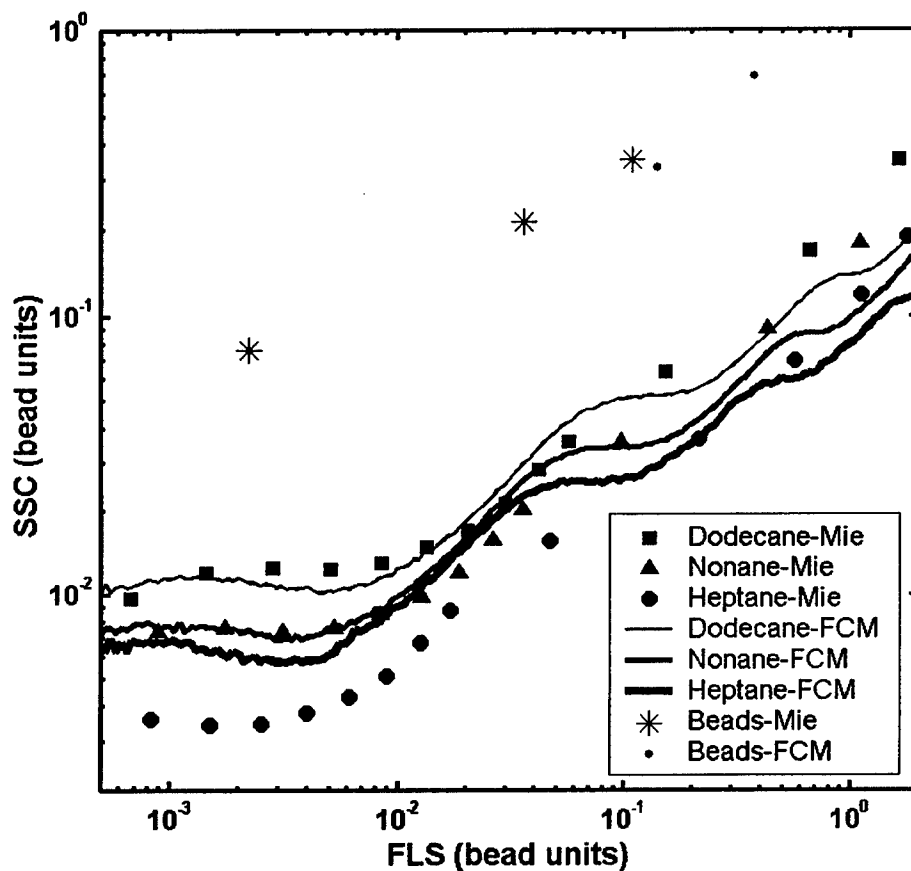
24% and underestimating n by 7%.

Figure 1. Comparison of theory-based estimates (asterisks) and FCM measurements
(lines and dots) of forward angle light scattering, FLS, and side angle light scattering,
SSC, for beads and oil dispersions. Polystyrene beads were 0.28, 0.46, and 0.57 μm in
diameter, and oil dispersions included heptane, nonane, and dodecane. Note that the
measured and theoretical positions of the 0.28 μm are approximately the same.

50272-101

REPORT DOCUMENTATION PAGE	1. REPORT NO. MIT/WHOI 2002-10	2.	3. Recipient's Accession No.

4. Title and Subtitle

Scale Closure in Upper Ocean Optical Properties:

From Single Particles to Ocean Color

5. Report Date June 2002
6.

7. Author(s)   Rebecca E. Green

8. Performing Organization Rept. No.

9. Performing Organization Name and Address

MIT/WHOI Joint Program in Oceanography/Applied Ocean Science & Engineering

10. Project/Task/Work Unit No.
MIT/WHOI 2002-10

11. Contract(C) or Grant(G) No.

(C) N00014-95-1-0333

(G) N00014-96-1-0965

12. Sponsoring Organization Name and Address

National Aeronautics and Space Administration

13. Type of Report & Period Covered
Ph.D. Thesis

14.

15. Supplementary Notes

This thesis should be cited as: Rebecca E. Green, 2002. Scale Closure in Upper Ocean Optical Properties:
From Single Particles to Ocean Color. Ph.D. Thesis. MIT/WHOI, 2002-10.

16. Abstract (Limit: 200 words)

Predictions of chlorophyll concentration from satellite ocean color are an indicator of primary productivity, with implications for foodwebs, fisheries, and the global carbon cycle. Models describing the relationship between optical properties and chlorophyll do not account for much of the optical variability observed in natural waters, because of the presence of seawater constituents that do not covary with phytoplankton pigments. In order to understand variability in these models, the optical contributions of seawater constituents were investigated. A combination of Mie theory and flow cytometry was used to determine the diameter, complex refractive index, and optical cross-sections of individual particles. In New England continental shelf waters, eukaryotic phytoplankton were the main particle contributors to absorption and scattering. Minerals were the main contributor to backscattering (bb) in the spring, whereas in the summer both minerals and detritus contributed to bb. *Synechococcus* and heterotrophic bacteria were relatively unimportant optically. Seasonal differences in the spectral shape of remote sensing reflectance, Rrs, were contributed to approximately equally by eukaryotic phytoplankton absorption, dissolved absorption, and non-phytoplankton bb. Differences between measurements of bb and Rrs and modeled values based on chlorophyll concentration were caused by higher dissolved absorption and non-phytoplankton bb than were assumed by the model.

17. Document Analysis   a. Descriptors

optical

particles

flow cytometry

b. Identifiers/Open-Ended Terms

c. COSATI Field/Group

18. Availability Statement

Approved for publication; distribution unlimited.

19. Security Class (This Report) UNCLASSIFIED	**21. No. of Pages** 168
20. Security Class (This Page)	**22. Price**

(See ANSI-Z39.18)   *See Instructions on Reverse*   OPTIONAL FORM 272 (4-77)
(Formerly NTIS-35)
Department of Commerce